NTNU
Norwegian University of
Science and Technology

# DC/DC Converters for Multi-terminal HVDC Systems

Based on Modular Multilevel Converter

Hasan Inanc Sari

Wind Energy
Submission date: August 2016
Supervisor: Elisabetta Tedeschi, ELKRAFT
Co-supervisor: Pavol Bauer, ELKRAFT

Norwegian University of Science and Technology
Department of Electric Power Engineering

# DC/DC Converters for Multi-terminal HVDC Systems

## Based on Modular Multilevel Converter

H. Inanc Sari

Master Thesis of Science

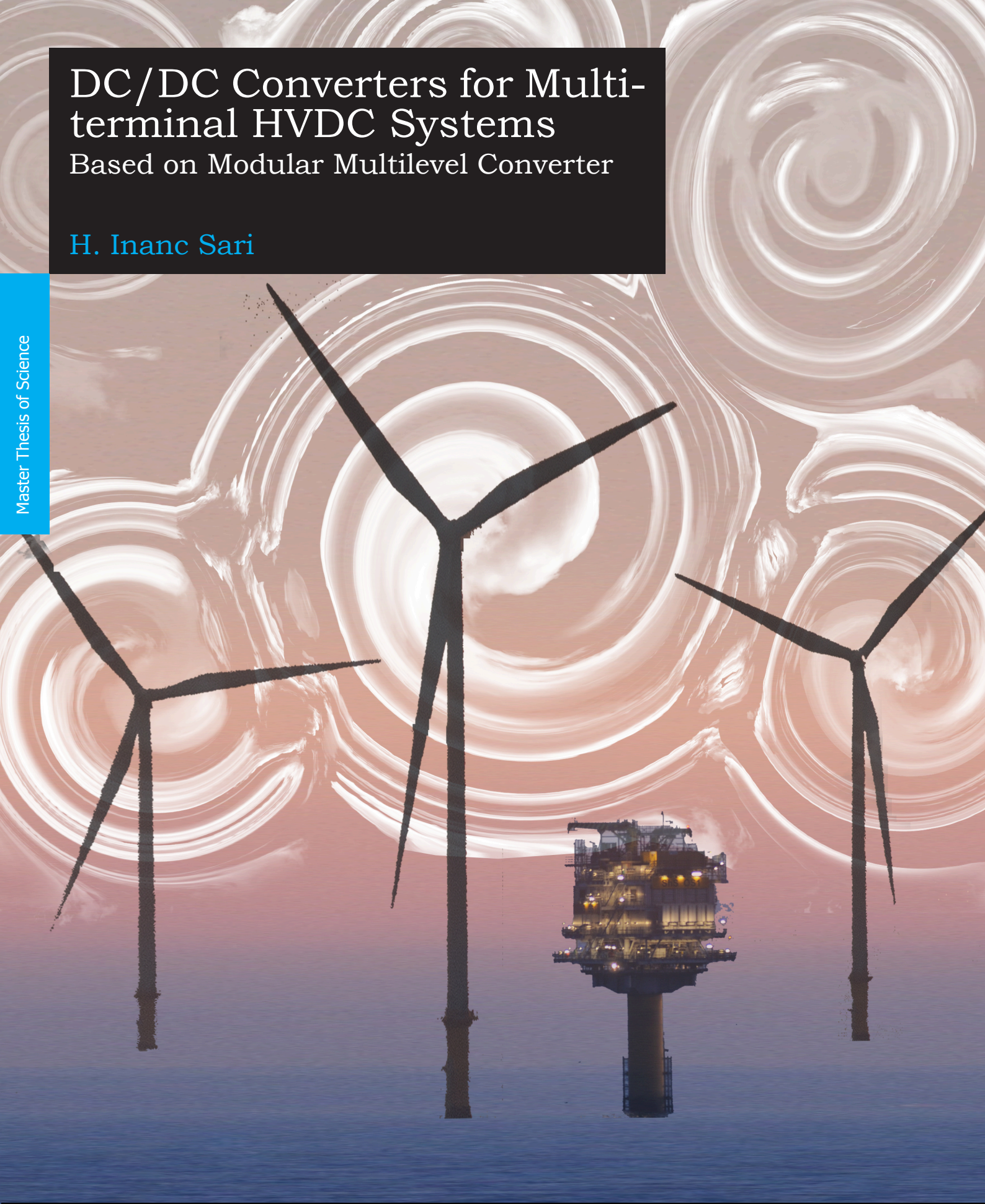

EWEM

TU Delft

NTNU

DTU

European Wind Energy Master – EWEM - Electric Power Systems Track

# DC DC Converters for Multi-terminal HVDC Systems

## Based on Modular Multilevel Converter

Master of Science Thesis

by

**H. Inanc Sari**

In partial fulfillment of the requirements for the degree of

**Master of Science**

in Electrical Engineering
at Delft University of Technology

&

**Master of Science**

in Technology-Wind Energy
at Norwegian University of Science and Technology

within the **European Wind Energy Master - EWEM**
Electric Power Systems Track

August 11th, 2016

European Wind Energy Master - EWEM
Norwegian University of Science and Technology
Delft University of Technology



NTNU
Norwegian University of
Science and Technology

DELFT UNIVERSITY OF TECHNOLOGY DEPARTMENT OF ELECTRICAL SUSTAINABLE ENERGY
AND
NORWEGIAN UNIVERSITY OF SCIENCE AND TECHNOLOGY DEPARTMENT OF ELECTRIC POWER ENGINEERING

The undersigned hereby certify that they have read and recommend to the Delft University of Technology Department of Electrical Sustainable Energy and Norwegian University of Science and Technology Department of Electric Power Engineering for acceptance a thesis entitled **"DC/DC Converters for Multi-terminal HVDC Systems Based on Modular Multilevel Converter"** by **H. Inanc Sari** in partial fulfillment of the requirements for the degree of Master of Science.

Dated: August 11th, 2016

Supervisor: _____
Prof. Elisabetta Tedeschi, NTNU Trondheim

Supervisor: _____
Prof. dr. ir. Pavol Bauer, TU Delft

Co-supervisor: _____
Jon Are Suul, SINTEF Energy Research

Reader: _____
Dr. ir. Laura Ramirez Elizondo, TU Delft

# Acknowledgements

This master thesis is the result of my time at Norwegian University of Science and Technology (NTNU) - Department of Electric Power Engineering in Trondheim. It is the requirement for the concluding work of European Wind Energy Master (EWEM) coordinated by Delft University of Technology (TU Delft).

This double degree work would not have been possible without the supervision of professors in both NTNU and TU Delft. I am eternally grateful to my supervisor Prof. Elisabetta Tedeschi, NTNU Trondheim for her immense range of knowledge, her constant supervision, patience and precious time throughout this work. I would also like to express my deep gratitude to Prof. Pavol Bauer, TU Delft. Their enthusiasm and energy for power electronics and renewable energy have fascinated and kept me motivated to complete this work.

Likewise, I would like to express special and many thanks to my co-supervisor Jon Are Suul for sharing his deep knowledge and guiding me on technical problems. He always found time to answer my questions even during his most busy times.

I also express my gratitude to Gilbert Bergna-Diaz, research scientist in SINTEF, for his invaluable explanations about modular multilevel converters and for his support about simulation models especially for multi-terminal DC grid.

I am thankful to whole European Wind Energy Master Committee for giving me this great opportunity to complete my master study in three universities and granting me the Erasmus Mundus Scholarship. Many thanks must be given to Linda Gaffel, Coordinator European Wind Energy Master, for replying all my endless e-mails very quickly prior to and during my study and for her enormous efforts during the EWEM summer schools and other extra-curricular activities. Special acknowledgements to Dr. ir. Henk Polinder, TU Delft coordinator of EWEM-Electric Power Systems Track for his continuous guiding throughout my entire master study. I would also like to thank the other EWEM students for the two unique years we spent in Copenhagen, Delft and Trondheim.

Finally, my parents who have always been with me in spite of the distance deserve grate thanks for their infinite support, patience, confidence and love. I would like to express my sincere gratitude to my dearest sister for her advices and cover image of this work.

*H. Inanc Sari*
*Trondheim, August 2016*

# Abstract

The increase in the energy demand has resulted in searching for new energy sources. Due to the increased prices of fossil fuels and the environmental issues, renewable energy sources has become popular in Europe. Renewable energy generation such as wind, solar and wave has point-to-point connections with the main grid. In order to minimize the disadvantages of renewable energy sources like energy fluctuations, multi-terminal systems are favoured interconnecting energy generation stations among them with the main grid.

The long distance interconnection especially for offshore wind farms and intercontinental connections is not possible with traditional alternating current (AC) technology because of the limited power transfer. Therefore, high voltage direct current (HVDC) technology is considered as the main element for the future multi-terminal grid. The conversion between AC and DC is preferred via voltage source converters (VSC) as they offer more flexible power control compared to traditional current source converters in other words line commutated converters (LCC).

HVDC power transmission schemes have been constructed depending on the technology of the time, which means that there is no standardization in voltage levels and configurations of the HVDC schemes. Therefore, the connection of such systems operating at different voltage levels and/or in different schemes such as monopole and bipolar systems for the future multi-terminal DC grids requires DC/DC converters. Although the voltage level and the configurations are the same for both DC systems, DC/DC converter may be required for the power flow control in multi-terminal DC grid. The modular multilevel converter (MMC) seems as the most suitable converter in this application due to its advantages such as low switching losses, high scalability and modularity.

MMC control structures are introduced and front-to-front connection of two MMC forming a DC/AC/DC converter is modelled and simulated for different applications such as interconnecting systems with same voltage levels, different voltage levels or different configurations in this study. The passive element sizes of MMC submodules are also compared for different AC side frequency as the component sizes can be decreased thanks to the increase in the AC frequency which has a disadvantage of higher switching losses. Moreover, the designed converters are tested in multi-terminal DC grids to check their performance and functionality.

# Contents

# List of Figures

# List of Tables

# Abbreviations

| | |
|---|---|
| AC | Alternating Current |
| CCSC | Circulating Current Suppressing Controller |
| CIGRÉ | Conseil International des Grands Réseaux Électriques<br>International Council on Large Electric Systems |
| DC | Direct Current |
| GTO | Gate Turn-Off Transistor |
| HVAC | High Voltage Alternating Current |
| HVDC | High Voltage Direct Current |
| IGBT | Insulated-Gate Bipolar Transistor |
| LCC | Line-Commutated Converters |
| LSPWM | Level-Shifted Pulse Width Modulation |
| MMC | Modular Multilevel Converter |
| MO | Modulus Optimum |
| MTDC | Multi-Terminal Direct Current |
| NLM | Nearest Level Modulation |
| OHL | Overhead Line |
| PI | Proportional Integral |
| PR | Proportional-Resonant |
| PSPWM | Phase-Shifted Pulse Width Modulation |
| PWM | Pulse Width Modulation |
| SM | Submodule |
| SVM | Space Vector Modulation |
| VSC | Voltage Source Converter |
| WF | Wind Farm |

# 1

# Introduction

*The main motivations for the relevance of the topic investigated in the thesis and a short overview are presented in this chapter. The objective, main contributions and thesis structure are also provided.*

The total energy demand of the world has been increasing rapidly, 48% increase by 2040 [1], and this has resulted in taking cognizance of reliable and plentiful renewable energy sources. About 2000 GW of the net global electricity generation was supplied by renewable energy sources (hydropower, solar, wind, bioenergy) and around 22% of renewable energy generation was from wind in 2015 [2]. As shown in Figure 1.1, installed wind power generation capacity has significantly increased in the last two decades, from 7.5 GW in 1997 to 435 GW in 2015 [3].

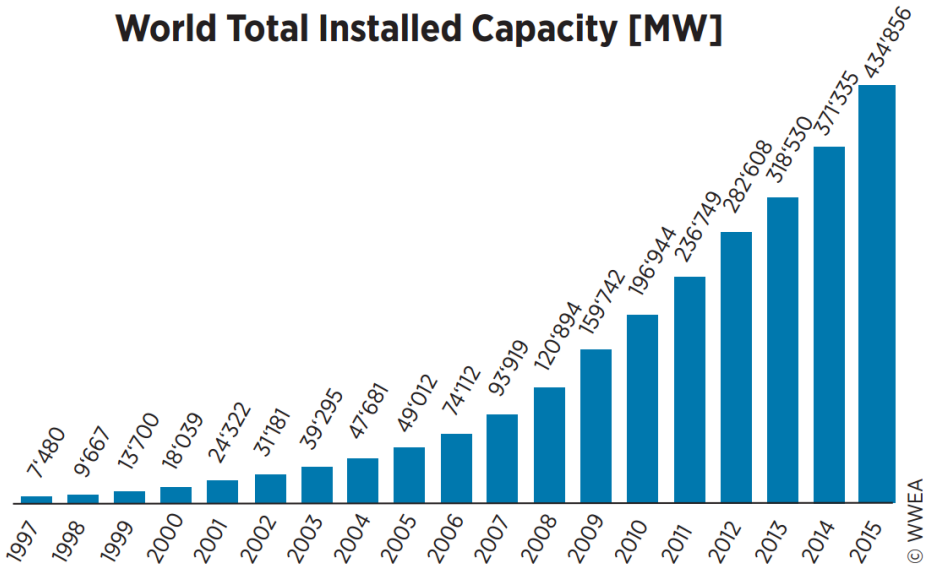


**Figure 1.1:** Global installed wind power generation capacity [3]

In order to utilize powerful and continuous wind as maximum as possible over the oceans, offshore wind plants have been installed since 1991 and 12.2 GW of energy was globally generated by offshore wind farms in 2015 [2]. Although offshore wind farms require more investment in the construction and grid connection processes, they generate high amount of sustainable power in long term. Moreover, constructing wind farms offshore can compensate the cost for valuable properties where the population is densely clustered and onshore growth is opposed.

Since the generation in the offshore wind farms is far away from the consumption side, existing high voltage alternating current (HVAC) grid is not suitable for the power transmission from offshore

due to the limited power transfer arising from high capacitive current component in long alternating current (AC) cables. Furthermore, the goal of increasing the renewable energy will require a revision on the existing transmission systems because the power fluctuation arising from renewable energy sources may be a problem in the AC grid. It is considered that renewable energy sources should be connected to a direct current (DC) grid in order to operate them more effectively [4]. Therefore, the main element for connection of offshore wind farms and the transmission of energy between countries is considered as high voltage direct current (HVDC) transmission technologies in order to avoid cable loss and reactive power compensator [5, 6]. To illustrate, in DolWin2 project, in German North Sea, wind farms are connected through AC cables to a ±320 kV HVDC converter station installed on an offshore platform and the generated power is transmitted through DC subsea cable between converter station and the onshore. After this point, DC land cables are used for the power transmission till HVDC onshore converter station where the system is connected to the grid. Thanks to HVDC transmission technologies, electrical losses can be decreased 1% per converter station while a rated power of 916 MW is transmitted from the offshore [7].

While the existing HVDC transmission schemes have point-to-point connections between the generation and the consumption side, the future HVDC grid is expected as a fully integrated multi-terminal DC (MTDC) Supergrid as proposed by several experts [8–12] since the MTDC is the best and most efficient solution for long distance transmission. It is also considered that HVDC Supergrid will compensate the unstable behaviour of the renewable energy sources [13]. However, the existing HVDC schemes have not been standardized; i.e. they are in different configurations and/or voltage levels depending on the technology of the time they were constructed. Therefore, DC/DC conversion at high voltage level is required for the interconnection of such HVDC schemes and offshore wind farms.

Considering the advantages of voltage source converters (VSC) over conventional line commutated converter (LCC) technology such as independent active and reactive power control, reduced footprint and fast power flow reversal without interruption, VSC is more suitable for the development of MTDC grid and interconnection of offshore wind farms by operating several terminals in parallel. Moreover, VSC-based MTDC transmission systems allow less power loss with more stable system [8]. HVDC-Light, HVDC-MaxSine and HVDC-Plus are the commercial names of VSC-based HVDC technology implemented by three distinguished companies [14–16].

Among different topologies of VSC, the modular multilevel converter (MMC) is seen as more promising solution for high power high voltage applications due to its several advantages such as high scalability and less distorted output voltage which eliminates bulky filters and decreases the footprint size further. For instance, Siemens used MMC topology for low loss power supply in order to interconnect San Francisco´s City Center electrical power grid with a substation near Pittsburg, California by constructing 88 km subsea HVDC transmission link which transmits up to 400 MW at a DC voltage of ±200 kV [17].

Although usage of MMC has been growing rapidly in HVDC applications and there is considerable amount of technical literatures on AC/DC/AC converters with MMC topology, there are relatively few publications about using MMC in DC/DC converter applications. Therefore, the performance of DC/DC converters implemented by front-to-front connection of two MMC has been studied in this thesis.

## 1.1. Objectives

This thesis mainly focuses on the implementation of MMC to high power high voltage DC/DC converters and multi-terminal applications with the above mentioned motivations. The objectives of the thesis are:

- Analysing the importance of HVDC for the power transfer from offshore wind farms.
- Motivations for MTDC transmission grid and DC/DC converters.
- Brief review of several topologies for high power high voltage DC/DC converters.
- Investigating MMC for HVDC applications.

- Detailed analysis of MMC in terms of modelling and control in order to provide bidirectional power flow and implementing the control strategies in Matlab/Simulink.
- Analysis of MMC based DC/DC converter in the connections of DC networks with similar configurations and voltage levels with the purpose of controlling the power flow in MTDC grid and its simulation.
- Analysis of MMC based DC/DC converter with the purpose of connecting DC networks with different configurations and voltage levels and its simulation.
- Analysis of the effect of AC side frequency on MMC components sizes.
- Verifying the designed DC/DC converters in a MTDC system including DC/DC converters for the power flow control and interconnection of DC systems operating at different voltage levels with dissimilar configurations.

## 1.2. Main Contributions

The main purpose of the work is to analyse high power high voltage DC/DC converters for interconnection of DC networks. The thesis contribution is to provide a MMC model, including control structures and its usage as a DC/DC converter with front-to-front connection of two MMC. At this point DC/DC converter is classified depending on the purpose: Power flow control between two similar HVDC networks and interconnection of dissimilar HVDC networks together with power flow control. By this method, DC networks operating with similar configuration and voltage levels or networks with different configuration and voltage levels are connected. Furthermore, the work also includes the applications of DC/DC converters in MTDC systems formed by monopole and bipolar DC systems together with the analysis of the increased AC side frequency which allows to decrease converter component sizes.

## 1.3. Thesis Structure

After the motivations and objectives are explained in Chapter 1, following chapters are organized as follows:

- Chapter 2 presents basics of HVDC systems. Firstly, it explains the historical development of HVDC technology and advantages of DC transmission over AC systems. Furthermore, this chapter includes different types of converters designed for HVDC networks together with implementations of these converters used in the projects throughout the world. The application areas of HVDC technology and its configurations, mainly monopole and bipolar transmission, are also presented in Chapter 2. Finally, importance of MTDC grids and their different configurations are discussed in this chapter as well as officially commissioned MTDC projects.
- Chapter 3 explains why DC/DC converters are required for high power HVDC transmission systems. Moreover, a classification for DC/DC converters is presented in this chapter. After the application areas and advantages of converters with and without galvanic isolation are introduced, the main DC/DC converter types suitable for high power HVDC transmission systems are explained in brief.
- Chapter 4 presents the operation principles of MMC. Operating states of submodules used in MMC arms, sizing of submodule capacitor and different modulation techniques are explained in this chapter. A mathematical model is built depending on the MMC equations and it is simulated in Matlab/Simulink for both single phase and three phase systems. Moreover, a switching model including power electronic devices is constructed with low number of submodules (8 submodules in a phase leg) in order to verify the results obtained from mathematical model.
- Chapter 5 demonstrates a MMC model based on controlled voltage sources with nearest level modulation in order to achieve high number of submodules for high voltage applications. Furthermore, the control structure is expanded and circulating current suppressing controllers based on dq vector and PR controllers, active and reactive power controllers and current controllers are described in this chapter. Simulation results are provided for the control systems.

- Chapter 6 presents front-to-front connection of two MMC used as a DC/DC converter without galvanic separation. This system is used to interconnect HVDC systems operating at similar voltage levels in order to control power flow. The control structure of the total system and the simulation results are also provided in this chapter.
- Chapter 7 includes front-to-front connection of two MMC with a galvanic separation in the form of transformer coupling in order to connect two HVDC systems operating at different voltage levels or having different configurations. Firstly, the interconnection of systems with different voltage levels is achieved by a two-winding transformer. Secondly, connection of different configurations are performed by two-winding and three-winding transformers. The control structures and simulation results are shown for all systems.
- The effect of the middle AC stage frequency of DC/DC converter on the converter component sizes is investigated in Chapter 8. The theory of the decrease in submodule capacitance value, thus the size of the converter, explained in Chapter 4, is simulated in this chapter for both converters with and without transformer coupling. It is also presented that the increase in the AC side frequency reduces the core size of the transformer although the change is not as linear as other component sizes.
- MTDC grid designed by International Council on Large Electric Systems (CIGRÉ) B4 working group is examined in Chapter 9. After the system components including AC/DC converters with the connection of onshore and offshore stations, DC/DC converters connecting similar or different DC networks, and transmission lines modelled using pi equivalent models are introduced, the converters designed in previous chapters are tested. The simulation results for converters used for power control and interconnection of dissimilar DC networks are provided in this chapter.
- Chapter 10 presents the summary of the thesis with conclusions and the extension of the possible topics for the future work.

# 2

# HVDC and MTDC Networks

*This chapter includes general information about HVDC power transmission systems. After the development of HVDC systems is introduced, advantages of such systems are described. Two types of converters used in HVDC technology, line commutated and voltage source converters, are explained and the applications of HVDC are exemplified. The chapter also presents configurations of HVDC technology, namely monopole and bipolar transmission systems. Moreover, multi-terminal DC grids are discussed.*

## 2.1. History of HVDC Systems

The bulk power transmission in electrical systems is performed thanks to direct current in HVDC transmission networks. The concept of power transmission via DC current emerged even before HVAC networks by an electrical engineer, Marcel Deprez (1843-1918), who worked on DC power transfer over long distances during the second half of the 19$^{th}$ century. His first successful prototype was constructed between Miesbach and Munich in 1882 for the Munich Electrical Exhibition. This system reached 1.5 kW rated power at 2 kV by transmitting power over a distance of 57 km; however, its efficiency was less than 50% [18]. René Thury (1860-1938) developed the work of Deprez and created a commercial HVDC transmission system in 1889 in Genoa, Italy by transmitting 630 kW rated power at 14 kV over 120 km in 1889. For the both Deprez's and Thury's systems, generators and loads were connected in series and operated at the same voltage level.

The limitations for the early HVDC transmission systems were the lack of voltage transform and the loss of power at all loads in case of a power failure. Due to the series connection of generators and loads, the current flow stops at all loads if there is a break in the circuit, which makes the system vulnerable. Therefore, conversion of high transmission DC voltage to lower voltages took importance; however, the transformer developed in 1880s worked in AC systems. Therefore, AC transmission systems were favoured because of cheaper, reliable and more efficient AC transformers till the invention of mercury arc valves by Peter Cooper Hewitt (1861–1921) in the early 20$^{th}$ century [19].

Based on mercury arc valves, the Elbe Project started in 1941 for the city of Berlin with 60 MW power rating at ±200 kV and line of 115 km. As a result of increasing demand of electrical power and development in the technology, HVDC transmission systems increased popularity during 1950s. After the thyristor became a controlled switch for high power applications, first thyristor based HVDC scheme was constructed by General Electric in Canada in 1972 with 350 MW rated power. The HVDC technology continued to develop and voltage source converters emerged in 1990s in Hellsjön–Grängesberg project in Sweden by providing smaller HVDC systems [18]. Today, there is more than 140 GW installed HVDC transmission capacity worldwide and it is expected to build around 300 GW of new HVDC transmission capacity by 2020 to connect especially renewable sources [20].

## 2.2. Advantages of HVDC Technology

Modern HVDC systems do not only transmit electric power from one station to another but also they have significant advantages over conventional AC transmission systems by combining all economical, technical and environmental benefits. Some of the main benefits are:

- More Power:
  - HVDC systems can transmit 40% more power when compared the AC systems with the same insulation level and conductor cross section [21].
  - This percentage is even larger in the systems due to the lack of reactive power, dielectric losses, skin and proximity effects in DC systems.
  - HVDC systems can be used to increase the transfer capability of the existing transmission corridors. For the same tower body and foundation, the power transfer can be increased 300% as shown in Figure 2.1.

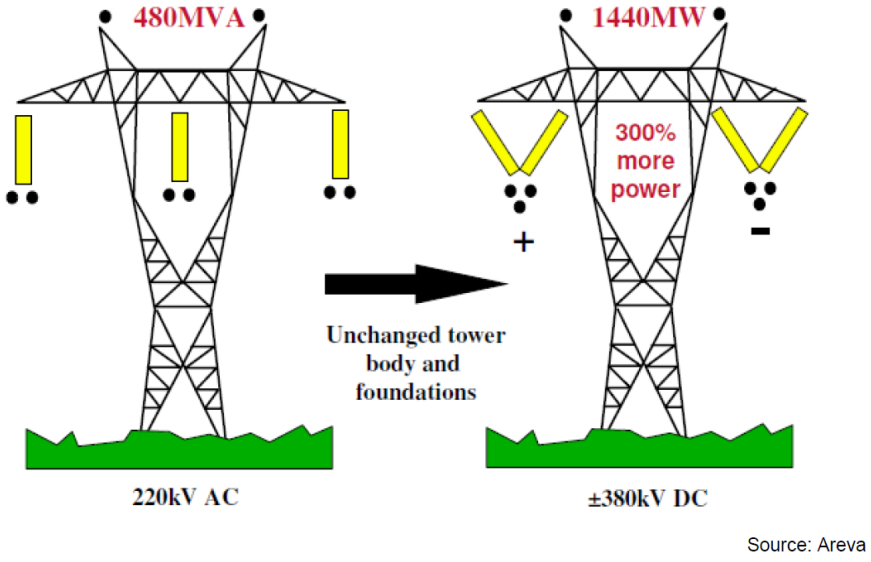


**Figure 2.1:** Increased power transfer using the existing transmission corridors [21]

- Less Loss:
  - When same amount of electric power is transmitted, HVDC systems have 50% less transmission losses than AC transmission systems with the same insulation level and same resistances since the required current in DC is $1/\sqrt{2}$ times AC current.
  - HVDC transmission systems have less corona loss.
  - There is no dielectric losses in DC cables.
  - DC systems provide more efficient transmission of electric power due to less losses.
- HVDC systems require simpler line construction, which saves lands when compared to AC systems. Therefore, the environmental effect is decreased by reduced HVDC overhead corridor or HVDC underground cable instead of large AC transmission corridors.
- For the same transmission capacity, HVDC transmission lines require less investment costs. Although expensive converter stations are necessary for HVDC system terminals, HVDC systems bring economical benefits over a certain distance which is called break-even or critical distance. The break-even distance is approximately 700-800 km for overhead lines while it is much shorter, 40-90 km, for submarine cables. The investment cost comparison of AC and DC systems is shown in Figure 2.2.

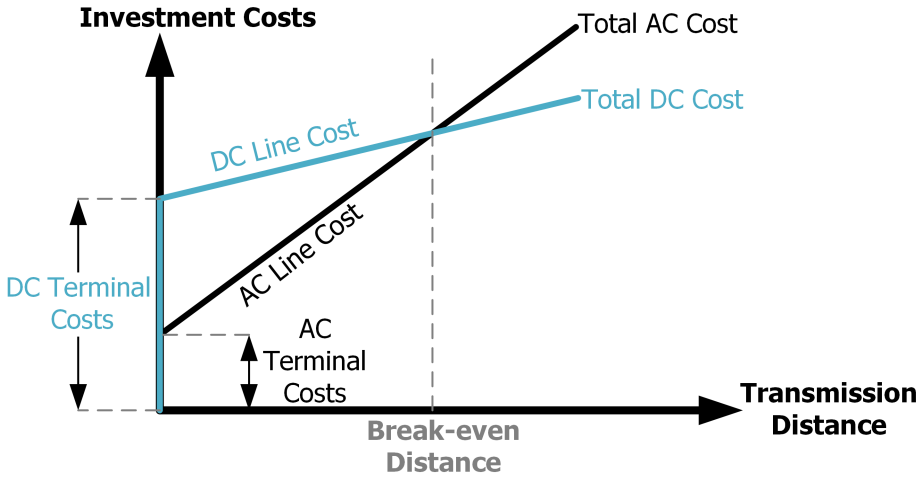


**Figure 2.2:** The comparison of investment costs for AC and DC systems

- HVDC links can connect and stabilize asynchronous AC networks operating at different frequencies. To illustrate, HVDC is used in the connection of systems with nominal frequencies of 50 Hz and 60 Hz in Japan or South America. There are also examples that systems are not synchronous although the operating frequencies are the same [22].
- Power flow can be easily controlled in HVDC systems. Thanks to control facilities of HVDC transmission, it is also possible to enhance the performance of AC systems.
- HVDC systems can be used in offshore applications and they can connect oversea countries using the submarine DC cables as in the case of Iceland and Europe [23] while the active power transfer is limited by the large cable capacitance and charging current in AC cables. As shown in Figure 2.3, the capacitive component of the current increases with the cable length while keeping the total current at thermal limit constant, which causes a decrease in active current component. In DC systems there is no charging current component; therefore, reactive power compensation for the cables used in long distances is not necessary.

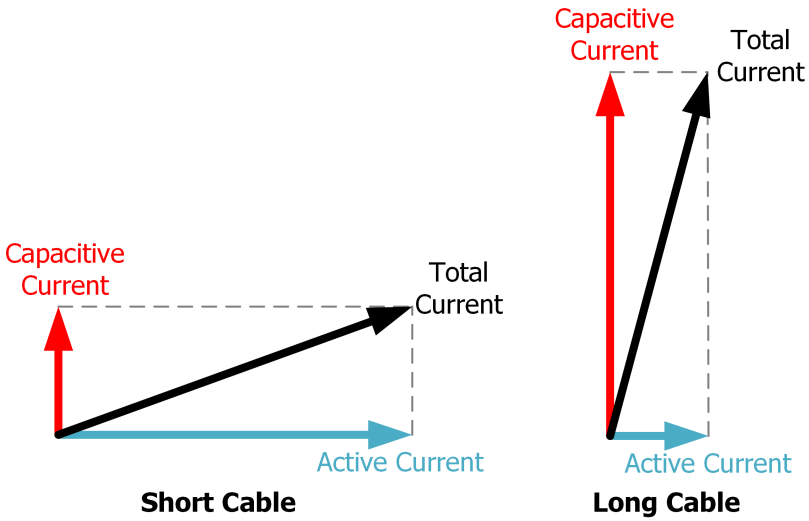


**Figure 2.3:** Increase in charging current in AC cables with the cable length

- HVDC systems have less radio interference and longer useful life.

In the light of all the advantages mentioned above, HVDC technology can be used in onshore wind farms through overhead lines and in offshore wind farms through submarine cables.

## 2.3. Converters for HVDC Technology

The main element in the conversion process between AC and DC in HVDC systems is the converter which operates as either rectifier (AC to DC conversion) or inverter (DC to AC conversion). Electro mechanical conversion was used in the early prototypes of converters such as in Thury systems; however, after the invention of mercury arc valves, electronic converters have been used since 1941.

Electronic HVDC converter technology can be divided into two categories: Line commutated converters (LCC) and voltage source converters (VSC).

### 2.3.1. Line Commutated Converters (LCC)

LCC-based HVDC converters are still in the operation today for the high power transmission over long distances. In LCC systems uncontrolled power electronic devices that can be only turned on are used in converter arms. Due to the lack of control in HVDC converters using diodes, mercury arc valves were used in the early LCC-based HVDC systems. After 1970s, thyristors took place since mercury arc valves needed high maintenance. Due to the considerably less breakdown voltage of thyristors compared to high voltage applications, thyristor valves are utilized where large amount of thyristors, typically tens or hundreds, are connected in series.

Six pulse bridges were used in the basic configuration of LCC including 6 power electronic switches for a three phase system each connecting one AC terminal to the DC terminal as shown in Figure 2.4.

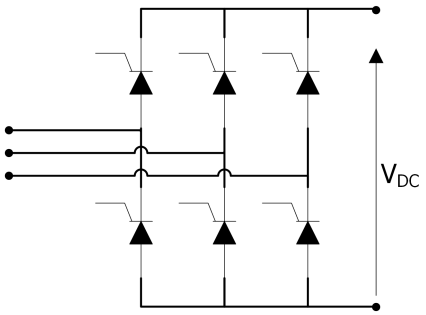


**Figure 2.4:** LCC configuration using six pulse bridge

However, this configuration includes large amount of harmonics at both AC and DC sides. Therefore, twelve pulse bridge configuration has been used where two six pulse bridges are connected in series at DC side. In this configuration, AC side is separated into two parts supplied by the secondary side of a transformer having delta and star connection as shown in Figure 2.5. Thanks to this method, 30° phase difference is created between delta and star connected windings which provides considerably reduced harmonics. Due to the less harmonic distortion of this method, the twelve pulse bridge is seen as the standard solution in LCC-based HVDC converters. To illustrate, in NorNed project which interconnects electrical grids of Feda in Norway (300 kV AC voltage) and Eemshaven in the Netherlands (400 kV AC voltage) with the longest submarine cable of 580 km LCC-based HVDC converters were used. Twelve pulse converter configuration was utilized for the converters located at both ends of the HVDC link operating at ±450 kV [24].

Although LCC-based HVDC converters are still the main solution for high bulk power transmission, typically 100-9000 MW, over long distances with a very low power loss, they have some drawbacks:

- They use thyristors which can only turn-on by control action and it requires an external commutation from the AC system for the turn-off of the device. Thus, there is no black start capability and it requires stronger AC systems [25].
- They require special converter transformers having both delta and star connections on the secondary side in order to adjust AC voltage level to the DC voltage.

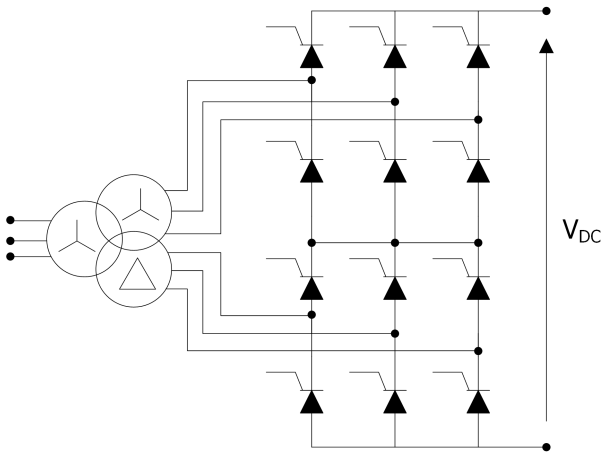


**Figure 2.5:** LCC configuration using twelve pulse bridge

- They require filters both on AC and DC side in order to remove the harmonics generated.
- Reactive power compensation is necessary since converters absorb reactive power 50-60% of the transmitted DC power [26]. Therefore, they require capacitor banks.
- Due to the bulky filters and capacitor tanks, they require large areas and investment cost in order to build the converter station.
- The DC current is only in one direction which complicates the power flow reversal.
- Reversing the power flow direction is achieved by reversing the polarity of terminal voltages.
- Magnitudes of the power and DC current are controlled by terminal voltage difference.

### 2.3.2. Voltage Source Converters (VSC)

Due to the low degree of freedom in the control of thyristor valves, HVDC operation is limited with LCC. Gate turn-off thyristor (GTO) or mainly insulated gate bipolar transistor (IGBT) which can be controlled for both turn-on and turn-off have been used in order to design a self-commutated converter. The first project was realized for achieving 3 MW power transmission between Hellsjön and Grängesberg, Sweden through a 10 km of HVDC link operating with 10 kV in 1997 [27]. This experimental project performed by ABB proved the existence of VSC and its advantages and since then VSC-based HVDC converters have been built with higher powers, lengths and voltage levels.

A basic back-to-back VSC-based HVDC system is shown in Figure 2.6. VSC-based HVDC scheme includes two converters operating as rectifier and inverter. In these converters, large number of transistors are connected in series in order to provide high blocking voltage. IGBT modules includes anti-parallel diodes in order to maintain four quadrant operation. Moreover, control and cooling equipments are inside of the power electronic modules which provides easy transportation and assembly. On the AC side ordinary transformers are used in order to adjust voltage level suitable for the conversion. The capacitor on the DC side can supply the energy storage for power flow control and it can also provide DC harmonics filtering [28].

The advantages of VSC-based HVDC schemes compared to LCC systems are:

- They have black start capability thanks to fully controlled power electronic devices and they can operate independently of the AC grid.
- They are based on pulse width modulation (PWM) which brings several advantages in terms of power control:

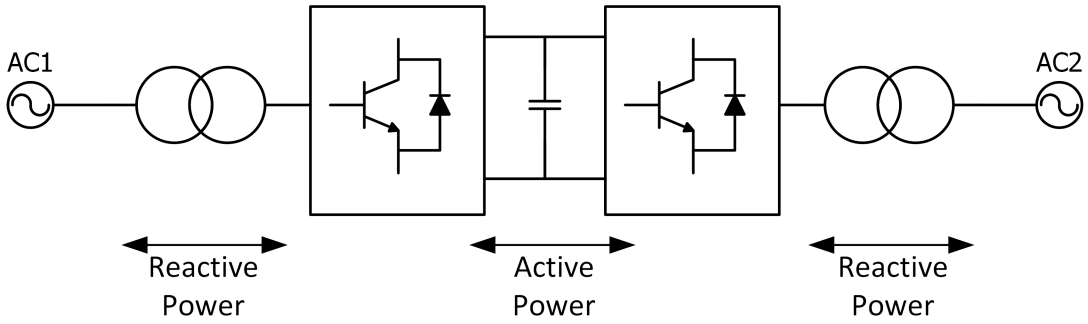


**Figure 2.6:** HVDC system based on VSC

  - Both active and reactive power can be controlled independently by decoupling direct and quadrature components of the current. Therefore, reactive power is independent of the DC power transmitted in contrast to LCC.
  - VSC keeps the DC voltage polarity constant. Thus, direction of the power flow is controlled by the direction of current which provides fast reversal of power flow.
- They can generate or consume reactive power depending on the demand which eliminates the reactive power compensation and bulky capacitor banks from the converter station.
- They require little or no filtering.
- Thanks to the removal of huge capacitor banks and filters from the converter stations, they have more compact dimensions which provides less footprint, visual impact, investment costs and station losses.
- Their compact dimensions make them suitable for offshore grids and interconnection of wind farms with lighter offshore platforms.
- With reduced application engineering, it can be possible to connect networks without complex studies and system support.
- Due to higher degree of power control and easy power reversal, they are ideal for multi-terminal HVDC applications.
- VSC stations can use simpler and more conventional ordinary transformers instead of specialised transformers designed for LCC systems.

Besides many advantages of VSC-based HVDC schemes, high switching losses of the converter due to high switching frequency resulting from PWM method is the main drawback of these systems.

The converters used in VSC-based HVDC systems can be in different topologies: Two level or Multilevel converters.

### Two Level Converter

Two level converter topology was used in early VSC-based HVDC systems. In this topology, IGBT valves and anti-parallel diodes are used as power electronic devices in six pulse bridge as shown in Figure 2.7. The AC voltage switches between two discrete voltage levels depending on the switching of IGBT valves ($+V_{DC}/2$ or $-V_{DC}/2$).

In addition to switching losses resulting from high switching frequency of PWM, two level converters required advanced circuits for driving the gates since IGBT valves require high number of series connected IGBTs in order to achieve high DC voltages.

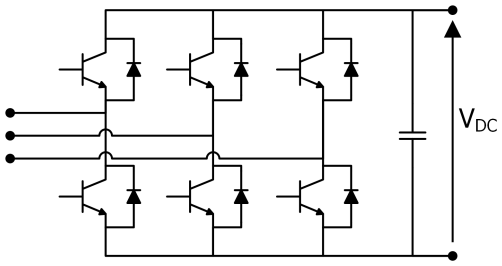


**Figure 2.7:** Three phase two level VSC

VSC-based HVDC projects using two level converters include Estlink Transmission System. After a competition between LCC and VSC technologies, VSC was determined as a more appropriate solution considering maintenance and investment costs, losses, overload capacity and installation time. Estlink Transmission System has been in operation since 2007 connecting Estonia and Finland operating at 330 kV and 400 kV AC voltage, respectively, with 105 km long HVDC link at ±150 kV and 350 MW rated power [29].

### Multilevel Converter

In order to improve the harmonic performance of two level VSC for high power applications operating at medium or high voltage, multilevel converter topologies have been developed. These converter topologies can supply more than two discrete voltage levels on the AC side. They can be either three level converters supplying $-V_{DC}/2$, 0 and $+V_{DC}/2$ or in cascaded topologies as in modular multilevel converters (MMC) supplying many voltage levels.

Three level converters can be divided into two categories: Diode-clamped (neutral-point-clamped) and flying capacitor topologies where four IGBT valves are attached in each phase as shown in Figure 2.8a and 2.8b, respectively. The voltage level of $+V_{DC}/2$ is obtained by turning on two top IGBT valves, 0 output voltage is obtained by turning on two middle IGBT valves and $-V_{DC}/2$ is obtained by turning on bottom two IGBT valves.

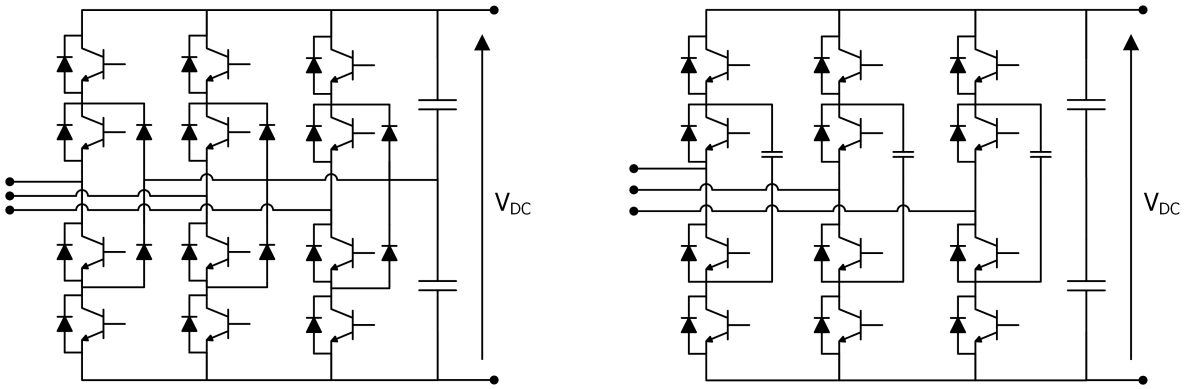


**(a)** Diode-clamped (neutral-point-clamped) topology

**(b)** Flying capacitor topology

**Figure 2.8:** Three level converter topologies

Three level neutral-point-clamped converter topology was used in 220 MW Murraylink Transmission Interconnection Project in Australia connecting Berri (132 kV AC voltage) and Red Cliffs (220 kV AC voltage) stations with 177 km long underground cable operating at ±150 kV [30].

Another multilevel VSC topology is modular multilevel converters (MMC) using cascaded connections of submodules as first introduced by Lesnicar and Marquardt in 2003 [31]. Detailed operation principle

of MMC is explained in following sections. Tres Amigas SuperStation Project is an example of implementation of MMC topology for VSC based HVDC systems. It is supposed to transmit 5000 MW of power between two main U.S. power grids, the Eastern Interconnection and the Western Interconnection [32].

Multilevel converters bring further advantages to VSC. Some of these advantages are listed as:

- They are highly scalable in terms of number of levels.
- The generation of harmonics is very low.
- They allow converters to operate with low switching frequencies in high voltage applications.
- Thanks to low switching frequencies, high frequency noise and switching losses are decreased.

## 2.4. HVDC Applications

HVDC systems can be used in different applications such as interconnection of asynchronous networks using back-to-back connection, long distance bulk power transmission or long submarine transmission.

### 2.4.1. HVDC Back-to-Back

Back-to-back connected HVDC systems include two converters as shown in Figure 2.9. Both rectifier and inverter are located in the same converter station without any HVDC transmission link between them. Since there is no HVDC cable or overhead line which restricts the selection of high voltage level for the optimum values, implementation of such system is relatively easier. Back-to-back connection is use for the interconnection of asynchronous systems operating at different frequencies.

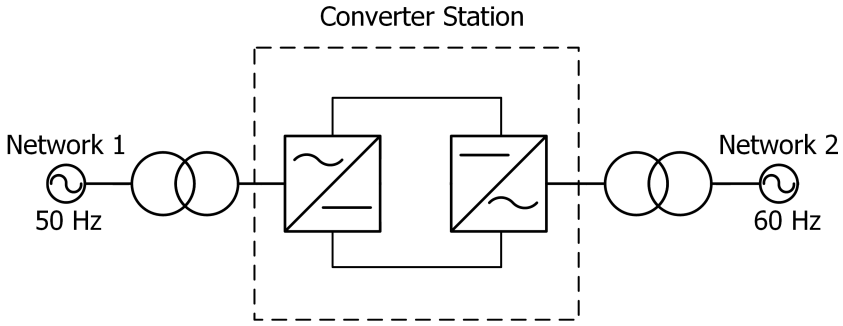


**Figure 2.9:** HVDC back-to-back

### 2.4.2. Long Distance Overhead Line Transmission

The most economical way of bulk power transfer over long distances is seen as the HVDC overhead line transmission in addition to its lower power loss. As stated in Section 2.2, point-to-point connected DC overhead lines offer more economical solution if the distance is greater than 700 km.

### 2.4.3. Long Submarine Transmission

As stated in Figure 2.2, transmission of power via HVDC submarine cables for the distances longer than 40-90 km provides more economical solution. This also allows interconnection of offshore wind farms with the main grid. The connection of large offshore wind farms with the main grid requires a transmission system with high reliability and minimum maintenance while it can retain its performance in harsh offshore environmental conditions. Moreover, the transmission system must comply the connection regulations and grid codes. As a result, HVDC transmission system is seen as the best solution in order to meet these requirements.

## 2.5. Configurations for HVDC Systems

HVDC systems offer the connection of two separate AC networks by means of a DC transmission link. In order to provide this connection, HVDC systems can be in different configurations depending on the functionality. The most common configurations are explained as below:

### 2.5.1. Monopole HVDC Transmission

Monopole HVDC transmission system is divided into two categories: Symmetric and asymmetric monopole systems.

#### Symmetric Monopole System

The symmetrical monopole system includes two fully insulated HVDC conductors each of which are exposed to ± half of the rated DC voltage in order to transmit DC current. Since converters are grounded via high impedances, there is no DC ground current. The schematic of a symmetric monopole system is shown in Figure 2.10.

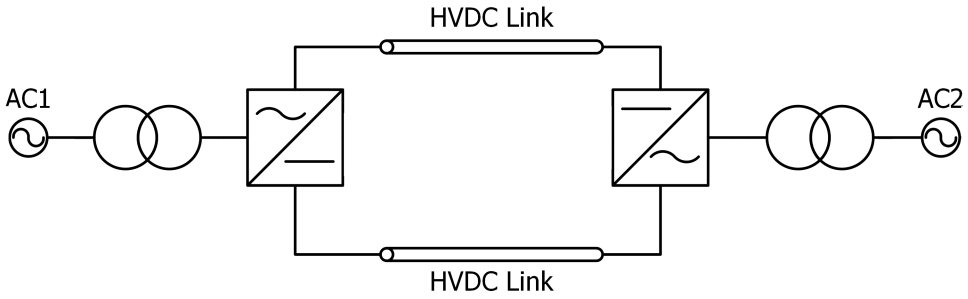


**Figure 2.10:** Symmetric monopole system

#### Asymmetric Monopole System

The asymmetric monopole systems include single HVDC conductor subject to a single DC voltage. In this configuration, one terminal of each converters located at each side of HVDC link is connected to ground. This type of monopole HVDC systems can be later expanded to a bipolar system [33]. According to grounding schemes, there are two types of asymmetric monopole HVDC system:

**Asymmetric Monopole with Ground Electrode**
For the long distance power transmission, a grounding system using ground electrodes is seen as the most convenient solution. Using single HVDC conductor decreases transmission losses and investment costs. The schematic of asymmetric monopole system with ground electrode is shown in Figure 2.11.

**Asymmetric Monopole with Metallic Return**
When environmental effects or the infrastructure does not allow to use of ground electrodes or the transmission distance is short, grounding with a metallic return can be used although it increases costs and losses due to the impedance of metallic return path. An asymmetric monopole system with metallic return is illustrated in Figure 2.12.

### 2.5.2. Bipolar HVDC Transmission

Bipolar HVDC transmission systems include four converters and two HVDC lines each rated for the full

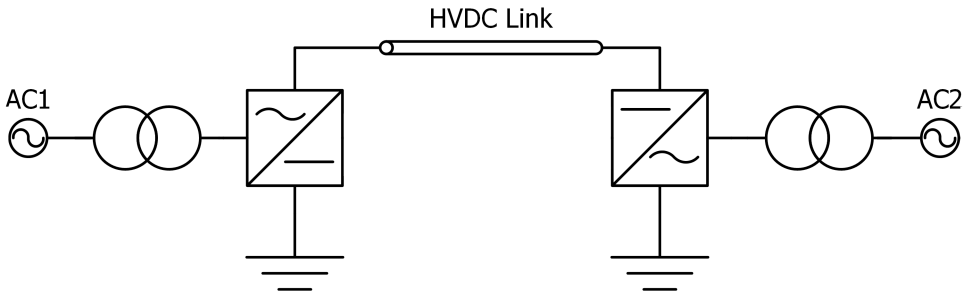


**Figure 2.11:** Asymmetric monopole system with ground electrode

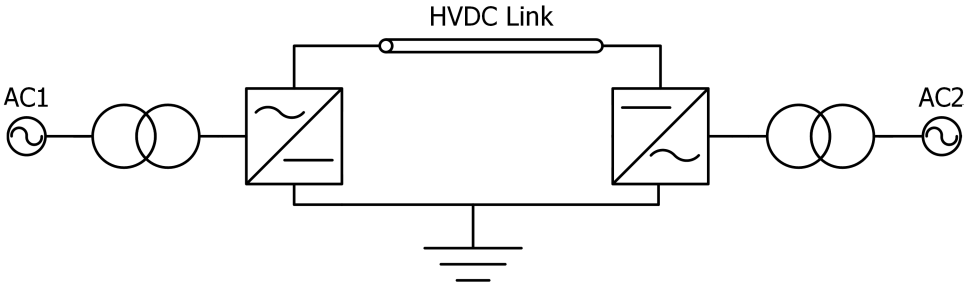


**Figure 2.12:** Asymmetric monopole system with metallic return

voltage with opposite polarities. Although additional equipments increases losses and costs, bipolar HVDC transmission systems are more suitable if the required power transmission exceeds monopole capacity or if more reliable solution is required. If one of the DC links is lost in bipolar configuration during a maintenance, for example, the half of the power can still be transmitted via the other DC link [34]. Bipolar systems can be implemented using ground electrodes or metallic return as in asymmetric monopole systems as shown in Figure 2.13a and 2.13b.

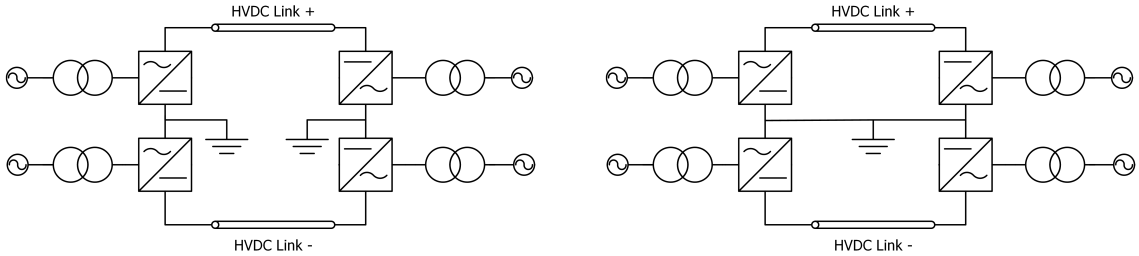


**(a)** Bipole system using ground electrodes **(b)** Bipole system using metallic return

**Figure 2.13:** Bipolar HVDC transmission schemes

## 2.6. MTDC Grids

Nowadays, most of the DC systems have point-to-point connection with the main grid. Due to the increased proportion of renewable energy sources in many countries and the stochastic behaviour of renewable energy sources such as photovoltaic systems or wind farms, the power balance may not always be provided between supply and demand [35]. VSC-based multi-terminal HVDC transmission system is seen as the key solution for the unstable behaviour of renewable energy resources by connecting more than two power sources within the same DC grid since it can provide a flexible power transmission with more efficiency. European MTDC grid in long-term plans is shown in Figure 2.14 [36].

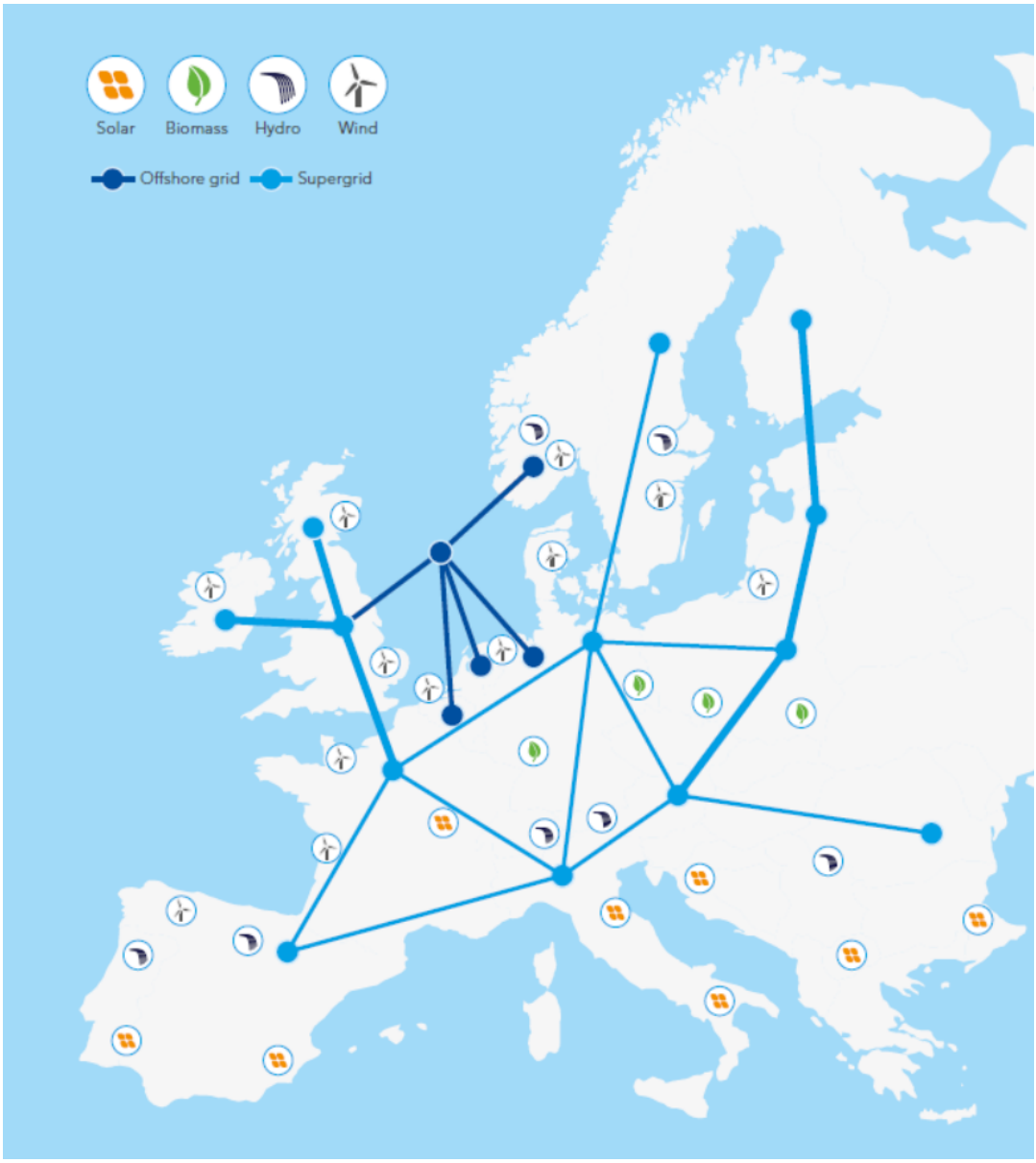


**Figure 2.14:** European MTDC grid in long-term plans [36]

There are two possible architectures for MTDC systems: Series and parallel configurations.

### 2.6.1. Series Configuration

In series configuration, converters are connected along a line so that they create a loop as a four-terminal system is shown in Figure 2.15. The system is grounded at a point that can be shifted depending on operating conditions [9]. The same DC current, $I_{DC}$, flows around the network and the rated voltages of converters are adjusted by their individual power ratings. Series connected MTDC systems have some disadvantages:

- A DC fault at one terminal of the system creates a total outage in MTDC grid.
- Insulation coordination is a difficult task due to different insulation levels of each converter.

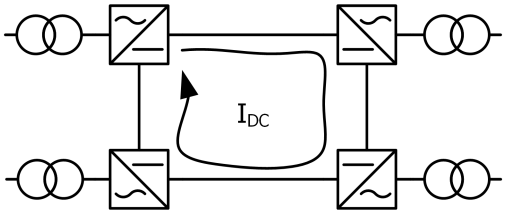


**Figure 2.15:** Series configuration of four-terminal MTDC system

### 2.6.2. Parallel Configuration

Converters are connected in parallel in this configuration and they have the same voltage level set by one of the converters. Individual power ratings of each converter adjust their rated currents. Parallel connection can be in radial or meshed types as shown in Figure 2.16.

Parallel configuration of MTDC systems are accepted more due to their advantages listed below [10]:

- The control of parallel type of MTDC systems is easier.
- Parallel type of MTDC systems have lower losses.
- They can provide more flexible solution which makes them suitable for future expansion of grids.
- Even though one terminal of the system fails, others can continue their operations.

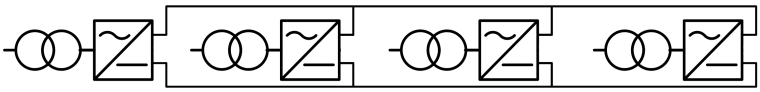

**(a)** Radial MTDC network

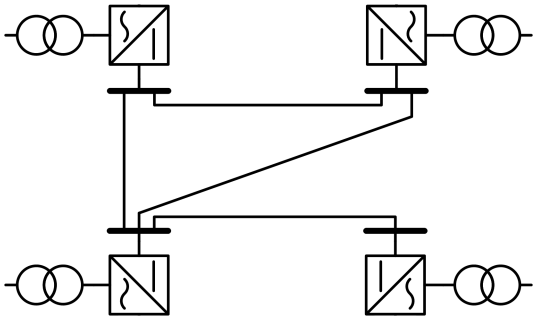

**(b)** Mesh MTDC Network

**Figure 2.16:** Parallel configurations of MTDC system

First VSC-based MTDC system was constructed in 2013 in Shantou, China in order to connect renewable energy sources with the main power grid [11]. The projects interconnects the Nanao Island, where two wind farms (WF) are located with Guangdong grid, using 32 km long HVDC link including submarine cables, land cables and overhead lines at ±160 kV. MTDC system has three terminals with 200 MW, 100 MW and 50 MW power ratings. The schematic of the project is shown in Figure 2.17.

In 2014, another MTDC project including five terminals was constructed in Zhoushan, China in order to interconnect five islands with the main power grid. Converter stations located in the islands with 1000 MW total power rating (400 MW, 300 MW and three 100 MW) are connected by submarine cables with 129 km of total length operating at ±200 kV [37].

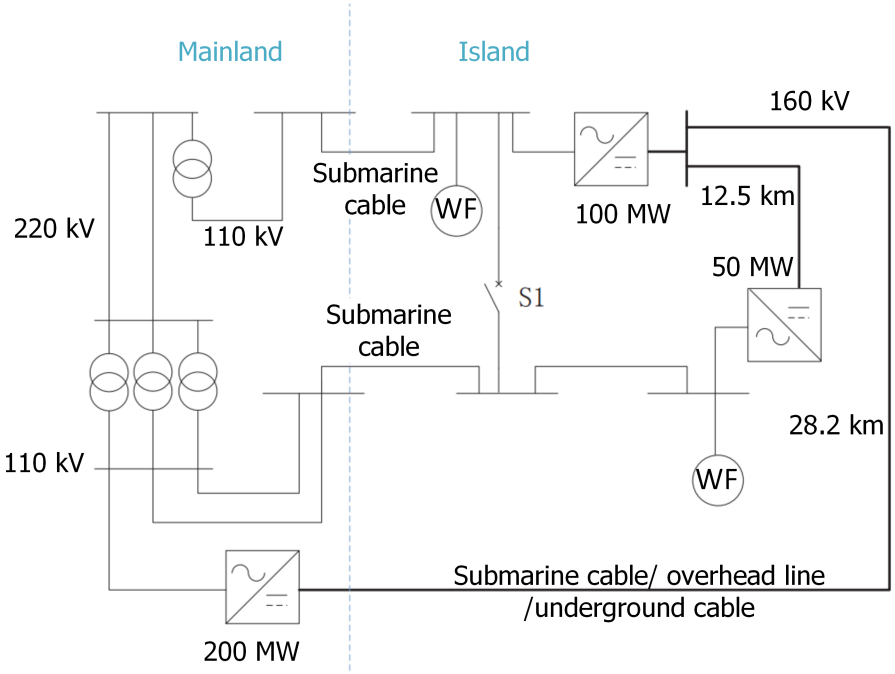


**Figure 2.17:** The schematic of Nanao Island MTDC project [12]

# 3

# High Voltage DC/DC Converters

*This chapter discusses the need for DC/DC converters in high voltage high power transmission systems. It also presents the classification of high voltage DC/DC converters. Finally, the main topologies are explained briefly.*

## 3.1. Introduction

Future expectation is the development of a fully integrated meshed multi-terminal HVDC grid in order to achieve integration of renewable energy sources and bulk electric power transmission. In addition to interconnection of existing point-to-point HVDC links, recently constructed renewable energy sources will be connected to the main grid in this MTDC system. However, existing HVDC power transmission schemes were constructed depending on the technology of the time, which means that there is no standardization in voltage levels and configurations. Therefore, the construction of new HVDC transmission interconnections requires the use of DC/DC converters at high voltage and high power levels because of justifications listed below:

- In order to achieve desired power flow control between HVDC networks, DC/DC converters can be used.
- Interconnection of HVDC terminals operating in similar configurations but at different voltage levels requires DC/DC converters.
- In order to connect HVDC networks with different configurations, DC/DC conversion stage is necessary although their voltage levels are the same.
- DC fault isolation can be achieved by DC/DC converters so that a fault on one DC system does not affect the others.

## 3.2. Classification of High Voltage DC/DC Converters

DC/DC converter to be used in high power high voltage applications can be constructed by converting DC system into an AC system first and converting back AC to DC. The middle AC stage can be one or three phase but three phase is preferred due to its higher power density and less current stress on power electronic devices.

High power high voltage DC/DC converters can be classified into two groups according to their function in HVDC systems depending on DC voltage step ratio and DC system configurations [38]:

- DC/DC converters without galvanic isolation as shown in Figure 3.1a.

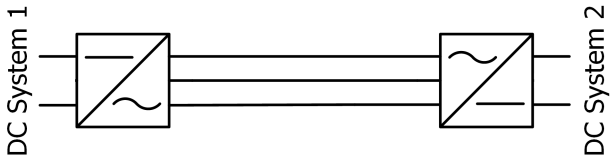


**(a)** Without galvanic isoation

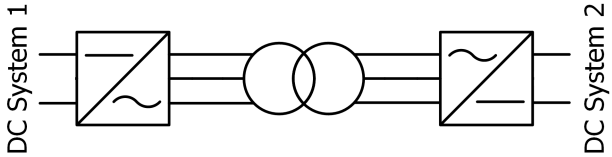


**(b)** with galvanic isolation

**Figure 3.1:** DC/DC converter topologies

- DC/DC converters with galvanic isolation as shown in Figure 3.1b.

DC voltage ratio nomenclature between two DC systems is defined according to Table 3.1 [38].

**Table 3.1:** DC voltage step ratio nomenclature

| | |
|---|---|
| **Low Ratio** | $\frac{V_{DC_{high\ voltage\ side}}}{V_{DC_{low\ voltage\ side}}} \leq 1.5$ |
| **Medium Ratio** | $1.5 < \frac{V_{DC_{high\ voltage\ side}}}{V_{DC_{low\ voltage\ side}}} \leq 5$ |
| **High Ratio** | $5 < \frac{V_{DC_{high\ voltage\ side}}}{V_{DC_{low\ voltage\ side}}}$ |

### 3.2.1. DC/DC Converters without Galvanic Isolation

DC/DC converters without galvanic separation can be used for the interconnection of HVDC terminals with similar configurations (either monopole or bipolar) and similar voltage levels, i.e. having low voltage step ratio [38–41]. The main purpose of these converters is the control of power flow in DC supergrid. They are preferred due to their cost effective solution for DC/DC conversion eliminating the investment cost for transformer coupling. However, a DC fault in one terminal may propagate to the other DC system due to the direct current path between converter stations [38]. Each front-to-front connected DC/AC converters can be determined among VSC topologies; therefore, the types of DC/DC converters without galvanic isolation are:

- Front-to-front connection of two level converters
- Front-to-front connection of modular multilevel converters

#### Front-to-Front Connection of Two Level Converters

In this topology, the converter consists of two front-to-front connected DC/AC voltage source converters without having a transformer coupling between the converters using the AC system as a middle stage (First DC to AC conversion, and the AC to DC conversion). Each DC/AC converter is a two level converter including six IGBT valves as shown in Figure 3.2. The control structure and the simulation of front-to-front connected two level converters are presented in [39]. The main drawback of this system is the requirement of high switching frequency for the converters resulting in increase in losses.

#### Front-to-Front Connection of Modular Multilevel Converters

The front-to-front connection of MMC without a galvanic separation can be used to interconnect two

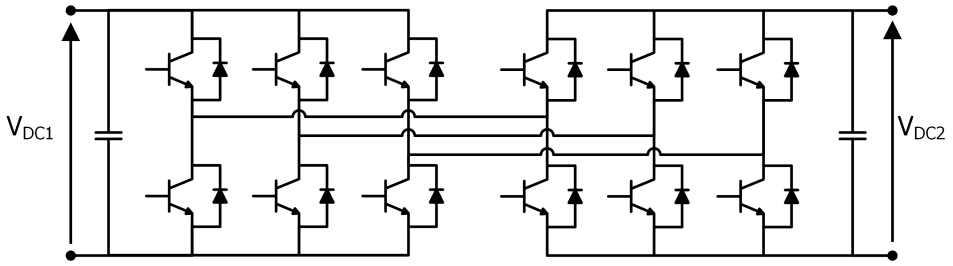


**Figure 3.2:** Front-to-front connection of two level converters

DC systems operating in similar voltage levels and configurations [38]. A MMC consists of 6 arms each operating as a controllable voltage source thanks to a number of submodules in each arm. The submodules can be in either full bridge or half bridge configurations. The circuit diagram of front-to-front connection of MMC is shown in Figure 3.3. Operation principles, modelling and control of MMC is presented in details in the related chapters.

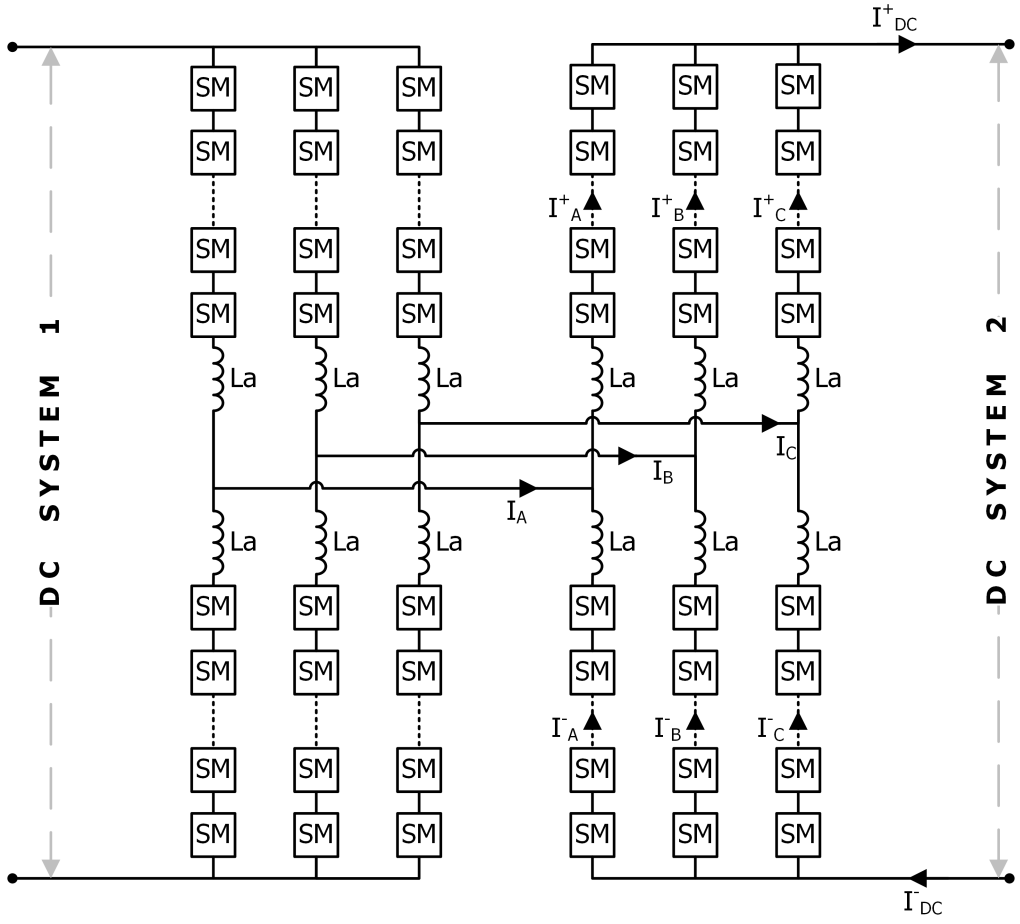


**Figure 3.3:** Front-to-front connection of modular multilevel converters

In this configuration, each submodule has its own capacitor; therefore, there is no DC link capacitors connected to DC terminals in contrast to two level converters. Although MMC requires sophisticated control systems, it is a promising candidate for future multi-terminal HVDC grids due to its several advantages listed below:

- The voltage level can be easily changed by adjusting the number of submodules connected in series.

- Thanks to the high modularity of the MMC, it can generate a stepwise AC voltage waveform with small voltage steps. This allows submodule IGBTs to switch at lower frequencies, which decreases the switching losses in a considerable amount.
- Due to low switching losses the power efficiency of the MMC becomes higher, thus the operation costs and the cost for the cooling equipment are decreased.
- Increasing the number of submodules in each arm allows the voltage waveform to have lower step size, which results in a more sinusoidal waveform.
- Since its AC voltage is less distorted and thus includes low harmonic contents, the need for an AC filter is eliminated. This also decreases the area covered by the converter station in the field.
- The modularity of the selection of submodule configuration is another benefit of the MMC. By using both half bridge and full bridge cells as in [42], benefits of both configurations can be combined. Therefore, low loss of half bridge submodules and short circuit proof feature of the full bridge submodules can be utilized in a single converter.
- Since the AC side is a middle stage for DC conversion, the frequency does not need to match with the grid. In other words, medium or high frequency voltage can be generated on the AC side which decreases the size of passive components such as submodule capacitors or arm inductors.

### 3.2.2. DC/DC Converters with Galvanic Isolation

The existing HVDC schemes have not been standardized; i.e. they operate in different configurations and different voltage levels depending on the technology of the time they were constructed. Converters with galvanic isolation can be used for the interconnection of existing DC systems with medium or high DC voltage ratios and various configurations or for the interconnection with an offshore wind farm [38, 43–46]. For utilizing the bulk power transmission, VSC and the conventional LCC can also be connected by DC/DC converters with galvanic separation [38]. Galvanic separation isolates two systems and provides DC fault blocking capability by preventing a direct current path between DC networks. Typically a transformer is used in order to electrically separate two systems. The AC stage frequency can be selected different than the grid side; therefore, the volume of the transformer can be decreased by choosing a higher frequency. The types of DC/DC converters with galvanic isolation are:

- Transformer coupled two level converters
- Transformer coupled modular multilevel converters

#### Transformer Coupled Two Level Converters

In this type of DC/DC converters, high voltage step ratio and the galvanic separation can be achieved by including a transformer in the AC side between two front-to-front connected two level converters as shown in Figure 3.4. Two level modulation and control strategy of DC/DC converter with transformer coupling is presented in [45]. The simulation of transformer coupled two level converters can be found in [47].

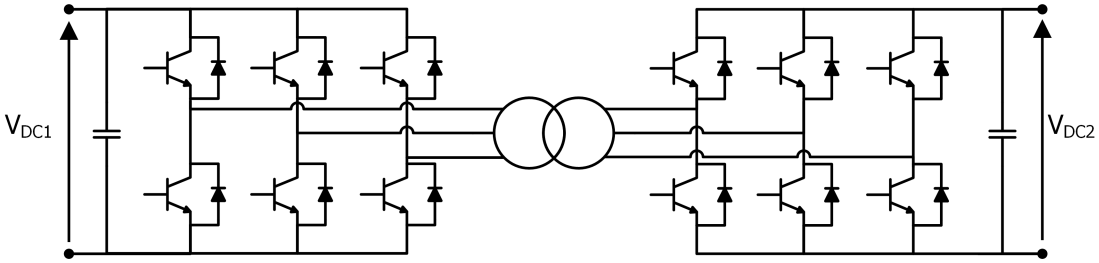


**Figure 3.4:** Transformer coupled two level converter

### Transformer Coupled Modular Multilevel Converters

The MMC can also be used in order to connect HVDC networks with different configurations and high voltage ratios by including a transformer coupling between front-to-front connected two MMC [43]. The circuit diagram of transformer coupled MMC is shown in Figure 3.5.

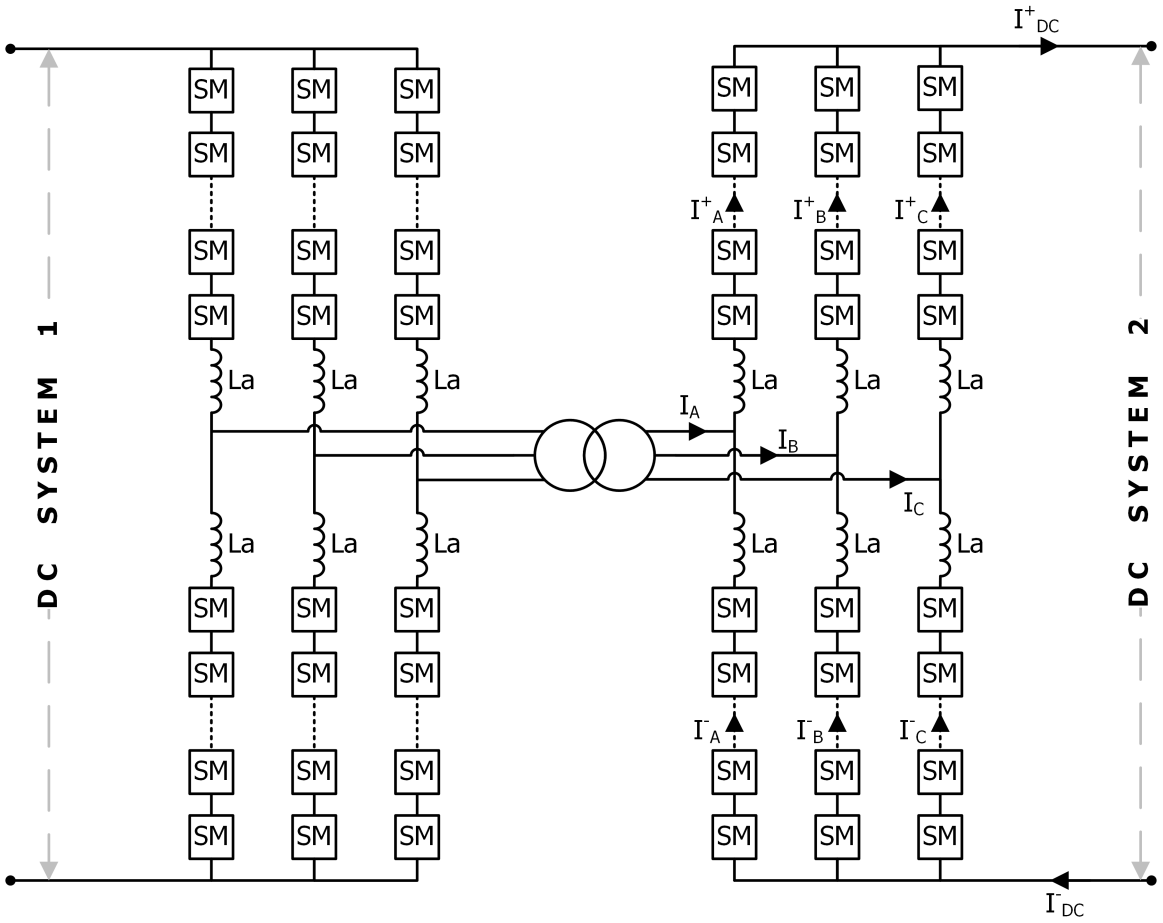


**Figure 3.5:** Transformer coupled modular multilevel converter

# 4

# Modular Multilevel Converter

*The operation principle of a Modular Multilevel Converter (MMC) is focused in this part of the report. A mathematical model is created based on MMC equations and submodule capacitor sizing is explained. Finally, simulation results are shown and compared with a switching model.*

A MMC includes six arms in total, two arms in each phase (a leg) which are called positive and negative. Each arm connects DC terminal to one AC terminal behaving as a controllable voltage source thanks to a number of submodules (SM) in series with an inductor, La, which limits the arm current. Each submodule includes its own storage capacitor instead of a DC link capacitor and by increasing the number of submodules, the MMC can generate a sine wave close to a pure sinusoid as much as possible.

The submodule can be in either half bridge or full bridge configuration as shown in Figure 4.1. The half bridge configuration of the MMC, in Figure 4.1a, contains half of the switching devices of the full bridge configuration which results in less switching losses while full bridge version, in Figure 4.1b, can handle DC faults by blocking the IGBTs by reversing the cell capacitor voltage, which forces to fault current be zero [48].

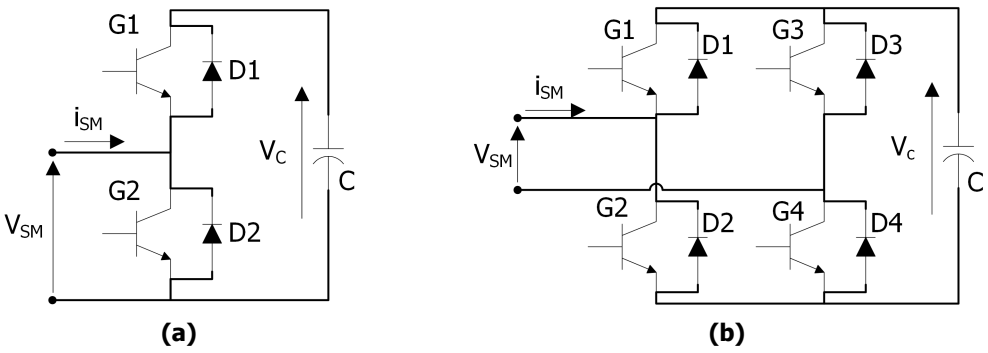


**Figure 4.1:** MMC submodules (a) Half bridge (b) Full bridge

## 4.1. Submodule Operating States

Mainly two operating states of the submodules are used in the normal operation of a MMC, namely active and bypass states. Half bridge configuration is used in this report in order to analyse submodule operation.

**1. Active State:** In the active state of the submodule, upper switching device (IGBT), G1, is ON, while the lower one, G2 is OFF. The output voltage of the submodule, $V_{SM}$, is equal to cell capacitor

voltage, $V_C$, independent of the direction of current. The direction of the submodule current, $i_{SM}$, affects electrical routes.

- If the current, $i_{SM}$, is positive, i.e. if the current enters the submodule, the current flows through the diode, D1, and it charges the capacitor as seen in Figure 4.2a.
- If the current, $i_{SM}$, is negative, i.e. leaving the submodule, the current flows through IGBT, G1, and the capacitor is discharged as shown in Figure 4.2b.

**2. Bypass State:** In the bypass state of the submodule, upper IGBT, G1, is OFF, whereas the lower IGBT, G2, is ON. The output voltage of the submodule in this state is zero independent of the direction of the current, $i_{SM}$, and the capacitor voltage remains constant. The direction of the current has an influence on only the electrical route.

- If the current, $i_{SM}$, is positive, entering the submodule, it flows through IGBT, G2, as seen in Figure 4.2c.
- If the current, $i_{SM}$, is negative, leaving the submodule, it flows through the diode, D2, as seen in Figure 4.2d.

The state in which both IGBTs, G1 and G2, are OFF is not a suitable operation point of the submodule because the capacitor is never discharged but it is charged through the diode, D1 if the current is positive and voltage across submodule terminals is greater than capacitor voltage [49].

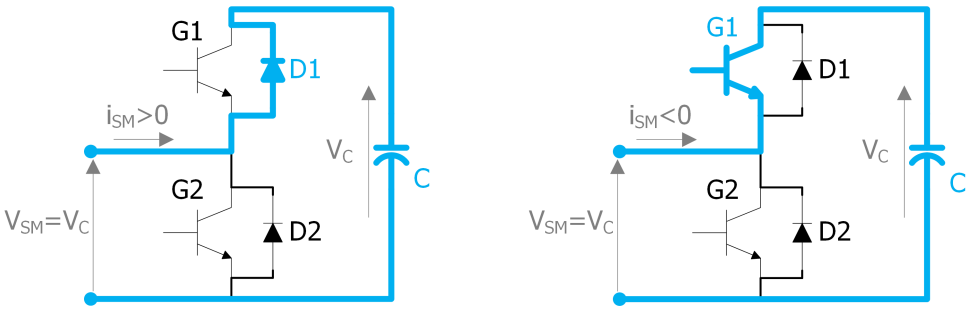


**(a)** Active state, positive current

**(b)** Active state, negative current

**(c)** Bypass state, positive current

**(d)** Bypass state, negative current

**Figure 4.2:** Operation states of a half bridge submodule

The submodule terminal voltages and capacitor status depending on current direction and switching states can be seen in Table 4.1 where S1 and S2 are gate signals of upper and lower switching devices in a submodule, respectively.

In order to give an understanding of the MMC operation, firstly a one phase MMC model is analysed. DC side consists of two constant voltage sources ($V_{PO}$=$V_{ON}$=$V_{DC}$/2) whereas the AC side includes an alternating voltage source ($V_g$), representing the grid, a resistor ($R_{out}$) and an inductor ($L_{out}$) as seen

**Table 4.1:** Switching states of a half bridge submodule

| Switching State | | Current Direction | $V_{SM}$ | Capacitor Status |
|---|---|---|---|---|
| S1 (Upper IGBT) | S2 (Lower IGBT) | | | |
| 1 | 0 | (+) | $V_C$ | Charging |
| 1 | 0 | (-) | $V_C$ | Discharging |
| 0 | 1 | (+) | 0 | Bypassed |
| 0 | 1 | (-) | 0 | Bypassed |
| 1 | 1 | | | Capacitor shorted |
| 0 | 0 | | | Only charging |

in Figure 4.3.

In order to obtain n steps in the output AC voltage when there are n submodules in a leg of MMC, i.e. n/2 submodules in upper and lower arms, switching signals have different meaning for upper and lower arms. For the upper arm submodules, S=1 means that the submodule is in bypass state; i.e. lower switching device conducts and the voltage across submodule terminals, $V_{SM}$, is zero while S=0 means that the submodule is in active state; i.e. upper switching device conducts and the voltage across submodule terminals, $V_{SM}$, is $V_C$, capacitor voltage. For the lower arm cells, S=1 means that the submodule is in active state; i.e. upper IGBT conducts and the voltage across submodule terminals, $V_{SM}$, is $V_C$, capacitor voltage while S=0 means that the cell is in bypass state; i.e. lower IGBT conducts and the voltage across submodule terminals, $V_{SM}$, is zero.

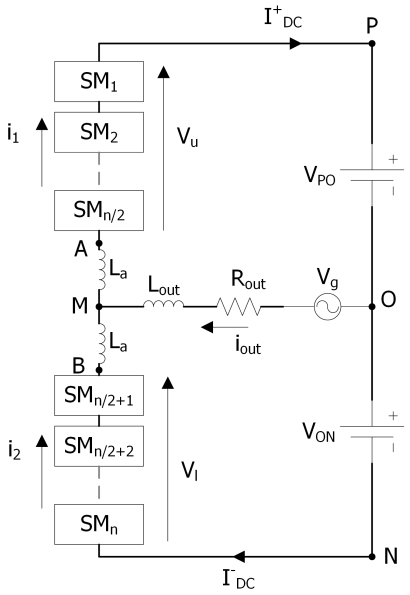


**Figure 4.3:** Circuit diagram of a single phase MMC

## 4.2. Modelling of MMC

In order to understand the concept of MMC, modelling is based on solving mathematical equations.

Firstly, upper and lower submodule voltages which depend on the states as described in Section 4.1 are calculated in (4.1) and (4.2), respectively.

$$\text{Upper arm: } V_{SMi} = V_{Ci}\,(1 - S_i) \tag{4.1}$$

$$\text{Lower arm: } V_{SMi} = V_{Ci}S_i \tag{4.2}$$

Therefore, voltage between different points are calculated where $n$ is the total number of submodules in a leg of MMC in Figure 4.3.

$$V_{AO} = V_{PO} - \sum_{i=1}^{n/2} V_{Ci}\,(1 - S_i) \tag{4.3}$$

$$V_{BO} = -V_{ON} - \sum_{i=n/2+1}^{n} V_{Ci}S_i \tag{4.4}$$

$$V_{AB} = V_{AO} - V_{BO} \tag{4.5}$$

Based on Kirchhoff's current law, the current equation can be written as in (4.6). In addition, the circulating or differential current is defined as the mean value of upper and lower arm currents, and is denoted by $i_c$, expressed in (4.7) [49].

$$i_1 = i_2 + i_{out} \tag{4.6}$$

$$i_c = \frac{i_1 + i_2}{2} \tag{4.7}$$

Equations (4.6) and (4.7) give explicit expressions for upper and lower arm currents as given in (4.8) and (4.9), respectively.

$$i_1 = \frac{i_{out}}{2} + i_c \tag{4.8}$$

$$i_2 = -\frac{i_{out}}{2} + i_c \tag{4.9}$$

As described in [50], the Thevenin equivalent circuit is shown in Figure 4.4 where $V_{th}$ is the voltage that drives output current and equal to output voltage when $i_{out}$ is zero; i.e. when no load is connected. $L_{th}$ is the thevenin inductance which is parallel connected inductances of upper and lower arm, $L_a//L_a = L_a/2$.

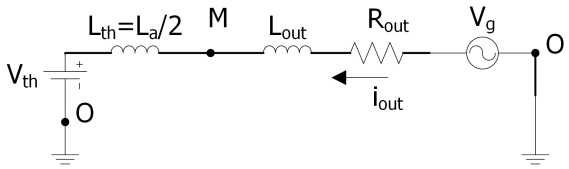


**Figure 4.4:** Thevenin equivalent of the circuit

In the condition that $i_{out}$ is zero and assuming upper and lower arm inductances are the same, the voltage drop in both inductors is equal. Therefore, thevenin voltage is obtained as in (4.11).

$$V_{MA} = V_{BM} = \frac{V_{BA}}{2} = -\frac{V_{AB}}{2} \tag{4.10}$$

$$V_{th} = V_{MO}|_{i_{out}=0} = V_{MA} + V_{AO} = -\frac{V_{AB}}{2} + V_{AO} \tag{4.11}$$

Using Kirchhoff's voltage law on the thevenin circuit of Figure 4.4, differential equation for $i_{out}$ can be obtained in (4.14).

$$V_{MO} = V_{th} + L_{th}\frac{di_{out}}{dt} \tag{4.12}$$

$$V_g - R_{out} i_{out} - L_{out} \frac{di_{out}}{dt} - L_{th} \frac{di_{out}}{dt} - V_{th} = 0 \tag{4.13}$$

$$\frac{di_{out}}{dt} = \left( \frac{1}{L_{th} + L_{out}} \right) \left( V_g - R_{out} i_{out} - V_{th} \right) \tag{4.14}$$

For the calculation of upper and lower arm currents, voltage on the upper and lower arm inductances are used.

$$V_{MA} = L_a \frac{di_1}{dt} \tag{4.15}$$

$$\frac{di_1}{dt} = \frac{V_{MA}}{L_a} = \frac{V_{MO} - V_{AO}}{L_a} \tag{4.16}$$

$$V_{BM} = L_a \frac{di_2}{dt} \tag{4.17}$$

$$\frac{di_2}{dt} = \frac{V_{BM}}{L_a} = \frac{V_{BO} - V_{MO}}{L_a} \tag{4.18}$$

Capacitor voltages are dependent on the upper and lower submodule states and currents. The capacitor equations, (4.19) and (4.20), are important in terms of charging and discharging of capacitors.

$$\text{Upper arm: } \frac{dV_{Ci}}{dt} = \frac{1}{C_i} i_1 \left( S_i - 1 \right) \tag{4.19}$$

$$\text{Lower arm: } \frac{dV_{Ci}}{dt} = \frac{1}{C_i} \left( -i_2 \right) S_i \tag{4.20}$$

Therefore, total upper and total lower submodule voltages are calculated as in (4.21) and (4.22).

$$V_u = \sum_{i=1}^{n/2} V_{Ci} \left( 1 - S_i \right) \tag{4.21}$$

$$V_l = \sum_{n/2+1}^{n} V_{Ci} S_i \tag{4.22}$$

## 4.3. Submodule Capacitor Sizing

The size of the capacitor in a MMC submodule is an important issue because they physically occupy a large proportion in the cell volume. It is even much more important if the converter station is placed inside of an expensive offshore platform as in the case of interconnection of offshore wind farms. Moreover, overcharging or undercharging of these capacitors may result in unstable conditions in the converter. Because of these reasons, the capacitance value of the submodule capacitor should be kept as low as possible. This part of the report is dedicated to calculate minimum cell capacitance value keeping the normal converter operation.

The peak to peak energy deviation of a MMC arm has the main influence on the cell capacitor sizing [51]. Therefore, formulation can be started from the total energy stored in a leg as in (4.23) where $n$ is the number of submodules in a leg, $C$ is the submodule capacitance and $V_C(t)$ is the cell capacitor voltage.

$$E_{leg}(t) = \frac{1}{2} nC \left( V_C(t) \right)^2 \tag{4.23}$$

Taking voltage and energy deviations into account, (4.24) can be written where $\Delta V$ is the maximum voltage deviation around the nominal cell voltage, $V_{C_{nom}}$, $\Delta E_{leg_{max}}$ and $\Delta E_{leg_{min}}$ are the maximum and minimum energy deviations from the initial condition $E_{leg}(0)$, respectively.

$$\frac{1}{2}nC\left(V_{C_{nom}}\left(1+\Delta V\right)\right)^2 = E_{leg}(0) + \Delta E_{leg_{max}} \tag{4.24a}$$

$$\frac{1}{2}nC\left(V_{C_{nom}}\left(1-\Delta V\right)\right)^2 = E_{leg}(0) + \Delta E_{leg_{min}} \tag{4.24b}$$

Since peak to peak energy deviation, $\Delta E_{leg}$, is the difference between maximum and minimum energy deviations as in (4.25a), by subtracting (4.24b) from (4.24a), minimum cell capacitance depending on peak to peak energy deviation can be found in (4.25b).

$$\Delta E_{leg} = \Delta E_{leg_{max}} - \Delta E_{leg_{min}} \tag{4.25a}$$

$$C = \frac{\Delta E_{leg}}{2nV_{C_{nom}}^2 \Delta V} \tag{4.25b}$$

In order to find the peak to peak energy deviation, $\Delta E_{leg}$, in the equation of cell capacitance, (4.25b) the calculation of the power exchange is necessary. The power exchange with the upper arm, namely the positive arm, can be calculated by multiplying the positive arm current, $i_1(t)$, and the positive arm voltage, $V_u(t)$ as in (4.26). The current has a negative sign in the equation because of the current definition in Figure 4.13.

$$P_{leg}^{+}(t) = V_u(t)\left(-i_1(t)\right) \tag{4.26}$$

The positive arm voltage and positive arm current can be defined as in (4.27a) and (4.27b), respectively assuming an equal share of AC current through both positive and negative arms and an even distribution of the DC current through each phase.

$$V_u(t) = \frac{V_{DC}}{2} - V_{AC}(t) \tag{4.27a}$$

$$i_1(t) = \frac{i_{AC}(t)}{2} + \frac{I_{DC}}{3} \tag{4.27b}$$

In order to allow the MMC to operate properly, the condition in (4.28) must be achieved where $\hat{V}_{AC_{nom}}$ is the nominal AC voltage amplitude and $k_{AC_{max}}$ is the maximum AC voltage magnitude deviation (e.g. 1.1 pu).

$$\frac{V_{DC}}{2} = \hat{V}_{AC_{nom}} k_{AC_{max}} \tag{4.28}$$

AC voltage and current equations can be defined as in (4.29), where $k_{AC}$ is the voltage magnitude deviation of the AC voltage (e.g. a value in between 0.9 and 1.1 pu) and $\hat{I}_{AC}$ is the AC current magnitude. $\phi$ in (4.29b) represents the phase difference between voltage and the current.

$$V_{AC}(t) = k_{AC}\hat{V}_{AC_{nom}} \sin(\omega t) \tag{4.29a}$$

$$i_{AC}(t) = \frac{\hat{I}_{AC}}{k_{AC}} \sin(\omega t + \phi) \tag{4.29b}$$

In order to calculate the DC current, apparent and active power can be used as in (4.30).

$$|\bar{S}| = \frac{3}{2}\hat{V}_{AC_{nom}}\hat{I}_{AC} \tag{4.30a}$$

$$P = |\bar{S}|\cos(\phi) = V_{DC}I_{DC} \tag{4.30b}$$

$$I_{DC} = \frac{3}{2}\frac{\hat{V}_{AC_{nom}}\hat{I}_{AC}}{V_{DC}}\cos(\phi) \tag{4.30c}$$

Therefore, the power exchange with the upper arm can be written as (4.31) by implementing (4.27)-(4.30) to (4.26).

$$P^{+}_{leg}(t) = \frac{|\bar{S}|}{3}\frac{k_{AC_{max}}}{2k_{AC}}\left[\frac{k_{AC}}{k_{AC_{max}}}\sin(\omega t) - 1\right]\left[\frac{k_{AC}}{k_{AC_{max}}}\cos(\phi) + 2\sin(\omega t + \phi)\right] \tag{4.31}$$

The energy variation of the upper arm can be calculated basically by integrating the power over time as in (4.32).

$$\Delta E^{+}_{leg}(t) = \int_0^t P^{+}_{leg}(\tau)d\tau \tag{4.32a}$$

$$= \int_0^t \frac{|\bar{S}|}{3}\frac{k_{AC_{max}}}{2k_{AC}}\left[\frac{k_{AC}}{k_{AC_{max}}}\sin(\omega\tau) - 1\right]\left[\frac{k_{AC}}{k_{AC_{max}}}\cos(\phi) + 2\sin(\omega\tau + \phi)\right]d\tau \tag{4.32b}$$

Although calculating the integral in (4.32) is complex because of many variables, peak to peak energy deviation can be calculated for the most extreme case, which causes the maximum deviation, resulting the maximum cell capacitance. As explained in [51], the energy deviation becomes the highest for a voltage magnitude deviation of ±10% when the AC voltage magnitude is 0.9 pu and the phase difference $\phi$=90° that is to say for the pure reactive power. For this extreme case, peak to peak energy deviation is calculated as in (4.33a), and thus by inserting it to (4.25b), cell capacitance can be derived as in (4.33b).

$$\Delta E_{leg} = 2.44\frac{|\bar{S}|}{3\omega} \tag{4.33a}$$

$$C \geq \frac{2.44|\bar{S}|}{6\omega n V^2_{C_{nom}}\Delta V} \tag{4.33b}$$

From the minimum cell capacitance equation, a very important inference can be made such that the cell capacitance is inversely proportional with the AC side frequency. This means that the frequency can be increased in order to decrease capacitance value, and thus physical capacitor size. Since the converter is used for interconnection of two DC systems, AC side is only a middle stage for the conversion; that is to say, the AC side frequency does not have to be the same with grid frequency, 50 Hz, it can be freely chosen. The behaviour of the cell capacitance with the AC side frequency can be seen in Figure 4.5 which is plotted according to the parameters specified by Table 4.2. According to these parameters, number of cells in a MMC leg is calculated as in (4.34).

**Table 4.2:** Design parameters for the cell capacitance calculation

| **Power Rating** | $\mathbf{V_{DC}}$ | $\mathbf{V_{C_{nom}}}$ | **ΔV** |
|---|---|---|---|
| 1000 MW | ±640 kV | 4 kV | 10% |

$$n = \frac{V_{DC_{total}}}{V_{C_{nom}}} = \frac{1280kV}{4kV} = 320 \tag{4.34}$$

As Figure 4.5 shows, raising the AC side frequency significantly decreases the size of the capacitor. Moreover, the core volume of the transformer is expected to reduce with increasing the frequency but due to other factors like the cooling equipment, the reduction in the total transformer volume is not linear [43]. In spite of its effect on the reduction of the cell capacitor size, increasing the AC side frequency results in a rise of switching losses. Therefore, the frequency should be selected carefully for keeping both the capacitor size and switching losses minimum while the converter operates properly. Selecting the AC connection frequency in between 350 Hz and 500 Hz seems like the best option because the converter losses are only 5% higher while the cost is 25% lower under 500 Hz operation when compared to frequency of 50 Hz [43], [52].

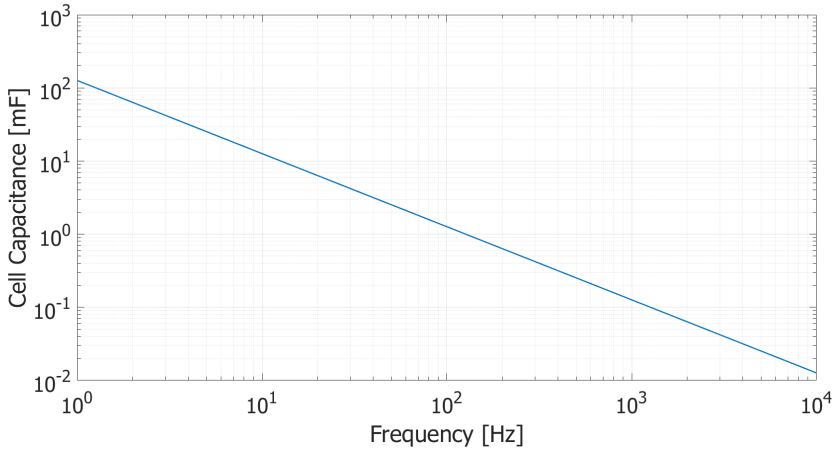


**Figure 4.5:** Behaviour of the cell capacitance with the AC side frequency

## 4.4. Control of MMC

A detailed control algorithm including power control is explained in Section 5.3. For the control of mathematical model, the control structure explained in [50] is used. This control scheme for a MMC consists of two main parts: an outer control loop which generates upper and lower arm reference voltages and an inner loop which includes balancing of submodule capacitor voltages.

### 4.4.1. Outer Control Loop

The outer control of the MMC includes two control loops: one controls the circulating current and the other controls the total voltage of the capacitors.

From the first control loop, reference value for the circulating current is calculated by a PI controller after subtracting the sum of all capacitor voltages from twice the value of DC voltage. Although the circulating current is an undesired element in a MMC, the reference value of the circulating current is not set to zero because by entirely suppressing the circulating current, there is no longer the possibility of reducing the capacitive energy fluctuations, as explained in [49]. Using twice the value of DC voltage is resulted from different meanings of the switching signals for upper and lower arms as explained in Section 4.1.

The control of circulating current indicates the reference voltage across upper and lower arm inductances, $V_{AB}$, as a result of equations (4.7), (4.15) and (4.17) as shown in (4.35).

$$\frac{di_c}{dt} = \frac{-V_{AB}}{2L_a} \tag{4.35}$$

After $V_{AB}^*$ is obtained, upper and lower reference voltages can be calculated as in (4.36) and (4.37). Creation of upper and lower reference voltages can be seen in Figure 4.6.

$$V_u^* = -V_{MO}^* - \frac{V_{AB}^*}{2} + V_{PO} \tag{4.36}$$

$$V_l^* = V_{MO}^* - \frac{V_{AB}^*}{2} + V_{ON} \tag{4.37}$$

### 4.4.2. Inner Control Loop

In order to provide an accurate operation of a MMC, charging and discharging of the submodule capacitors have a significant role so that capacitor voltages are kept in balance. Furthermore, total capacitor

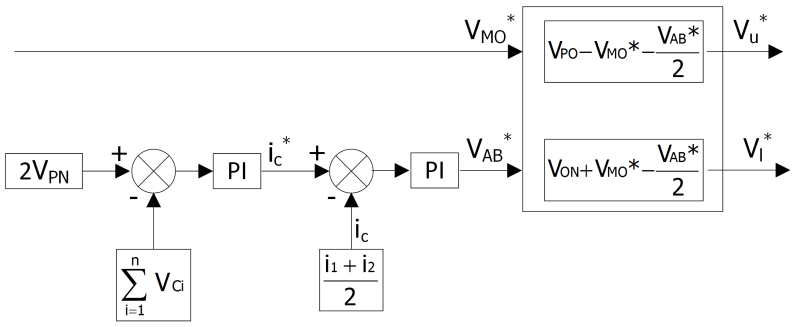


**Figure 4.6:** Control of circulating current and total voltage of capacitors and creation of reference voltages

voltage must be at a reference value in order to provide desired output voltage at the converter terminals. Balancing submodule capacitor voltages is performed by adding a balancing section to the modulation part which is explained in Section 4.5.

## 4.5. Modulation Methods of MMC

A large number of techniques is developed for the modulation of multilevel converters since MMC consists of large amount of power electronic switching devices which makes their modulation schemes more complex and extending traditional modulation techniques to multilevel topologies is a challenging task [53–59]. The main purpose of all different gate level modulation methods of the MMC is to keep all capacitor voltages at the same value which is performed by determining which capacitors should be charged or discharged by adjusting the gate signals, $S_i$. Generally, modulation for multilevel converters can be divided into three categories: Carrier-based Pulse-Width Modulation (PWM), Space Vector Modulation (SVM) and Nearest Level Modulation.

### 4.5.1. Carrier-based Pulse-Width Modulation

Carrier-based PWM technique is mainly based on comparison of a reference signal, generally a sinusoid, with a carrier signal, generally in triangular waveform in high frequency. Switching signals are generated at each time when an intersection occurs with reference and carrier signals. This method is extended for the multilevel case by using multicarrier signals which are used for the control and modulation of each submodule, independently [60].

The carrier signals can be positioned within levels (Level Shifted PWM) or having phase shifts (Phase-Shifted PWM):

**Level-Shifted PWM (LSPWM):** LSPWM includes triangular carrier signals with the equal number of submodules having the same amplitude and frequency but different offset values as seen in Figure 4.7. In this method of modulation, submodules have unequal switching patterns and the power delivered by submodules are not even which causes harmonics and undesirable distortions. This problem can be corrected by switching the level shifts between the carrier signals [61].

**Phase-Shifted PWM (PSPWM):** PSPWM includes triangular carrier signals with the equal number of submodules having the same amplitude and frequency but different phase shifts and the gate signals are determined after each intersection of reference signal and carrier waves.

The phase shift between the carriers is equal to 360°/n. Carrier waves belonging to the same arm have a phase shift of 720°/n. For example, for a MMC with 8 submodules, there should be 720°/8=90° phase shift between each consecutive carrier for both upper and lower carrier waves; i.e. phase of the upper carriers are 0°, 90°, 180° and 270° while phase of the lower carriers are 45°, 135°, 225° and

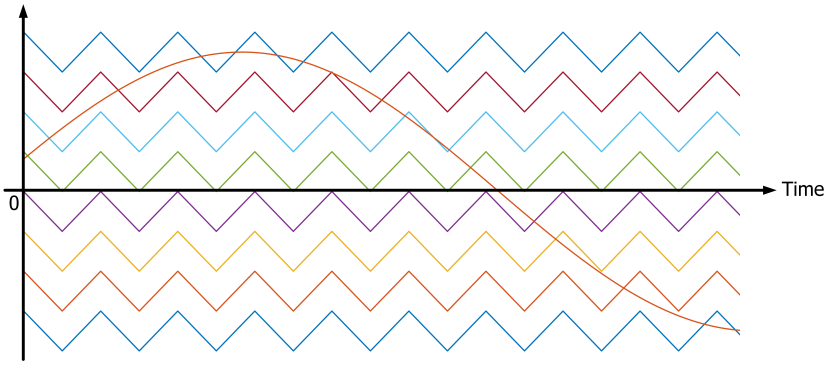


**Figure 4.7:** Level-shifted PWM carriers (triangular) and reference (sinusoidal)

315° [53].

Firstly, modulation algorithm sorts the upper or lower capacitor voltages after an intersection of carrier waves and upper or lower reference voltage. After this step, depending on the relation between reference and carrier waves and the direction of the current, gate signals are determined. The flowchart of the algorithm can be seen in Figure 4.8.

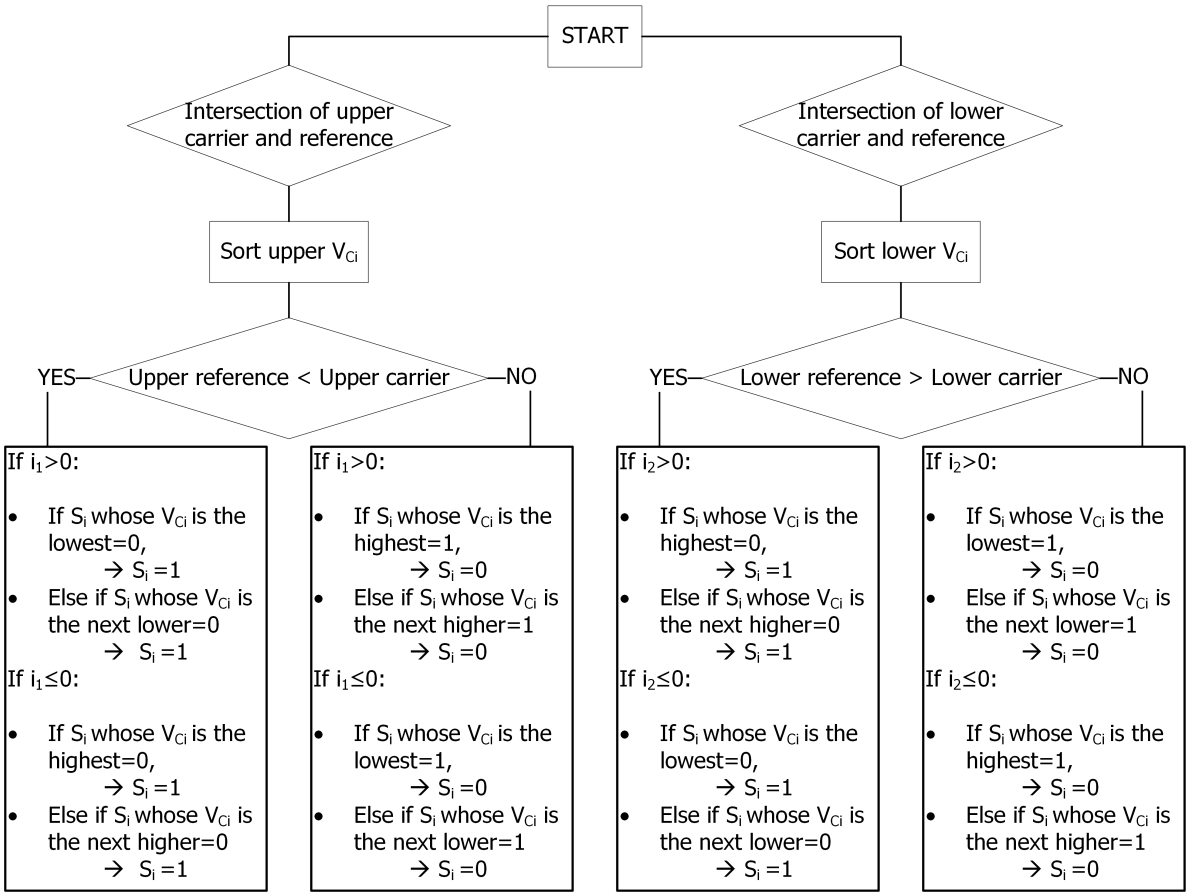


**Figure 4.8:** Flowchart of the modulation algorithm

### 4.5.2. Space Vector Modulation

For voltage source converters, SVM is preferred due to its flexibility to generate switching signals and its easy digital implementation since it does not require any triangular carrier wave [55]. All possible switching states of the converter provides discrete output voltage values which can be defined as possible voltage vectors to be achieved. In this method, reference voltage is represented as a vector and it is generated as a linear combination of voltage vectors. Traditional SVM method can be extended to multilevel case; however, this causes more complex algorithm for the calculation of the vectors and higher computational costs as the number of levels is increased since SVM requires coordinate transformations and look up tables [60]. Recently, a SVM method has proposed in [62] which operates independently from number of submodules without coordinate transformations and look up tables. These advantages make the developed SVM suitable for MMC with large number of submodules and HVDC applications.

### 4.5.3. Nearest Level Modulation

Nearest level modulation (NLM) technique is preferred when the MMC includes large number of submodules since it provides more flexibility and easy digital implementation due to the removal of any triangular carrier waveforms [63]. The main principle of the modulation is based on determining the number of submodules to be inserted or bypassed depending on the reference arm voltage values.

The reference arm voltage values for each phase, which are the output of control part, are used as an input for the NLM and it is normalized with DC voltage of the converter. The obtained value varying between 0 and 1 is exposed to a scaling in order to obtain the number of submodules inserted which is an integer value between 0 and n/2, where n/2 is the number of submodules in an arm in a phase.

$$n_{ON} = round(\frac{n}{2}\frac{V_{ref}(t)}{V_{DC}}) \tag{4.38}$$

By inserting the submodules according to (4.38), generated arm voltage follows the reference waveform with voltage steps as shown in Figure 4.9.

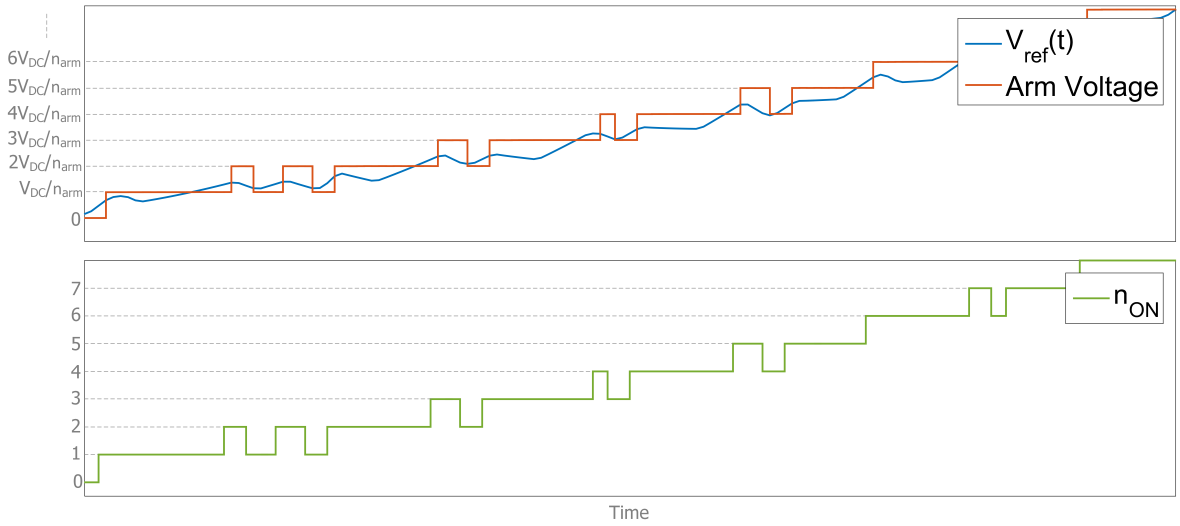


**Figure 4.9:** Reference and generated arm voltage waveforms and inserted number of submodules with NLM

## 4.6. Simulation Results

For the simulation of the converter, Matlab/Simulink is used. Firstly, a single phase MMC with 8 sub-

modules in a leg, i.e. 4 submodules in upper and lower arms, is simulated. As soon as the satisfied results are obtained from single phase simulation, three phase system is verified.

Design parameters for the simulation of MMC are shown in Table 4.3. The DC voltage is set to 500 V and the maximum grid voltage is set to 230 V in a frequency of 50 Hz. Triangular signals with the frequency of 2 kHz are used for the carrier waves for phase-shifted PWM. Upper and lower arm inductances, $L_a$, and output inductance, $L_{out}$, are set to 2 mH. Output resistance has a value of 0.1 Ω and the capacitance value for the capacitor in each submodule is 7.5 mF. The phase of the reference output voltage ($V_{MO}{}^*$) is set to zero in this part of the simulation.

**Table 4.3:** Design parameters for the simulation of MMC

| | | | |
|---|---|---|---|
| $\mathbf{V_{DC}}$ | 500 V | $\mathbf{L_a}$ | 2 mH |
| $\mathbf{V_g}$ **(max)** | 230 V | $\mathbf{R_{out}}$ | 0.1 Ω |
| $\mathbf{f_g}$ | 50 Hz | $\mathbf{L_{out}}$ | 2 mH |
| $\mathbf{f_c}$ | 2 kHz | **C** | 7.5 mF |

### 4.6.1. Simulation of the Modulation

The simulation result of the phase-shifted PWM algorithm with 8 submodules is shown in Figure 4.10 for the upper arm. At the first intersection of the reference voltage and the carrier wave, T4, capacitor voltages are sorted. From the intersection instant to next intersection, since the upper reference is greater than the carrier wave, T4, which the reference voltage intersects with and the upper arm current is positive at this interval, it is determined that "If Si whose VCi is the highest=1, Si=0". According to this command, gate signal for the second submodule, S2, is switched from one to zero since the highest capacitor voltage belongs to second submodule.

At the second intersection of the upper reference and the carrier, T1 in this case, capacitor voltages are sorted, again. Since the upper arm current is positive at this instant and the upper reference is less than the carrier, T1 after intersection instant, it is determined that "If Si whose VCi is the lowest=0, Si=1". According to this command, gate signal for the forth submodule, S4, is switched from zero to one since the lowest capacitor voltage belongs to forth submodule in this case.

Similarly, the simulation result of the modulation algorithm with 8 submodules for the lower arm is shown in Figure 4.11. At the first intersection of the reference voltage and the carrier wave, T7, capacitor voltages are sorted. From the intersection instant to next intersection, since the lower reference is greater than the carrier wave, T7, which the lower arm reference voltage intersects with and the lower arm current is negative at this interval, it is determined that "If Si whose VCi is the lowest=0, Si=1". According to this command, gate signal for the sixth submodule, S6, is switched from zero to one since the lowest capacitor voltage belongs to sixth submodule.

At the second intersection of the lower reference and the carrier, T5 in this case, capacitor voltages are sorted, again. Since the lower arm current is negative at this instant and the lower reference is less than the carrier, T5 after intersection instant, it is determined that "If Si whose VCi is the highest=1, Si=0". According to this command, gate signal for the eight submodule, S8, is switched from one to zero since the highest capacitor voltage belongs to eighth submodule in this case.

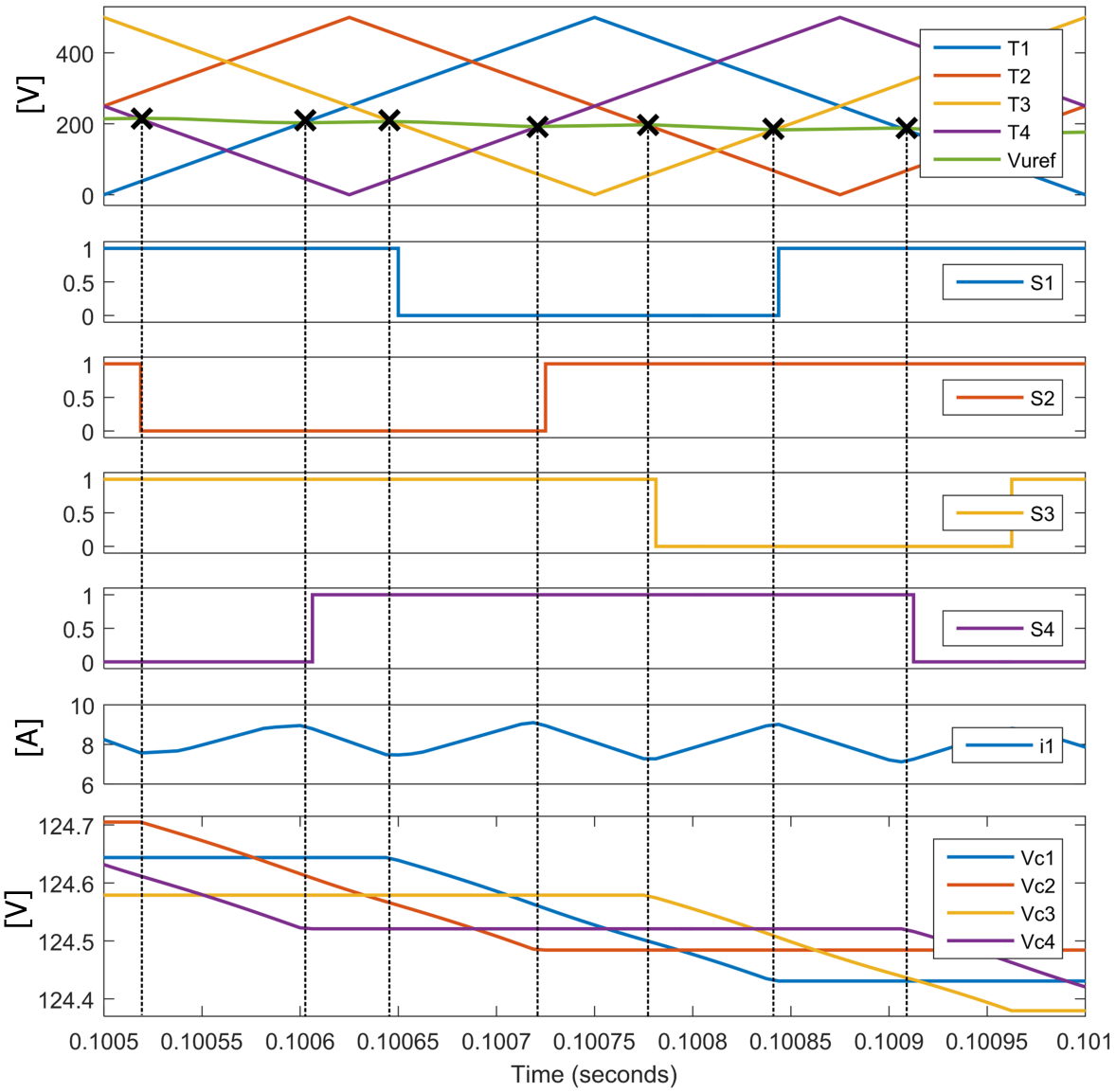


**Figure 4.10:** States and carrier signals for upper arm submodules

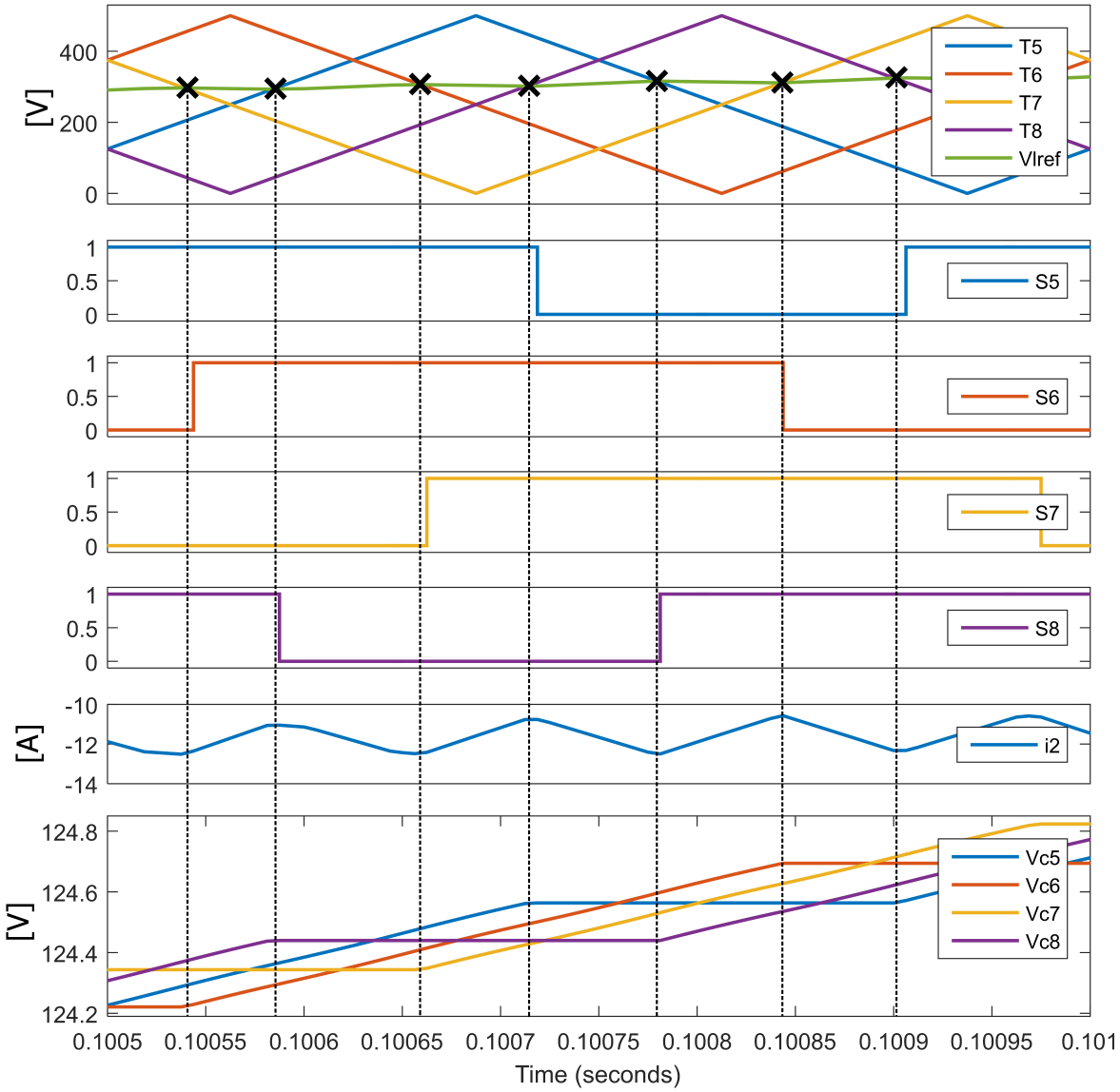


**Figure 4.11:** States and carrier signals for lower arm submodules

### 4.6.2. Single Phase MMC with 8 Submodules

Simulation results of the single phase system with 8 submodules can be seen in Figure 4.12. Since the DC voltage is 500 V, capacitors in each submodule are supposed to have an average of 125 V which results in 1000 V of total capacitor voltage. Figure 4.12a shows that total average capacitor voltage is about 1000 V after it reaches steady state. As can be seen in Figure 4.12c, the capacitors belonging to the same arm have the same voltage level thanks to modulation algorithm described in Section 4.5.1 and the average voltage value of each capacitor is 125 V.

From the difference between total capacitor voltages and the reference voltage, reference value for the circulating current is calculated. The circulating current follows its reference value as shown in Figure 4.12e and as explained in [64], its frequency is two times of the fundamental frequency.

Generated upper, lower and output voltages are shown in Figures 4.12b, 4.12d and 4.12f, respectively. They follow their reference values and the output voltage which is $V_{MO}$ in Figure 4.3 has 8 steps (9 levels) since there are 8 submodules in total. Figure 4.12g shows upper, lower and output currents which are in 50 Hz.

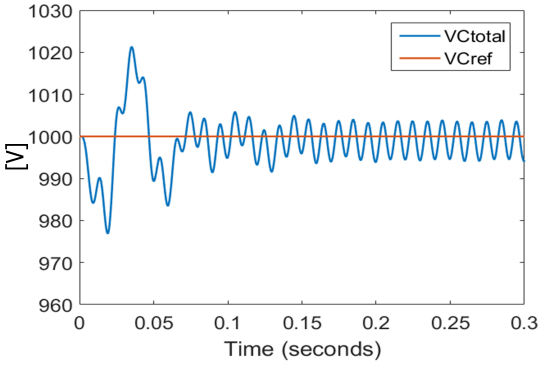


**(a)** The sum of all capacitor voltages

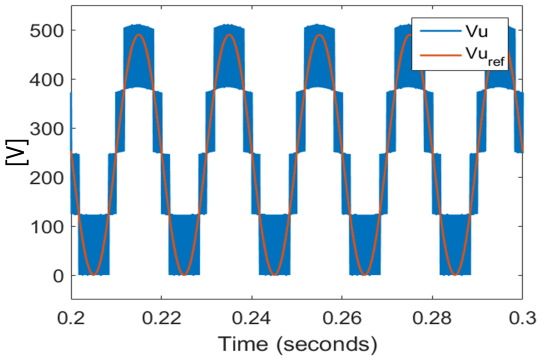


**(b)** Upper arm voltage and the reference

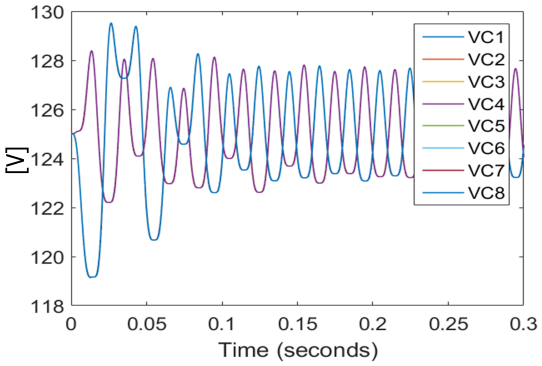


**(c)** Individual capacitor voltages

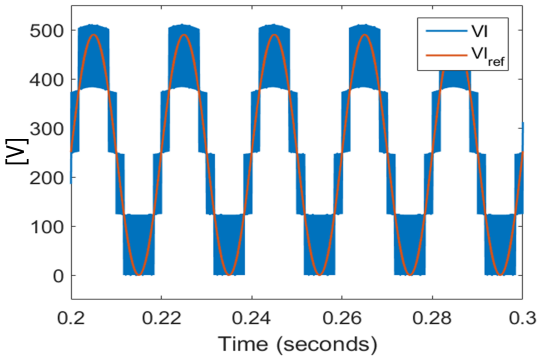


**(d)** Lower arm voltage and the reference

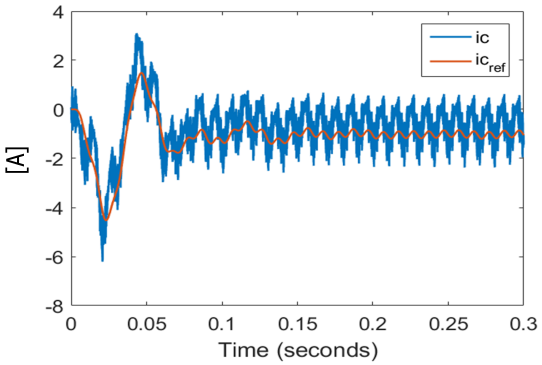


**(e)** Circulating current and the reference

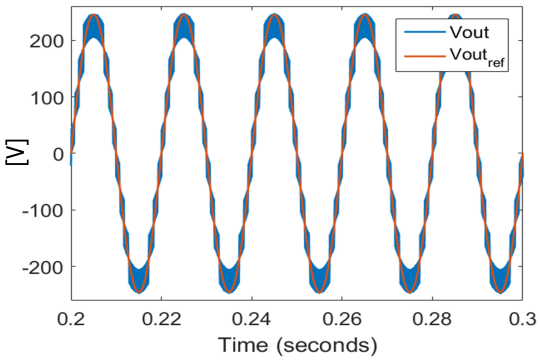


**(f)** Output voltage and the reference

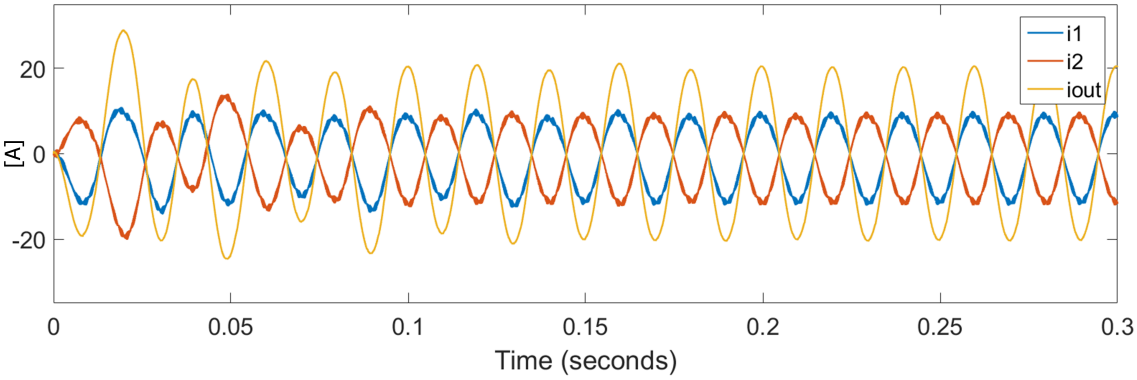


**(g)** Converter currents

**Figure 4.12:** Simulation results of the single phase MMC with 8 submodules

### 4.6.3. Three Phase MMC with 8 Submodules

In this part of the report, the simulation results for a three phase MMC with 8 submodules per phase are presented. After satisfied results are achieved from single phase simulations, the system is expanded for three phase as in Figure 4.13 and for high voltage applications. Therefore, the DC voltage is set to 640 kV and the maximum grid voltage is set to 294 kV in a frequency of 50 Hz as shown in Table 4.4.

**Table 4.4:** Design parameters for the simulation of three phase MMC

| | | | |
|---|---|---|---|
| $\mathbf{V_{DC}}$ | 640 kV | $\mathbf{L_a}$ | 2 mH |
| $\mathbf{V_g\ (max)}$ | 294 kV | $\mathbf{R_{out}}$ | 0.1 Ω |
| $\mathbf{f_g}$ | 50 Hz | $\mathbf{L_{out}}$ | 2 mH |
| $\mathbf{f_c}$ | 2 kHz | $\mathbf{C}$ | 7.5 mF |

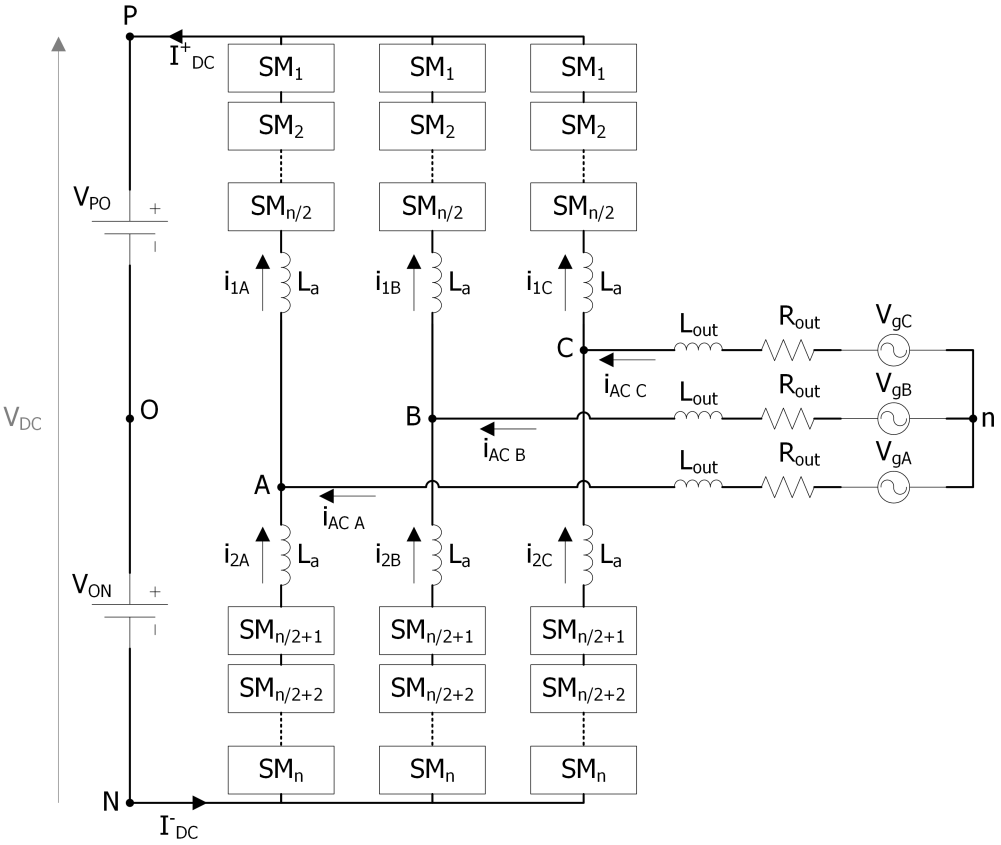


**Figure 4.13:** Circuit diagram of a three phase MMC

Figure 4.14 shows the simulation results of the three phase MMC with 8 submodules. Three phase output voltages and three phase output currents are shown in the figure. As can be seen in both plots, the waveforms are in 50 Hz with a 120° phase shift.

At this point of the simulation, it is recognized that there is a 90° phase difference between phase voltages and currents, which means that there is only reactive power transfer. It is noticed that the amplitude and phase of $V_{MO}^*$ has an effect on phase and amplitude of output current; therefore, $V_{MO}^*$ is set to a value which results in output voltage and current in phase in order to adjust power flow as purely active power.

For adjusting power flow as purely active, Kirchhoff's voltage law is applied to the circuit shown in Figure 4.4 and the output voltage, $V_{MO}$, is obtained as in (4.39). All voltages and currents are

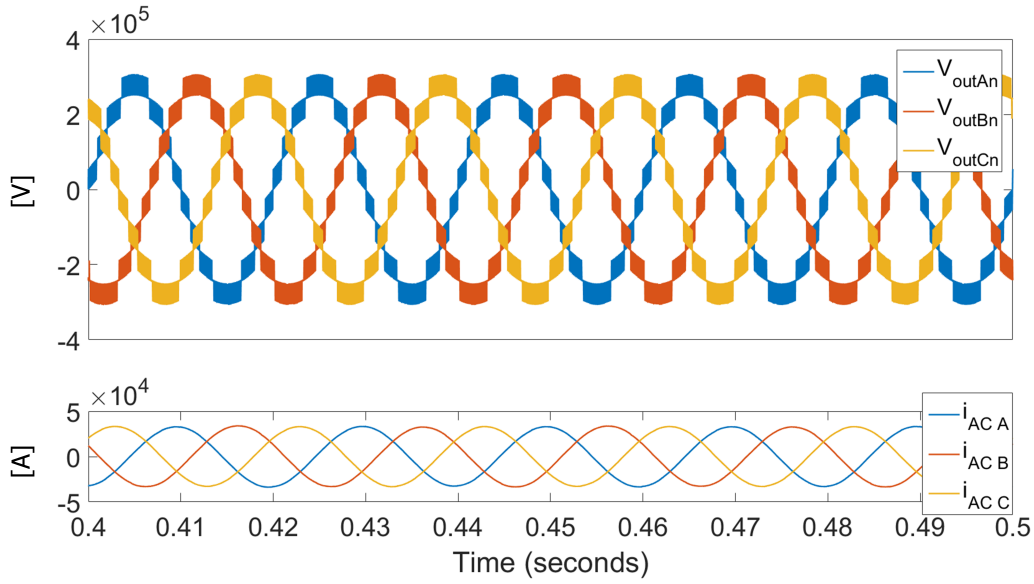


**Figure 4.14:** Simulation results of the three phase MMC with 8 submodules

written in explicit forms as in (4.40) where $\hat{V}_{MO}$ and $\hat{I}_{out}$ are amplitudes of output voltage and current, respectively, $\hat{V}_g$ is the amplitude of the grid voltage, $\omega$ is the angular frequency of the AC side, $2\pi f$, and $\phi$ is the phase shift of both output voltage and current for active power transfer.

$$V_{MO} = V_g - R_{out} i_{out} - L_{out} \frac{di_{out}}{dt} \tag{4.39}$$

$$\hat{V}_{MO} \sin(\omega t + \phi) = \hat{V}_g \sin(\omega t + 0) - R_{out} \hat{I}_{out} \sin(\omega t + \phi) - L_{out} \frac{d\left(\hat{I}_{out} \sin(\omega t + \phi)\right)}{dt} \tag{4.40}$$

Including all simulation parameters as in (4.41), for two $\omega t$ values, 0 and $\pi/2$, (4.42a) and (4.42b) can be derived.

$$\hat{V}_{MO} \sin(\omega t + \phi) = 294000 \sin(\omega t) - \hat{I}_{out} \left[0.1 \sin(\omega t + \phi) + 0.002\omega \cos(\omega t + \phi)\right] \tag{4.41}$$

$$\omega t = 0 \Rightarrow \quad \hat{V}_{MO} \sin(\phi) = -\hat{I}_{out} \left[0.1 \sin(\phi) + 0.6283 \cos(\phi)\right] \tag{4.42a}$$

$$\omega t = \frac{\pi}{2} \Rightarrow \quad \hat{V}_{MO} \sin\left(\frac{\pi}{2} + \phi\right) = 294000 - \hat{I}_{out} \left[0.1 \sin\left(\frac{\pi}{2} + \phi\right) + 0.6283 \cos\left(\frac{\pi}{2} + \phi\right)\right] \tag{4.42b}$$

Depending on $\hat{V}_{MO}$ value, $\hat{I}_{out}$ is extracted from both (4.42a) and (4.42b) with respect to phase shift, $\phi$. For the $\phi$ value which results the same $\hat{I}_{out}$ in (4.42a) and (4.42b) is determined as the phase shift of the reference output voltage, $V_{MO}{}^{*}$. In this case, $\hat{V}_{MO}$ =270 kV and $\phi$ =−16° give the expected results.

The currents and the individual capacitor voltages of phase A with controlled power can be seen in Figure 4.15. As seen in Figure 4.15b, arm currents has an offset which indicates that there is a transmission of active power as mentioned in [50].

Three phase output voltages and currents with purely active power are shown in Figure 4.16. As seen in Figure 4.16, voltages and currents belonging the same phase are in phase which results in a purely active power transfer.

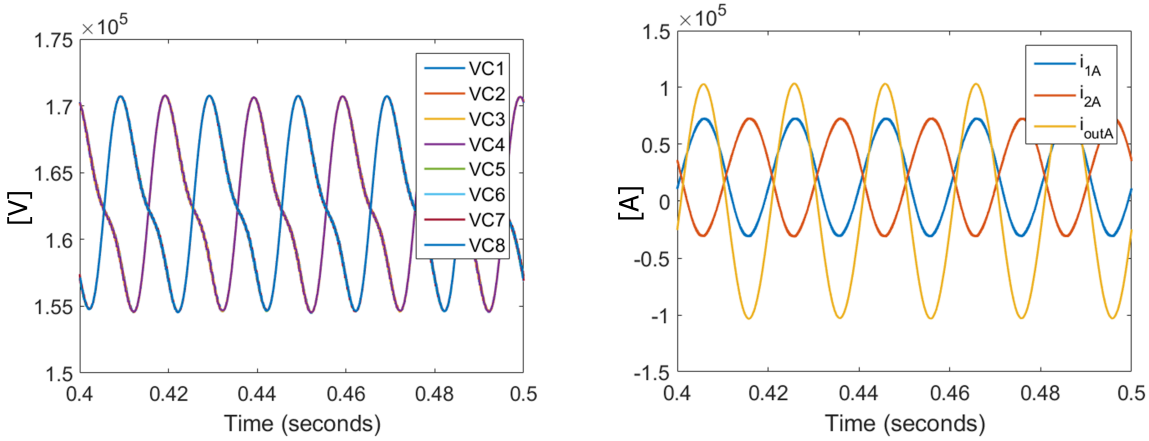


**(a)** Individual capacitor voltages of phase A **(b)** Upper, lower and output current of phase A

**Figure 4.15:** Simulation results of the phase A of the MMC

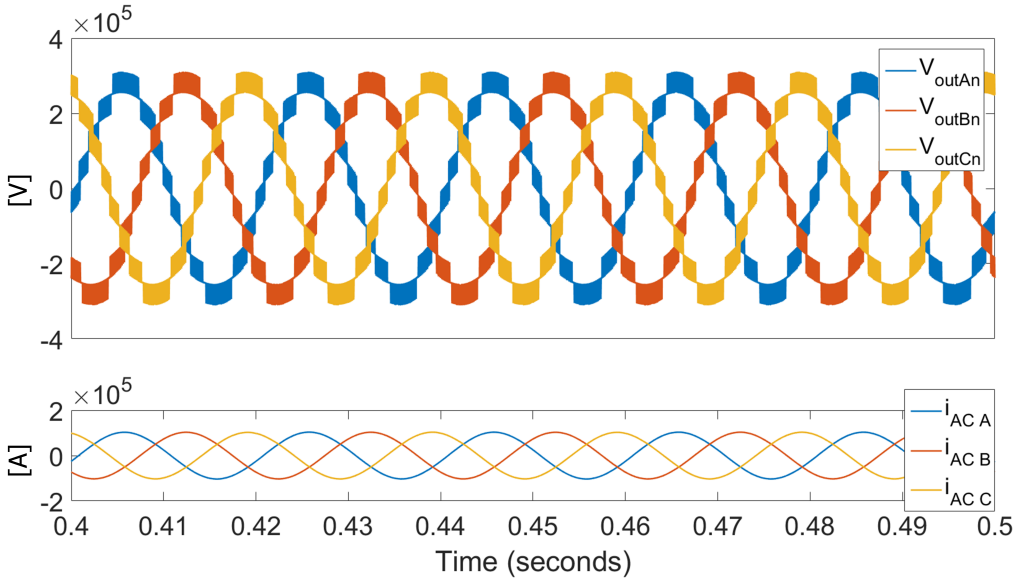


**Figure 4.16:** Simulation results of the three phase MMC with 8 submodules with purely active power

### 4.6.4. Switching Model Simulation

In order to compare the results obtained from three phase high voltage mathematical model of MMC with a model including IGBTs, a switching model is developed with 8 submodules in a leg. All simulation parameters are kept as in Table 4.4. Upper and lower arm capacitor voltages and upper arm, lower arm and output currents of phase A are shown in Figure 4.17a and Figure 4.17b, respectively. The waveforms are coherent with the results of mathematical model.

Three phase output voltages and currents are also plotted in Figure 4.18. The voltage waveforms are slightly distorted because of the harmonics resulting from switching of IGBTs. However, in terms of the amplitude and frequency, they are consistent with mathematical model.

The simulation time allows us to complete this simulation with 8 submodules since the number of submodules is not too high. Nevertheless, the simulation is time consuming because of switching schemes of power electronic devices and filtering may be required in order to reduce the harmonics in the system.

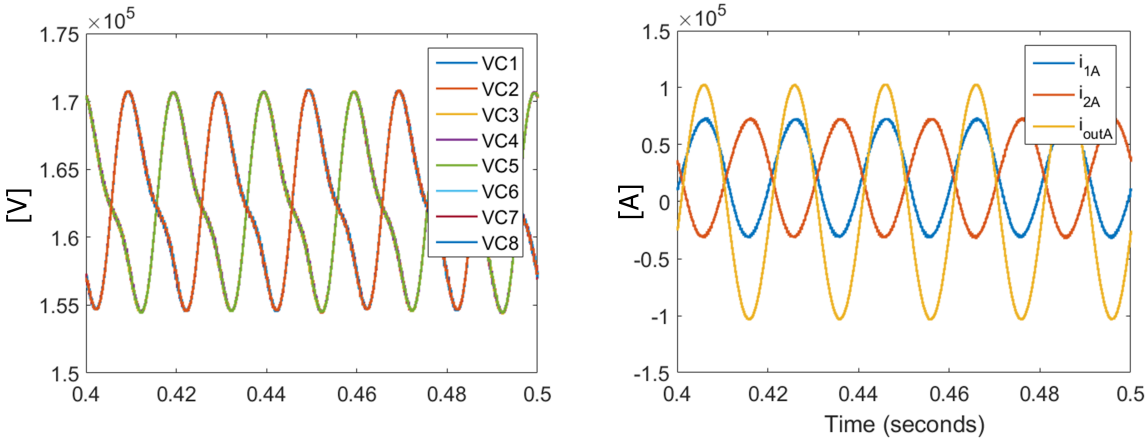


**(a)** Individual capacitor voltages of phase A

**(b)** Upper, lower and output current of phase A

**Figure 4.17:** Simulation results of the phase A of the MMC using switching model

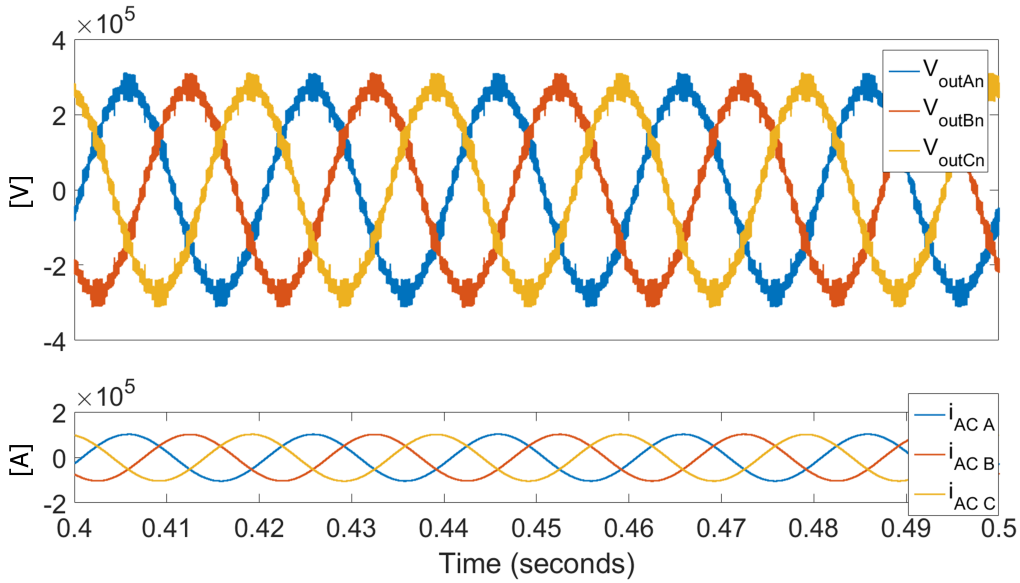


**Figure 4.18:** Simulation results of the three phase MMC with 8 submodules using a switching model

# 5

# Developed MMC Model

*This chapter presents a controlled voltage sources-based model of MMC including large number of cells. Advanced control structures for MMC, namely circulating current suppressing controller, active and reactive power controllers, AC rms voltage controller and current controllers are included and the generation of reference arm voltages is explained in this chapter.*

## 5.1. Introduction

Simulation results of the MMC in Section 4 proves that computing time is suitable for mathematical model including low number of submodules with phase-shifted PWM method. However, MMC for a high voltage application requires a large number of submodules, which increases the computing time significantly and restricts to simulate the previous model because of the increased number of carrier waves that have to be compared with the reference signals for the generation of gate signals of switching devices. Moreover, all the system is based on equations and there is no physical connection of circuit components in mathematical model. In order to perform a more realistic simulation and overcome the time-consuming process of PWM modulation for large number of submodules, a controlled voltage sources-based model with nearest level modulation is used for further analysis by operating the converter with a continuous insertion index.

## 5.2. Controlled Voltage Sources-Based Model of MMC

In this model, submodules on 6 arms of the three phase MMC are replaced by 6 controlled voltage sources. These voltage sources output the upper and lower arm voltages, $V_u$ and $V_l$, across their terminals while individual cell voltages, $V_{Ci}$, are also supplied depending on (4.19–4.22) to be used in other blocks. Controlled voltage sources-based model is shown in Figure 5.1.

Thanks to controlled voltage sources-based model and nearest level modulation method, the computing time is decreased in significant amount in order to simulate MMC with high number of submodules. The number of submodules are increased to 200 in a leg for each phase (100 submodules in upper and lower arms of each phase) for further analysis.

## 5.3. Developed Control of MMC

Controllers of a VSC determines the operating characteristics for a proper and stable operation. Although MMC brings many advantages as compared to traditional VSC, the control strategy is more complex. The control structure of MMC mainly consists of two main parts: inner control loop which controls the circulating current and balances submodule capacitors together with modulation algorithm [65] and outer control loop which controls power or voltage depending on the application through a

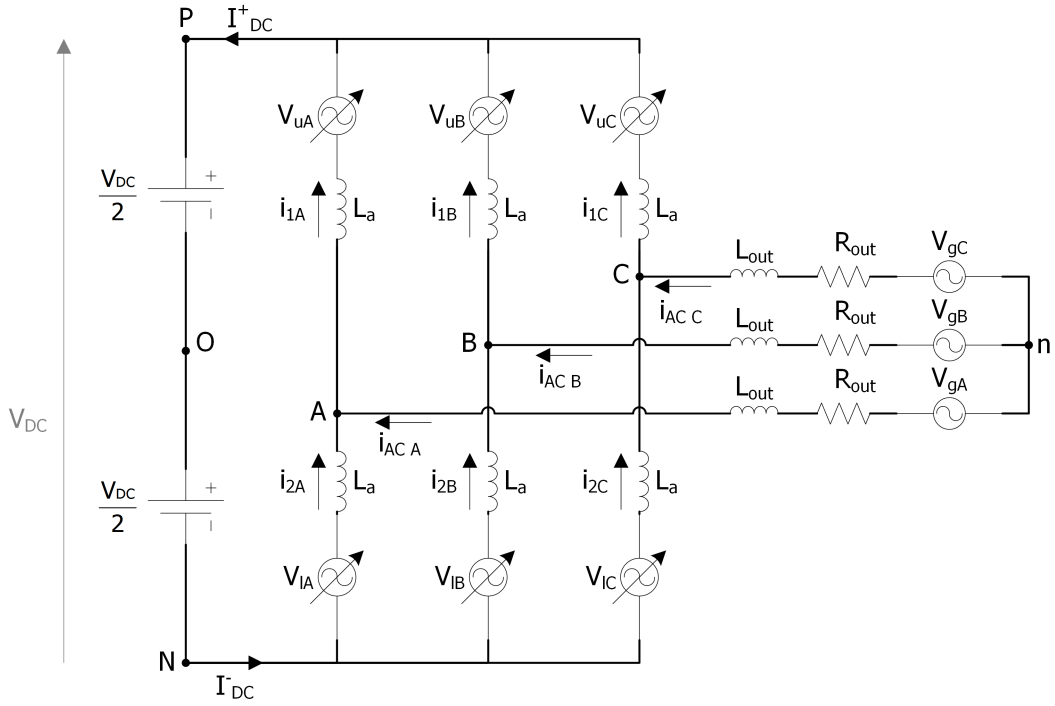


**Figure 5.1:** Controlled voltage sources-based model of MMC

current controller.

### 5.3.1. Inner Control Loop

Mainly, the circulating current is controlled in this control block since the balancing of submodule capacitor voltages is performed by modulation block. The circulating current is an inner current of converter, i.e. it does not occur in the output current or not directly affect the output voltage; however, it flows through the internal arms of the MMC, disturbs the sinusoidal arm currents and dissipates power. The increase of this current gives rise to losses and results in distortions and instability during transients [66]. While the aim of the arm inductor is to decrease the circulating current component, it cannot totally remove the circulating current. Moreover, it is not a cost-effective solution because of the fact that high-voltage inductors are costly [67, 68]. Therefore, elimination of this current component is a major problem in MMC and can be solved in different ways [49, 67–71]. Two of these methods are explained in this chapter.

#### Circulating Current Suppression Based on dq Coordinates

Circulating current suppressing controller (CCSC) based on its dq components is first proposed in [67] in order to eliminate circulating currents on MMC arms. According to this controller shown in Figure 5.2, the double line frequency circulating current for each phase is obtained from upper and lower arm currents based on (4.7) and direct and quadrature axis components are obtained via Park's transform at $2\omega$ on negative sequence rotational reference frame. d and q axis reference currents, $i_{cd}^*$ and $i_{cq}^*$, are set to zero in order to minimize $i_c$. Through PI controllers, d and q axis reference value for the voltage that drives circulating currents, $u_{cd}^*$ and $u_{cq}^*$ are generated. Finally, three phase reference signals, $u_{c\_ABC}^*$, are obtained by inverse Park's transform at $2\omega$ with negative sequence.

The dq vector control based CCSC is tested based on parameters given in Table 5.1 and the result is shown in Figure 5.3 which also presents the waveforms for the converter without any CCSC. As seen in Figure 5.3, the amplitude of the circulating current is suppressed significantly and the there is a clear improvement in output currents and voltages.

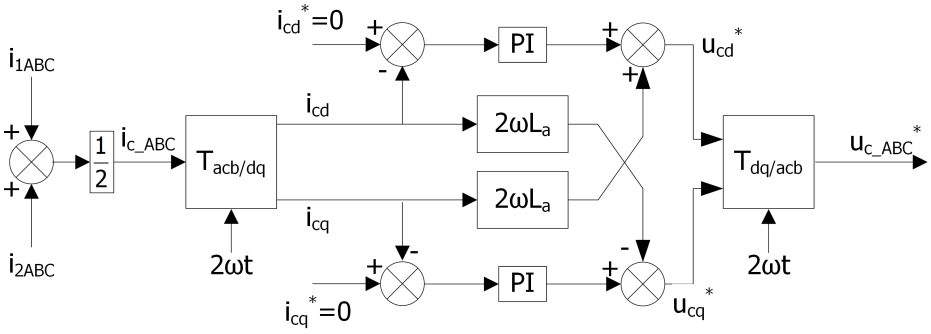


**Figure 5.2:** Circulating current suppressing controller based on dq coordinates

**Table 5.1:** Design parameters for the circulating current suppression based on dq vectrol control

| n (number of SM in one phase leg) | $K_P$ | $K_I$ |
|---|---|---|
| 200 | 20 | 2000 |

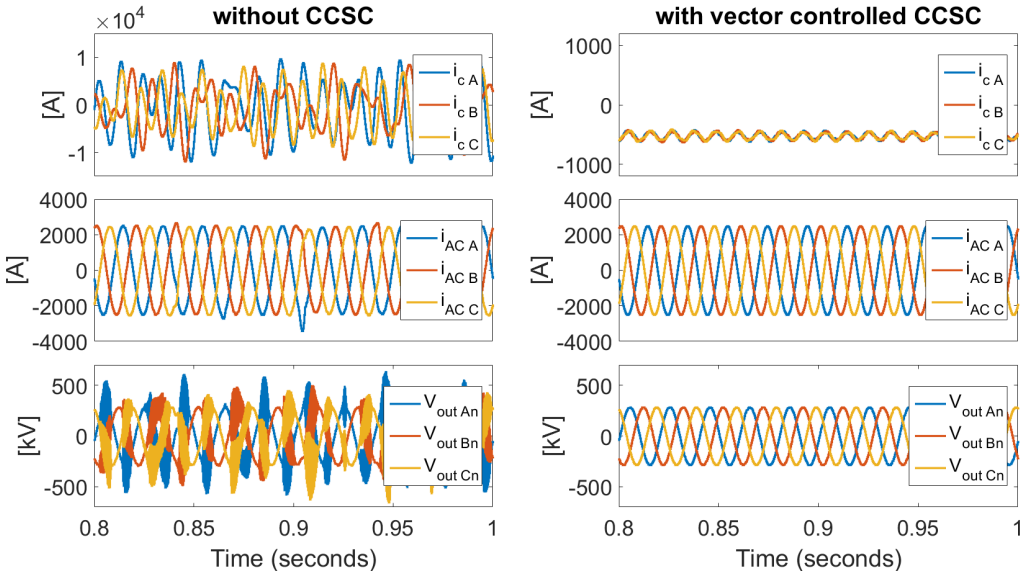


**Figure 5.3:** Circulating current and output currents and voltages without and with CCSC based on dq vectrol control

There are three main drawbacks of the circulating current suppression controller based on dq vector control:

- Total suppression of circulating current does not allow to reduce the capacitive energy fluctuations [49].
- Since it is based on Park's transformation, controlling three phase circulating current is a complex task [49].
- If the circulating current includes additional harmonics, additional Park's transformation is necessary, which makes the controller even more complex [71].

### Circulating Current Suppression Using a Proportional Resonant Controller

Due to the disadvantages of circulating current control using dq reference frame, proportional resonant (PR) controller is used in order to eliminate the circulating current as presented in [71]. The real value of the signal can follow the reference value at the resonant frequency thanks to the PR controller. Although the circulating current has only a double line frequency during steady state, it has a quadruple

harmonic component during the transient. Hence, the designed PR controller depicted in Figure 5.4 eliminates both harmonic components.

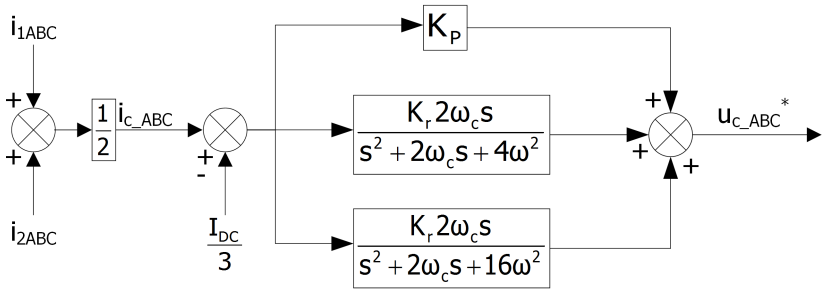


**Figure 5.4:** Circulating current suppressing controller based on PR controller

The circulating current suppression controller is tested using controlled voltage sources based model with the parameters given in Table 5.2. It should be noted that pu values are used for the input circulating current of the CCSC. As shown in Figure 5.5, usage of CCSC significantly decreases the amplitude of the circulating current and improves the output current and voltage waveforms.

**Table 5.2:** Design parameters for the circulating current suppression using PR controller

| n (number of SM in one phase leg) | $K_P$ | $K_r$ | $\omega_c$ |
|---|---|---|---|
| 200 | 0.06 | 5 | 5 |

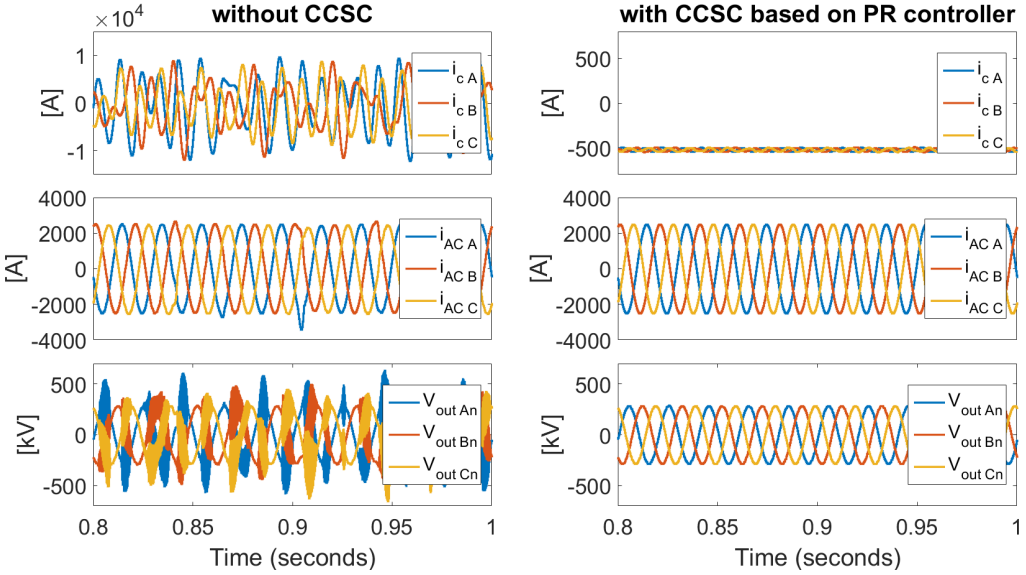


**Figure 5.5:** Circulating current and output currents and voltages without and with CCSC based on PR controllers

### 5.3.2. Outer Control Loop

The outer control loop of MMC generates the reference voltage for each phase that drives output currents. The outer control of MMC includes two steps for the generation of reference signals. The first step consists of DC voltage control, AC voltage control or power control block which are selected depending on the application of MMC and these blocks output the reference output currents. The second step of the outer control loop is the current control block which takes the reference currents generated by the first step and converts them to reference voltage values.

### Active and Reactive Power Control

The active and reactive power on the AC side of a three phase system and the power on the DC side can be calculated by (5.1–5.3) [72].

$$P_{AC_{ABC}} = V_{gA} i_{AC\_A} + V_{gB} i_{AC\_B} + V_{gC} i_{AC\_C} \tag{5.1}$$

$$Q_{AC_{ABC}} = \left(V_{gA} - V_{gB}\right) i_{AC\_C} + \left(V_{gB} - V_{gC}\right) i_{AC\_A} + \left(V_{gC} - V_{gA}\right) i_{AC\_B} \tag{5.2}$$

$$P_{DC} = V_{DC} I_{DC} \tag{5.3}$$

Instantaneous powers in dq reference frame can be expressed as in (5.4) and (5.5) using the three phase power equations.

$$P_{AC_{dq}} = V_{gd} i_{AC\_d} + V_{gq} i_{AC\_q} \tag{5.4}$$

$$Q_{AC_{dq}} = V_{gq} i_{AC\_d} - V_{gd} i_{AC\_q} \tag{5.5}$$

For a symmetric three phase system q component of the voltage is zero. Therefore, reference d and q components of the AC side currents can be obtained as in (5.6) and (5.7).

$$i_{AC\_d}^{ref} = \frac{P^{ref}}{V_{gd}} \tag{5.6}$$

$$i_{AC\_q}^{ref} = -\frac{Q^{ref}}{V_{gd}} \tag{5.7}$$

The resulting active and reactive power control structure is shown in Figure 5.6.

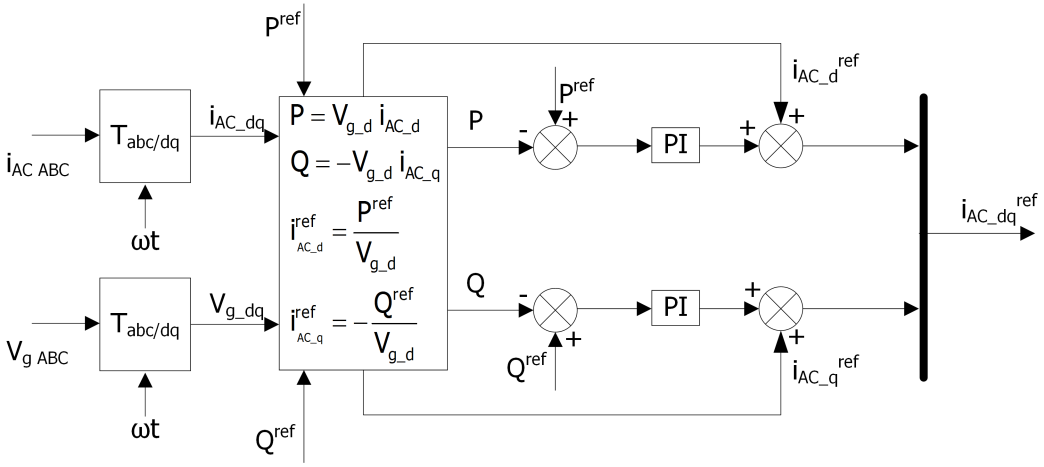


**Figure 5.6:** Active and reactive power controllers

In order to verify the accuracy of power control structure of MMC and the bidirectional power flow, reference power settings for active and reactive powers are changed from -1000 MW and -200 MVAR to 500 MW and 100 MVAR, respectively at t=0.5 s. As seen in Figure 5.7, the controller tracks the reference active and reactive power signals without any effect on output AC voltage. The output AC currents respond to power changes by reversing the direction and changing the amplitude.

According to (5.4–5.7), active and reactive powers depend on d and q axis of output currents, respectively while d axis voltage is common for both of them. dq axis voltages and currents are hence plotted in Figure 5.8 in order to verify that d and q axis currents are adjusted for the given power settings while dq axis voltages remain the same.

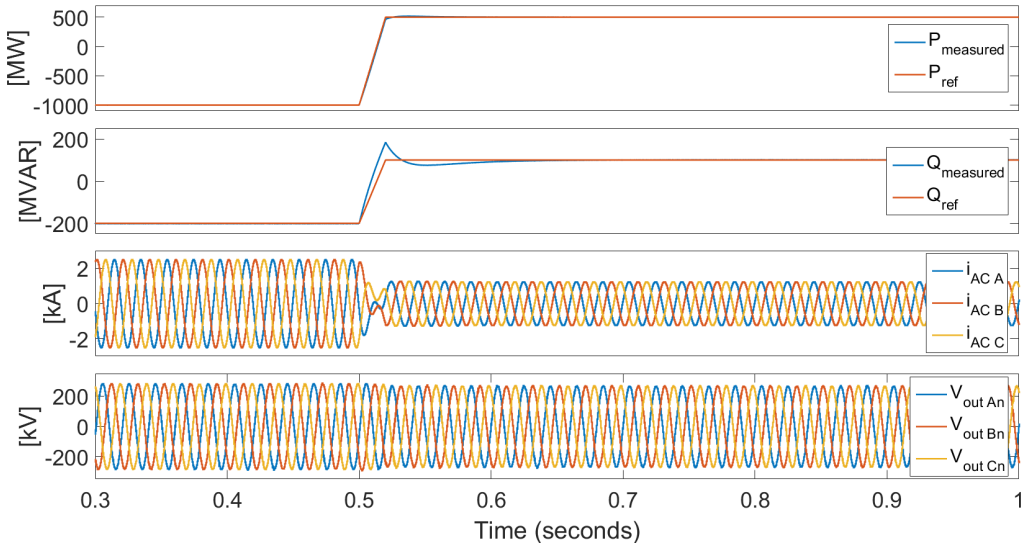


**Figure 5.7:** Active and reactive power response of the converter to power changes

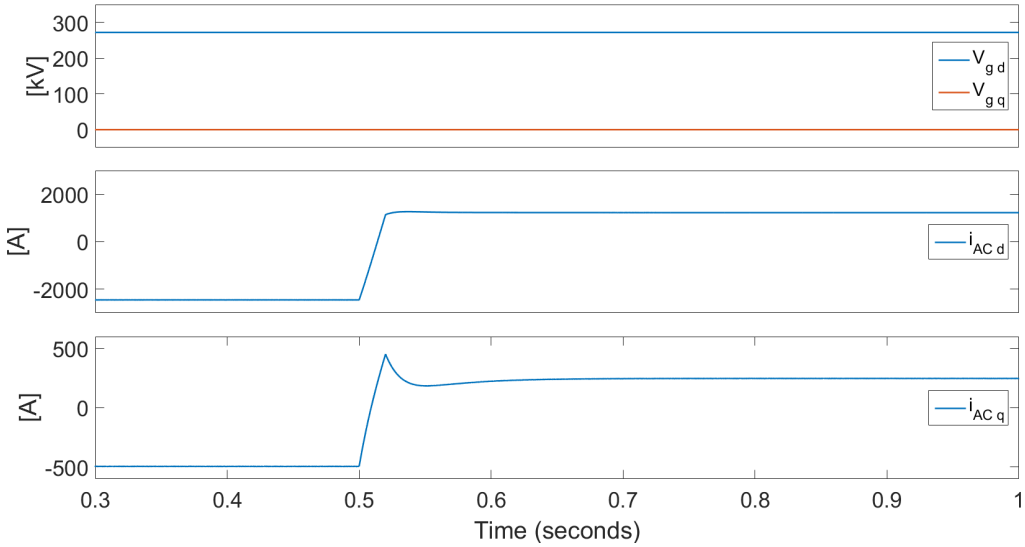


**Figure 5.8:** The response of dq axis voltages and currents to power changes

## AC Voltage Control

AC voltage at MMC terminals, $V_{ABC}$, can be controlled through AC voltage controller which provides the quadrature axis reference current, $i_q^*$. Therefore, it can be considered as an indirect way of reactive power control. The quadrature axis reference current is generated by comparing the rms value of reference voltages, $V_{ABC}^*$(rms), with the rms value of measured terminal voltages, $V_{ABC}$(rms), through a PI controller as shown in Figure 5.9 where the rms value of the voltage is calculated based on (5.8) [73].

$$V_{rms} = \sqrt{\frac{V_d^2 + V_q^2}{3}} \tag{5.8}$$

The response of the MMC to a 20% step change in AC voltage rms at t=0.5 s is presented in Figure 5.10 with the parameters given in Table 5.3. It should be noted that pu system is used in the

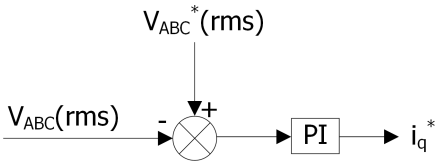


**Figure 5.9:** AC voltage controller

controllers.

**Table 5.3:** Design parameters for the AC voltage controller

| n (number of SM in one phase leg) | $K_P$ | $K_I$ | Change in AC rms voltage |
|---|---|---|---|
| 200 | 0.1 | 500 | 20% |

As expected, the amplitude of terminal voltages, $V_{ABC}$, decreases while the current amplitude increases in order to keep active power constant when the change is applied in AC rms voltage reference, $V^*_{ABC\ rms}$. The reactive power of the MMC increases due to the change in quadrature axis reference current which is the output of AC rms voltage controller.

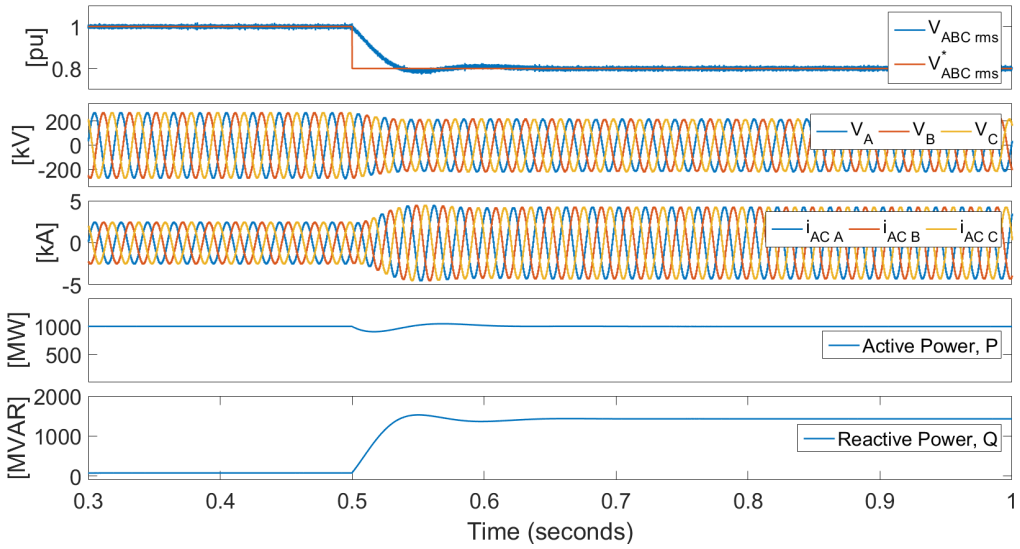


**Figure 5.10:** The response of the MMC to a step change in AC voltage rms at t=0.5 s

### Current Control

This step of the outer control loop has inputs of dq reference currents and it is required in order to generate the reference voltages, $e_{v\_ABC}{}^*$, that drive output currents of MMC and are used for the calculation of reference arm voltages as described in Section 5.3.2 (Generation of Reference Arm Voltages).

AC side dynamics of the converter can be defined as (5.9) where $i_{ABC}$ is the three phase AC side currents flowing out of converter phases.

$$V_{ABC} - V_{g\_ABC} = L_{out}\frac{di_{ABC}}{dt} + R_{out}i_{ABC} \tag{5.9a}$$

$$L_{out}\frac{di_{ABC}}{dt} = -R_{out}i_{ABC} + V_{ABC} - V_{g\_ABC} \tag{5.9b}$$

By means of Park's transform, three phase equations can be converted into dq axis reference frame as:

$$L_{out}\frac{di_d}{dt} = i_q\omega L_{out} - i_d R_{out} + V_d - V_{g\_d} \tag{5.10a}$$

$$L_{out}\frac{di_q}{dt} = -i_d\omega L_{out} - i_q R_{out} + V_q - V_{g\_q} \tag{5.10b}$$

The current control loop depicted in Figure 5.11 is constructed depending on (5.10a) and (5.10b).

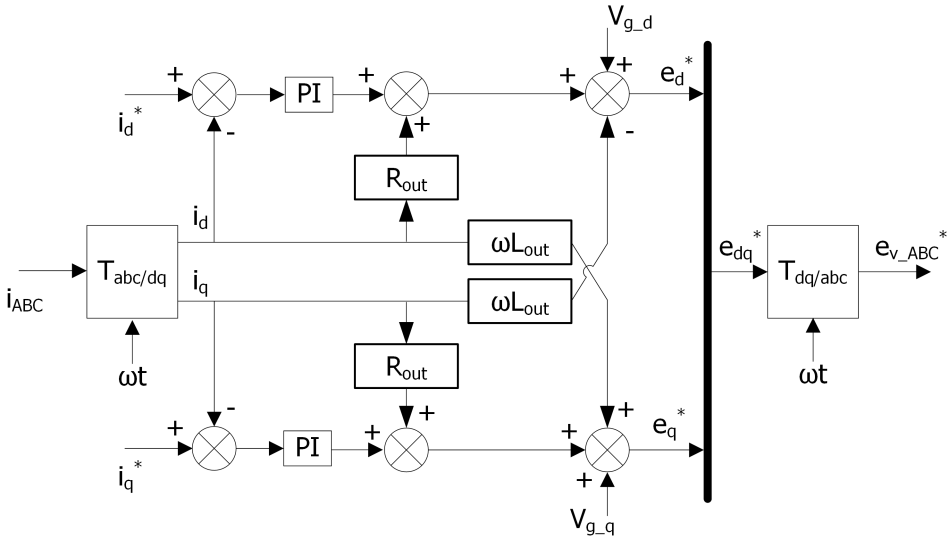


**Figure 5.11:** Current controler

**Tuning PI Controllers with Modulus Optimum Criteria**

Two PI controllers are used in current control block in order to adjust d and q axis currents to the reference values. These PI controllers are tuned based on modulus optimum (MO) criteria due to its simplicity and quick response [74, 75]. The current control loop can be represented as in Figure 5.12 by analysing the overall structure of MMC.

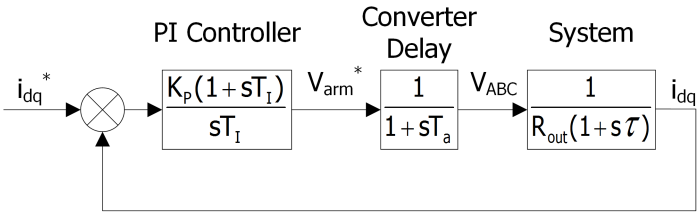


**Figure 5.12:** The general current control loop

In Figure 5.12, PI controller is modelled using proportional gain $K_P$ and integral time constant $T_I$=$K_P$/$K_I$. Converter delay represents the delay caused by switching of power electronic devices. Finally, the system is modelled using (5.9a–5.10b) where $\tau$=$L_{out}$/$R_{out}$ is the time constant of the AC network. Therefore, open loop transfer function of the current loop can be expressed as in (5.11).

$$G_{OL} = K_P\frac{1+sT_I}{sT_I}\frac{1}{1+sT_a}\frac{1}{R_{out}(1+s\tau)} \tag{5.11}$$

Proportional and integral gains of the PI controller are determined according to two main principles of MO criteria:

- Pole zero cancellation with the term having the largest time constant.
- Keeping the closed loop gain larger than or equal to unity for high frequencies.

Pole zero cancellation can be performed by defining the integral time constant $T_I=\tau$. The open loop transfer function of the current control loop after the first principle of MO criteria is applied can be expressed as in (5.12)

$$G_{OL} = \frac{K_P}{\tau R_{out}} \frac{1}{s\,(1+sT_a)} \tag{5.12}$$

Applying the second principle of MO criteria as in (5.13), proportional gain given in (5.14) is calculated.

$$\left|G_{CL}(j\omega)\right| = \left|\frac{G_{OL}(j\omega)}{1+G_{OL}(j\omega)}\right| = \left|\frac{K_P}{\tau R_{out} T_a (j\omega)^2 + \tau R_{out}(j\omega) + K_P}\right| = 1 \tag{5.13}$$

$$K_P = \frac{\tau R_{out}}{2T_a} \tag{5.14}$$

In order to verify the current control block, step response of d and q axis output currents are analysed in Figure 5.13. The reference value for the d axis current is changed at t=0.3 s from 0 to -1 kA while it is changed at t=0.6 s from 0 to 0.5 kA for q axis. As seen in the figure, the current change on one axis has almost no effect on the other one and currents track the reference signals.

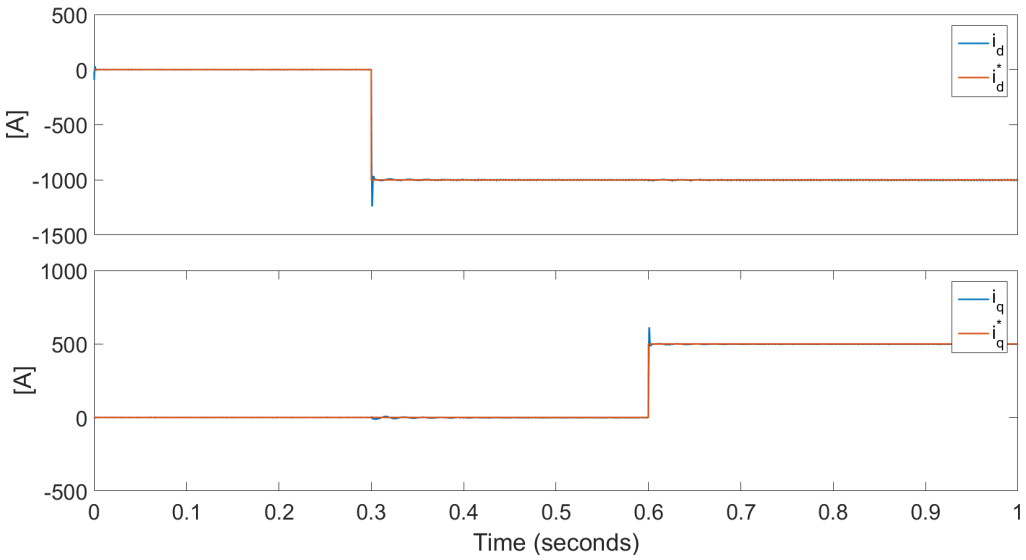


**Figure 5.13:** Step response of direct and quadrature axis currents

## Generation of Reference Arm Voltages

After the reference voltages that drive output currents and circulating currents, $e_{v\_ABC}^*$ and $u_{c\_ABC}^*$, are generated, reference arm voltages are required for the modulation block of MMC.

According to [66], circulating current of MMC has a relationship with DC and arm voltages as:

$$L_a \frac{di_{c\_ABC}}{dt} = \frac{V_{DC}}{2} - \frac{V_{u\_ABC} + V_{l\_ABC}}{2} \tag{5.15}$$

The left part of (5.15) is supposed as $u_{c\_ABC}$ and expressing $e_{v\_ABC}$ as (5.16), upper and lower arm voltages are obtained by summing and subtracting equations for $u_{c\_ABC}$ and $e_{v\_ABC}$.

$$e_{v\_ABC} = \frac{V_{l\_ABC} - V_{u\_ABC}}{2} \tag{5.16}$$

$$V^*_{u\_ABC} = \frac{V_{DC}}{2} - e_{v\_ABC} - u_{c\_ABC} \tag{5.17}$$

$$V^*_{l\_ABC} = \frac{V_{DC}}{2} + e_{v\_ABC} - u_{c\_ABC} \tag{5.18}$$

The overall control structure of MMC can be seen in Figure 5.14 including inner control, power control and current control blocks.

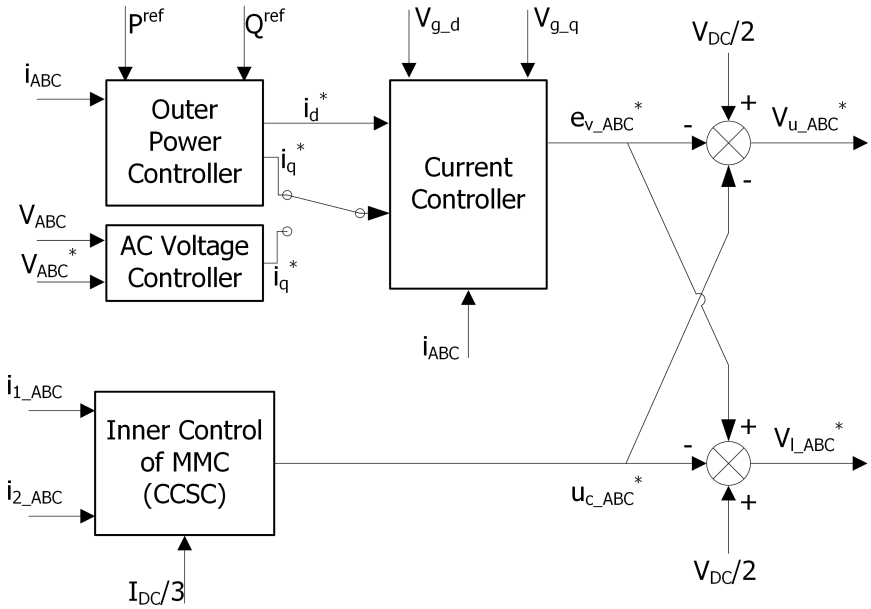


**Figure 5.14:** Overall control structure of MMC

# 6

# Front-to-Front Connected MMC without Galvanic Separation

*Front-to-front connection of two MMC without galvanic separation in DC/AC/DC configuration is implemented in this chapter in order to achieve a DC/DC converter. After the general control structure of the system is explained, simulation results are provided for the system having similar DC voltage levels and similar configurations with the purpose of power flow control.*

## 6.1. Control of DC/DC Converter in MMC Topology without Galvanic Isolation

The control algorithm of the DC/AC/DC converter is achieved such that one converter controls AC voltage on the middle AC stage while the other converter adjusts active and reactive power flow. Each converter has its own circulating current suppressing controller.

### 6.1.1. AC Voltage Controller

The amplitude and frequency of the AC voltage at the middle stage of DC/AC/DC converter are set by AC voltage controller. In order to obtain a three phase voltage on the AC side of the converter, one should apply a three phase sinusoidal signal with an amplitude of the base voltage of the system in desired frequency for $e_{v\_ABC}^{*}$. $\omega t$ used for the dq to abc transformation is generated by integrating $2\pi f$ angular frequency and it is used for the other dq/abc or abc/dq transformations. The control structure of the AC voltage controlled MMC is shown in Figure 6.1.

### 6.1.2. Power Flow Control

The power flow is controlled by the second converter thanks to outer power controllers. The structure of the power control block is the same with the one explained in Section 5.3.2 except the grid voltage. Since there is no AC grid represented by AC voltage sources in the simulations for DC/AC/DC case, the AC voltage is generated by the first converter as presented in Section 6.1.1. Therefore, the power flow control is performed by the second MMC which provides necessary AC currents in order to supply desired power while the AC voltage is adjusted by the other MMC.

The general control structure of the DC/AC/DC converter can be seen in Figure 6.2.

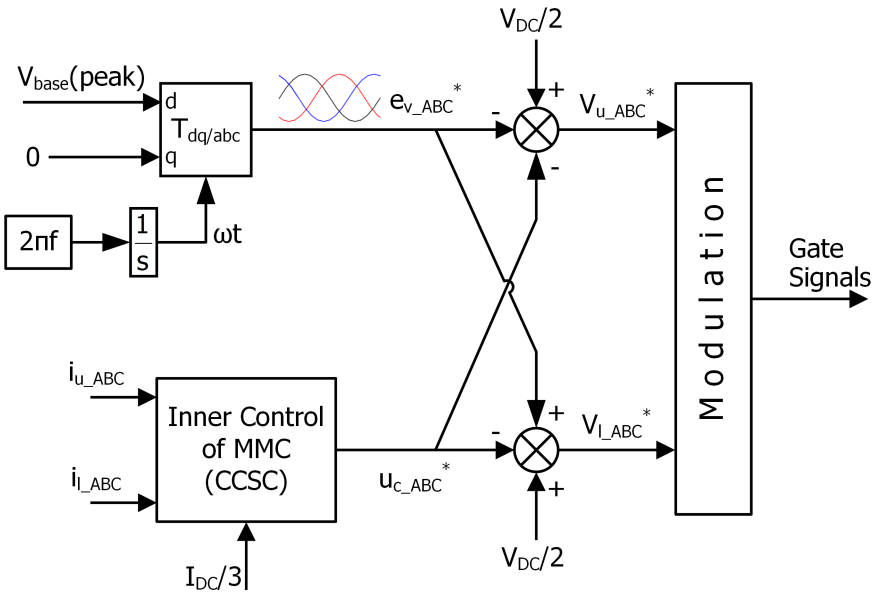


**Figure 6.1:** Control structure of the AC voltage controlled MMC

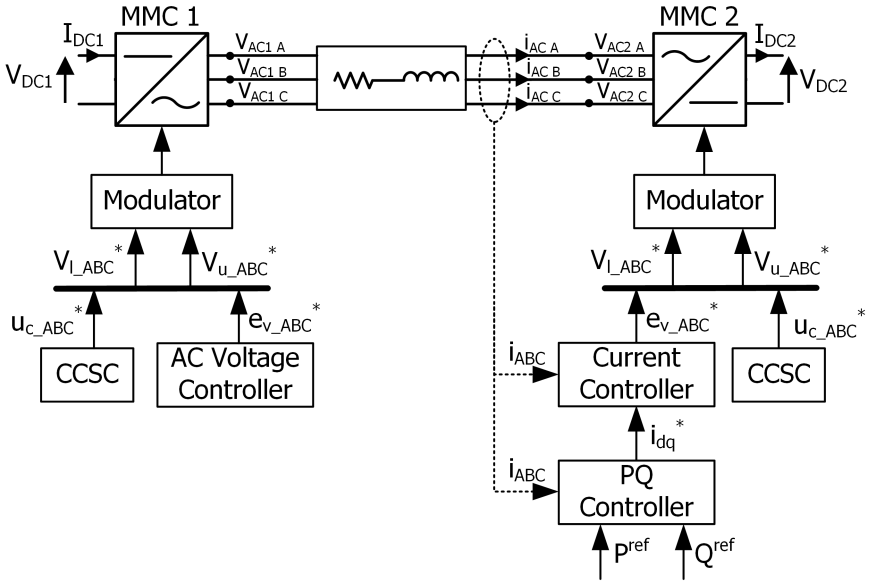


**Figure 6.2:** Control structure of DC/AC/DC converter in MMC topology without galvanic isolation

## 6.2. Simulation Results

The converter is simulated in Matlab/Simulink using controlled voltage sources-based model of MMC and nearest level modulation in order to control the power flow between two symmetrical monopole DC networks. The simulation parameters are shown in Table 6.1. Per unit system is used for the active and reactive power controllers and current controller.

In order to test the bidirectional power flow the active power reference is changed from -1000 MW to 500 MW at t=0.7 s. Reactive power flow reference is kept constant at 0 during the operation of DC/DC converter. The reference and measured DC active power and reactive power are shown in Figure 6.3.

**Table 6.1:** Design parameters for the simulation of DC/AC/DC converter

| | |
|---|---|
| **Apparent power, S** | 1200 MVA |
| **Number of submodules in one phase leg** | 200 |
| **Input voltage, $V_{DC1}$** | ±320 kV |
| **Output voltage, $V_{DC2}$** | ±320 kV |
| **AC voltage (line-to-line rms), $V_{AC}$** | 333 kV |
| **Frequency on AC side, f** | 50 Hz |
| **Submodule capacitance, C** | 2.5 mF |
| **Proportional gain of current controller for P, $k_P$** | 4 |
| **Proportional gain of current controller for Q, $k_P$** | 6 |
| **Integral time constant of current controller for P, $T_I$** | 0.04 |
| **Integral time constant of current controller for Q, $T_I$** | 0.004 |
| **Proportional gain of power controller for P and Q, $k_P$** | 10 |
| **Integral time constant of power controller for P, $T_I$** | 0.01 |
| **Integral time constant of power controller for Q, $T_I$** | 0.001 |
| **Proportional gain of CCSC, $k_P$** | 5 |
| **Resonant gain of CCSC, $k_r$** | 1000 |
| **Cut-off frequency of CCSC, $\omega_c$** | 0.5 rad/s |

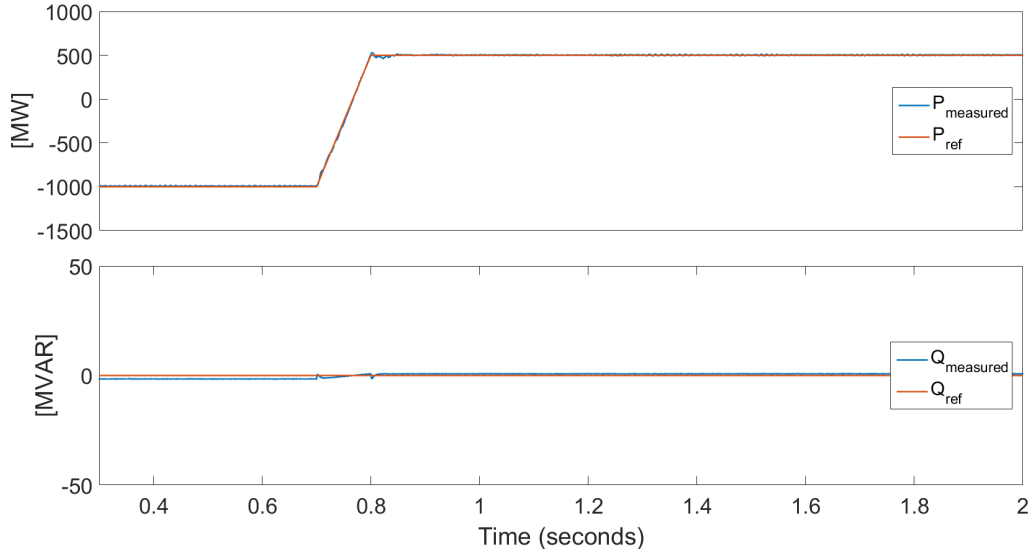


**Figure 6.3:** DC/DC converter response to the power change

As seen in Figure 6.3, active and reactive power tracks their reference values. The difference between the measured reactive power and the reference value results from the reactive power on the AC line inductors. As seen in the figure, the difference decreases when the magnitude of active power is decreased since the current has a lower amplitude during that time interval.

DC voltage and DC current plots are shown in Figure 6.4. As seen in the figure, the DC current changes its direction and magnitude in order to supply the power setting while the DC voltage is constant.

When the DC current plot is zoomed in, it can be seen that the operation of MMC generates current ripples. Figure 6.4 shows that the current ripple is only 3.8% (30 A peak-to-peak). In the real scenario, converters are connected to long DC cables and the current ripple can be damped on DC side by the capacitance and inductance of the DC cable [76].

Terminal AC voltage waveforms for both converters and the current waveform on the AC side are

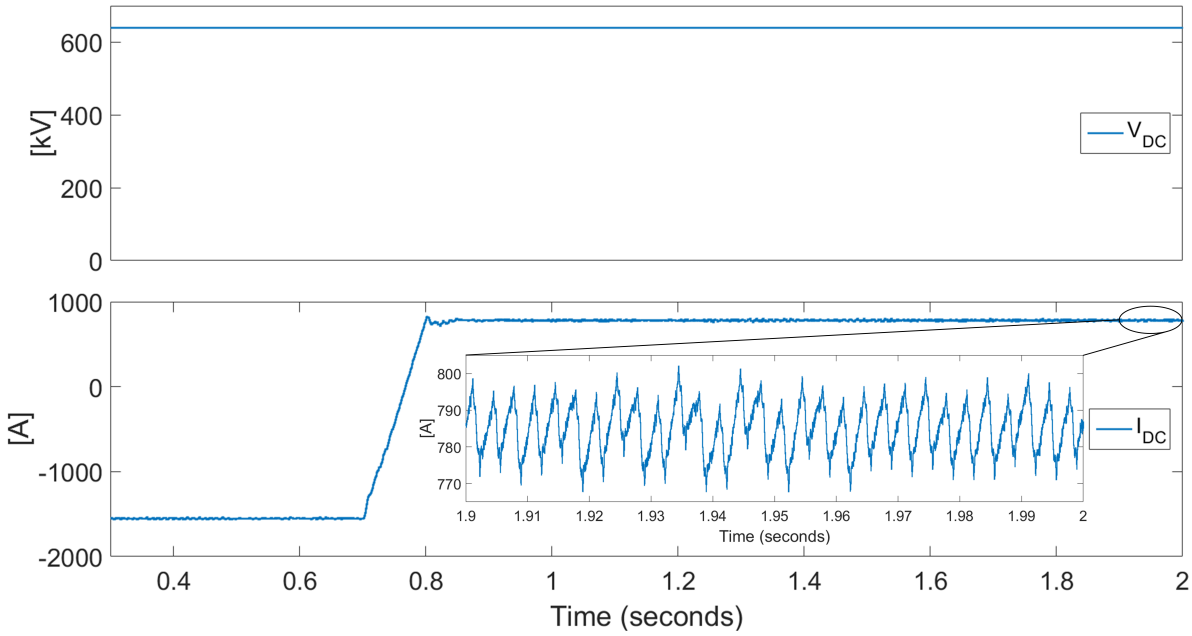


**Figure 6.4:** DC voltage and DC current in one terminal of DC/DC converter

shown in Figure 6.5. The first converter sets the amplitude and frequency of the AC voltage, while the other converter adjusts currents providing the power settings. Since the magnitude of the active power is decreased at t=0.7 s, the amplitude of the AC current decreases, too while the AC voltage is kept constant as seen in the figure. Moreover, sinusoidal waveforms of each plot have 120° phase difference between their phases and they are in 50 Hz as seen in the Figure 6.5. AC voltages have actually a stepwise waveform but it is not visible with this scale since there are 200 submodules on each phase which creates 200 steps on the waveform.

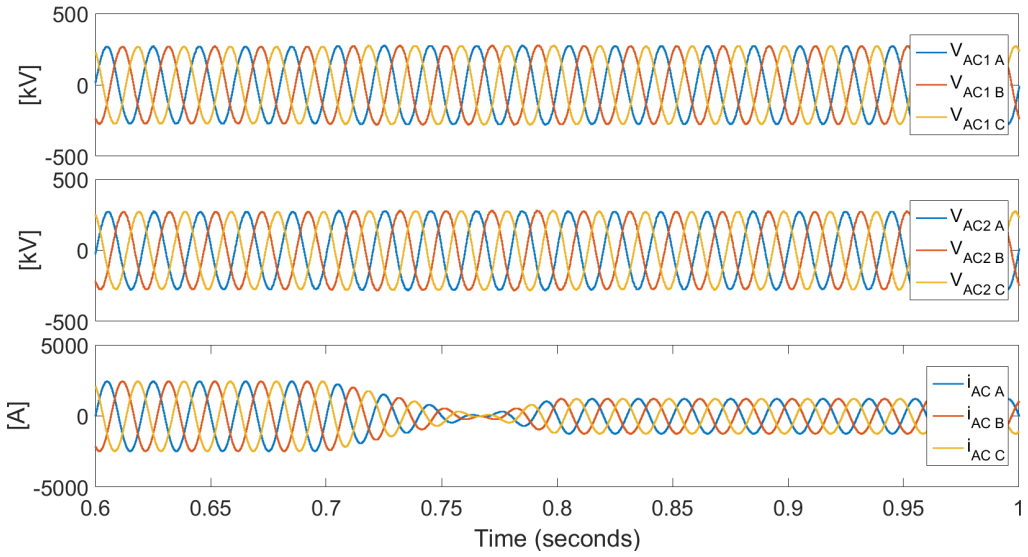


**Figure 6.5:** AC voltage waveforms in the AC terminals of both converters and the current waveform on the AC side

Upper and lower submodule capacitor voltages for both converters are also shown in Figure 6.6 in order to verify the proper operation of MMC and balancing algorithm. As seen in the figure, the

average level of the cell voltages is 1 pu at all power levels.

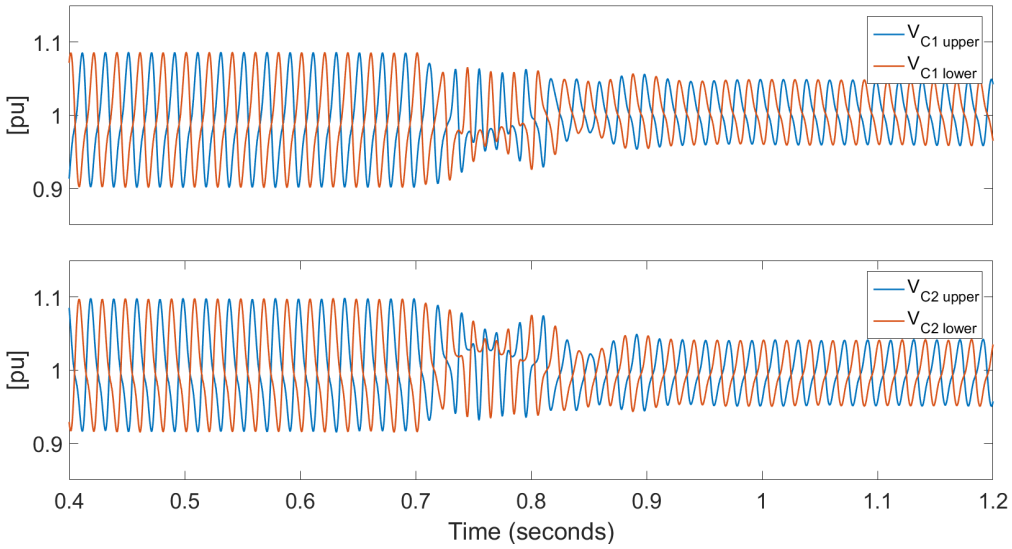


**Figure 6.6:** Upper and lower submodule capacitor voltages for MMC1 and MMC2

# 7

# Front-to-Front Connected MMC with Galvanic Separation

*Front-to-front connection of two MMC with galvanic separation in DC/AC/DC configuration is implemented in this chapter in order to interconnect dissimilar HVDC networks. Firstly, the control algorithm and simulation results for the interconnection of systems with different DC voltage levels are introduced. In addition, the topology is expanded for the interconnection of DC systems in different configurations and the control structure and simulation results are presented.*

## 7.1. Connection of DC Systems with Different Voltage Levels

Interconnection of DC networks operating in different voltage levels requires a DC/DC converter with medium or high voltage ratio. The voltage change can be performed on the AC side which is preferred in three phase arrangement in order to achieve high power levels. Such systems include two converters operating as an inverter or rectifier and an AC transformer. Y-Y connected two-winding transformer with grounded neutral is used for the implementation of the DC/DC converter in order to prevent from phase difference between primary and secondary sides of the transformer.

### 7.1.1. Control of DC/DC Converter in MMC Topology with Transformer Coupling

The control structure of the DC/DC converter connecting different voltage levels is similar to the one without galvanic separation except the transformer coupling on the AC side. One converter sets the AC voltage on one side of the transformer as explained in Section 6.1.1 while the other converter adjusts the active and reactive power flow using dq vector based control algorithm. The measurements for the active and reactive powers are taken from the secondary side of the transformer in the control algorithm used in simulations but it can also be taken from the primary side since the power is the same on both sides of the transformer. Each MMC includes its own circulating current suppressing controller together with balancing algorithm for cell capacitors in the modulation block. The control structure of medium or high voltage ratio DC/DC converter in MMC topology with transformer coupling is shown in Figure 7.1. It should be noted that transformer winding resistance and reactance values are used in the current controller block instead of AC line resistance and inductances for the generation of $e_{v\_ABC}^{*}$.

### 7.1.2. Simulation Results

The DC/DC converter used for interconnection of symmetric monopole systems with different voltage levels is simulated in Matlab/Simulink using controlled voltage sources-based MMC model and nearest

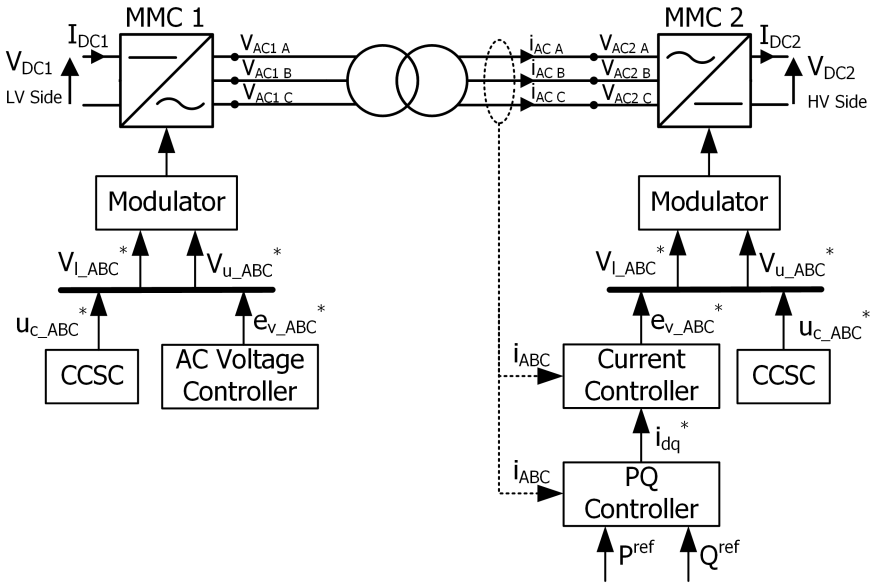


**Figure 7.1:** Control structure of transformer coupled DC/AC/DC converter in MMC topology

level modulation technique. The simulation parameters are shown in Table 7.1 and Table 7.2 for the transformer and both converters, respectively. Per unit system is used in CCSC of both converters and power and current controllers of the second converter.

**Table 7.1:** Design parameters of the transformer used in the simulation of DC/AC/DC converter

| | |
|---|---|
| **Nominal power** | 1200 MVA |
| **Nominal line-to-line voltages, $V_1$, $V_2$ (rms)** | 166.5 kV , 333 kV |
| **Turns ratio** | 1:2 |
| **Frequency** | 50 Hz |
| **Type** | Y-Y grounded neutral two-winding |
| **Resistance** | 1 mΩ |
| **Reactance** | 0.18 pu |

**Table 7.2:** Design parameters of the converters used in the simulation of DC/AC/DC converter with transformer coupling

| | **MMC1** | **MMC2** |
|---|---|---|
| **Apparent power, S** | 1200 MVA | 1200 MVA |
| **Number of submodules in one phase leg** | 200 | 200 |
| **DC voltage, $V_{DC}$** | ±160 kV | ±320 kV |
| **AC voltage (line-to-line rms), $V_{AC}$** | 166.5 kV | 333 kV |
| **Frequency on AC side, f** | 50 Hz | 50 Hz |
| **Submodule capacitance, C** | 10 mF | 2.5 mF |
| **Proportional gain of current controller for P, $k_P$** | | 4 |
| **Proportional gain of current controller for Q, $k_P$** | | 6 |
| **Integral time constant of current controller for P, $T_I$** | | 0.04 |
| **Integral time constant of current controller for Q, $T_I$** | | 0.004 |
| **Proportional gain of power controller for P and Q, $k_P$** | | 10 |
| **Integral time constant of power controller for P, $T_I$** | | 0.01 |
| **Integral time constant of power controller for Q, $T_I$** | | 0.001 |
| **Proportional gain of CCSC, $k_P$** | 0.06 | 0.06 |
| **Resonant gain of CCSC, $k_r$** | 5 | 5 |
| **Cut-off frequency of CCSC, $\omega_c$** | 5 rad/s | 5 rad/s |

It should be noted that the submodule capacitance value of the converter on low voltage side

(MMC1) is increased 4 times for the proper operation of MMC according to equation (4.33b) since the nominal cell voltage, $V_{C_{nom}}$, decreases to half of its former value when the voltage rating is decreased by half. The other method in order to keep the proper operation of MMC is by decreasing the number of submodules in an arm by half so that the nominal cell voltage, $V_{C_{nom}}$, becomes the same with previous case. The capacitance value of the cell capacitors must be increased to two times of its previous value in this case since it is inversely proportional with the number of submodules.

The bidirectional power flow is tested by changing the magnitude and direction of the power reference. The active power reference is switched from -500 MW to 1000 MW at t=1 s while the reactive power reference is kept constant at 0. The active power measured on DC side ($V_{DC}I_{DC}$) and the reactive power are shown in Figure 7.2 and Figure 7.3 for both low voltage and high voltage sides of the converter together with power references.

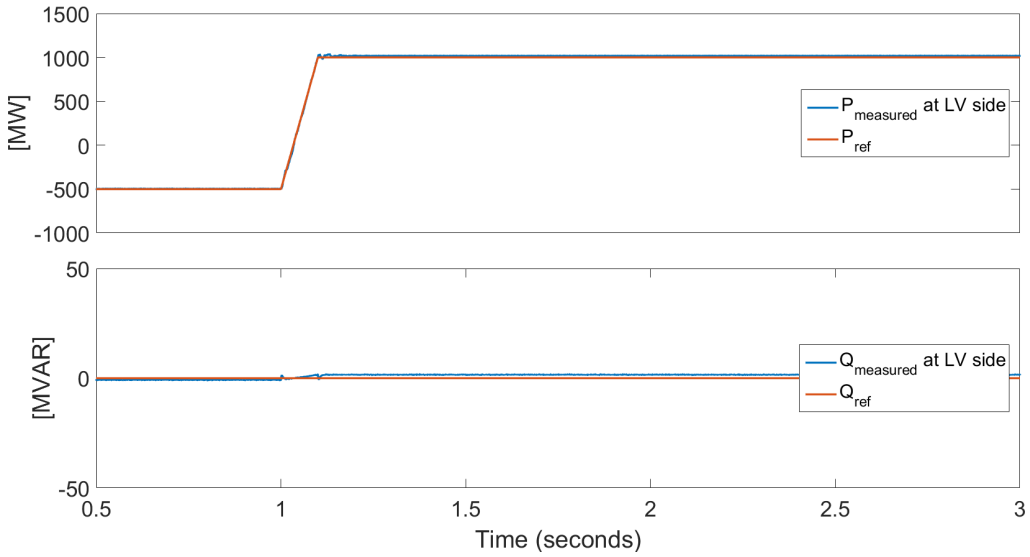


**Figure 7.2:** Response to the power change on the low voltage side of the converter

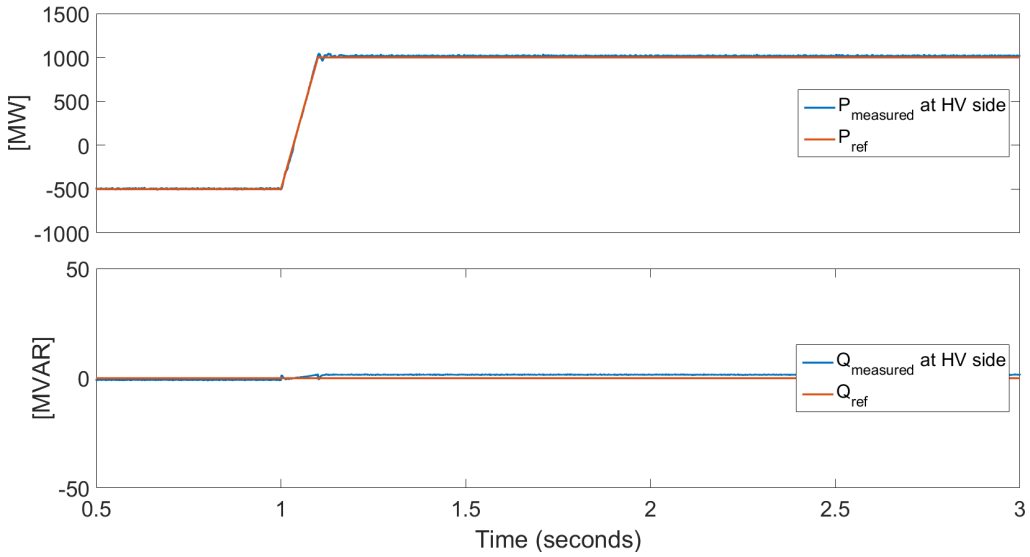


**Figure 7.3:** Response to the power change on the high voltage side of the converter

Active and reactive powers are almost the same in both Figure 7.2 and Figure 7.3 and they track

their reference values. The reactive power is slightly affected by the active power change, since the change in the magnitude of active power results in the change in AC side currents, too. Therefore, the change of the AC side currents causes difference in the reactive power on transformer inductances. This is the main reason for the slight difference between measured reactive power and the reference. As it can be seen in the figure, the increase in the active power at t=1 s, causes an increase in the difference between measured and reference value since the current amplitude increases, too.

DC voltage and current plots for both low voltage and high voltage sides are shown in Figure 7.4 and Figure 7.5, respectively. As seen in both figures, the DC current changes its direction and magnitude in order to set the active power demand while the DC voltages are kept constant.

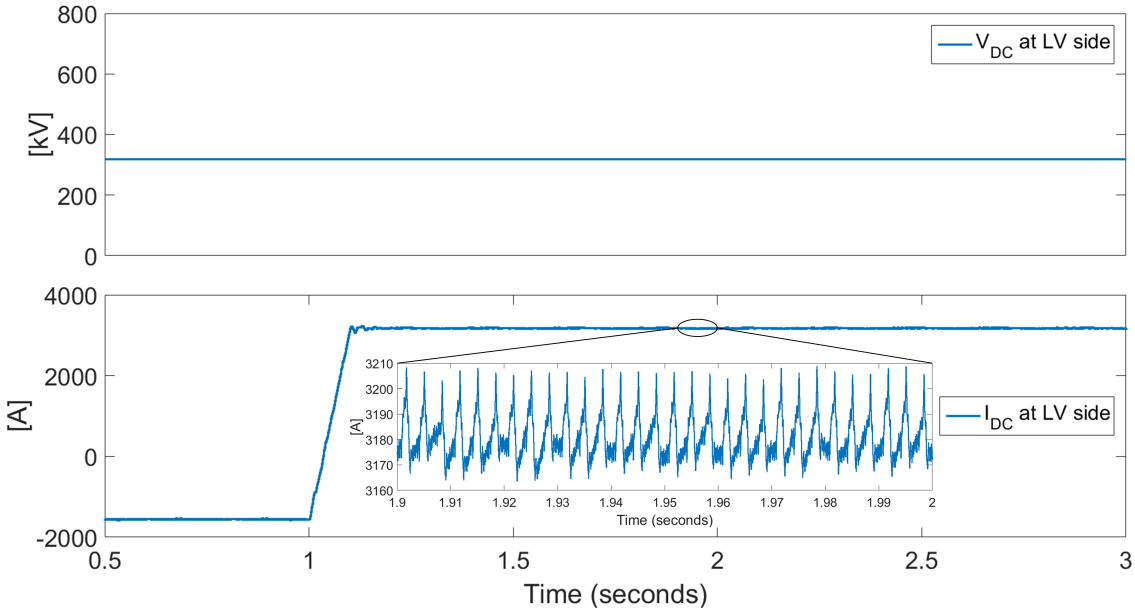


**Figure 7.4:** DC voltage and current on the low voltage side of the converter

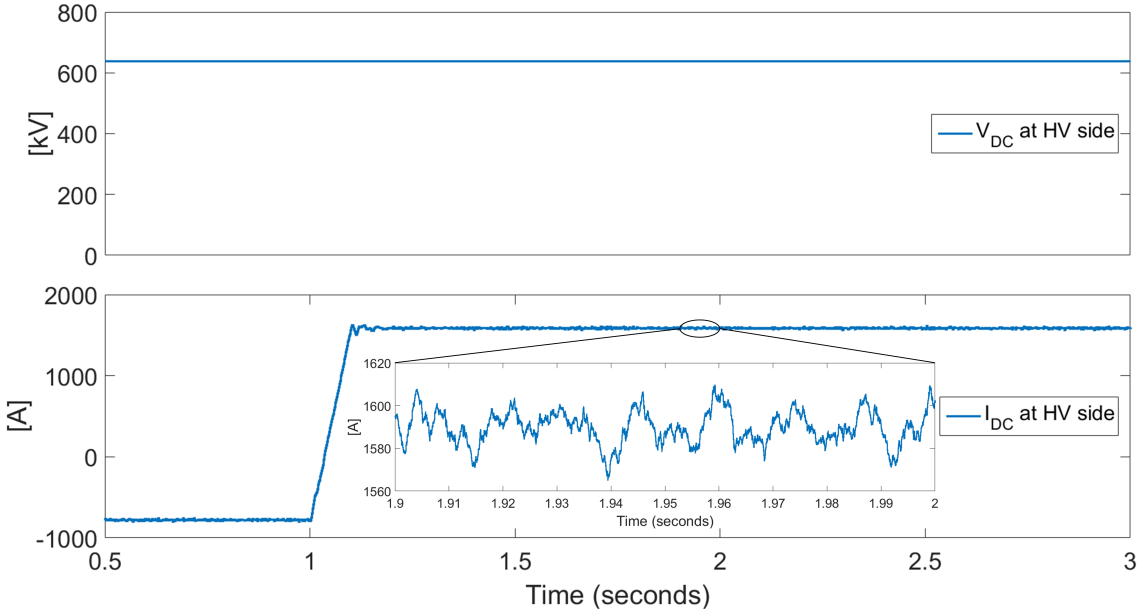


**Figure 7.5:** DC voltage and current on the high voltage side of the converter

As seen in Figure 7.4, the DC voltage on the low voltage side is constant at 320 kV while the current

has higher values than high voltage side and it slightly oscillates due to the operation of the MMC as seen in the zoomed in current plot. The figure shows that the current ripple is only % 1.2 (40 A peak-to-peak). Figure 7.5 presents that the DC voltage on the high voltage side has a constant value at 640 kV while the current is lower than low voltage side and there is a current ripple of % 2.5 (40 A peak-to-peak) because of converter operation.

Three phase AC voltage and current plots on low voltage and high voltage side of the converter are shown in Figure 7.6 and Figure 7.7, respectively. The magnitude and the frequency of the AC voltage is set by the first converter on the low voltage side while the AC current is adjusted according to power demand of the system. When both figures are compared, it can be clearly seen that transformer operates properly with a voltage ratio of 1:2. Since the magnitude of the active power increases at time t=1 s, the amplitude of the AC current increases at that time instant. Moreover, it is evident in both Figure 7.6 and Figure 7.7 that sinusoidal AC voltages and currents are in 50 Hz and the waveforms of each plot have 120° phase difference between their phases.

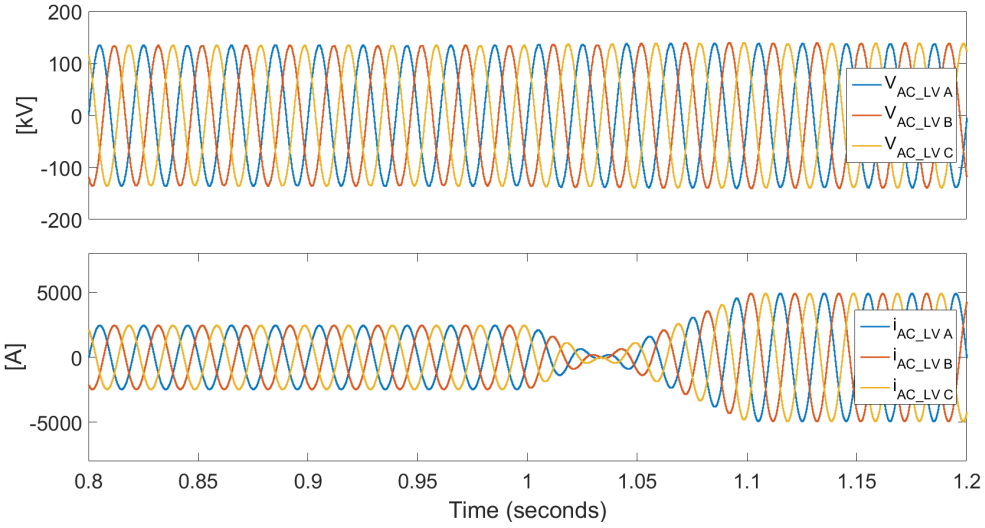


**Figure 7.6:** AC voltage and current on the low voltage side of the converter

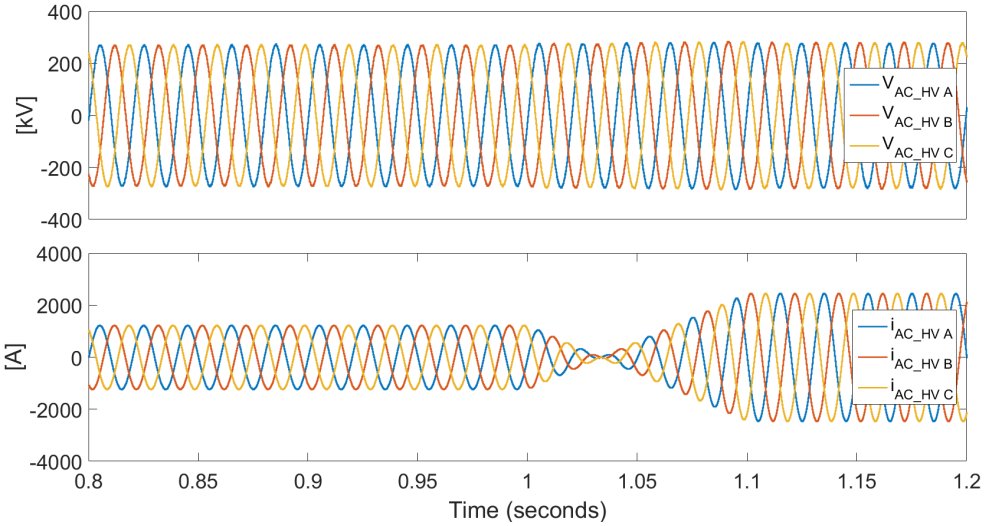


**Figure 7.7:** AC voltage and current on the high voltage side of the converter

Submodule capacitor voltages for the upper and lower arms of voltage controlled converter and

power controlled converter are shown in Figure 7.8 in order to check the proper operation of MMC and balancing algorithm. The figure presents that the average value of the submodule voltages are at 1 pu voltage level during all operation states.

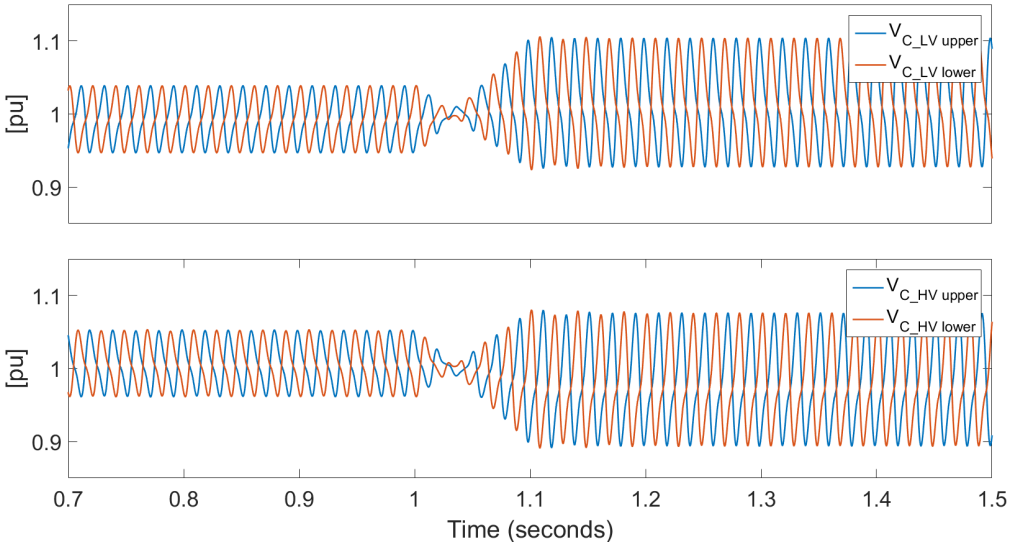


**Figure 7.8:** Upper and lower arm submodule voltages of MMC1 and MMC2

## 7.2. Connection of DC Systems with Different Configurations

For the future multi-terminal HVDC grid, interconnection of different type of DC networks is required. These connections can be among bipolar systems, asymmetric monopole systems or symmetric monopole systems as shown in Figure 7.9.

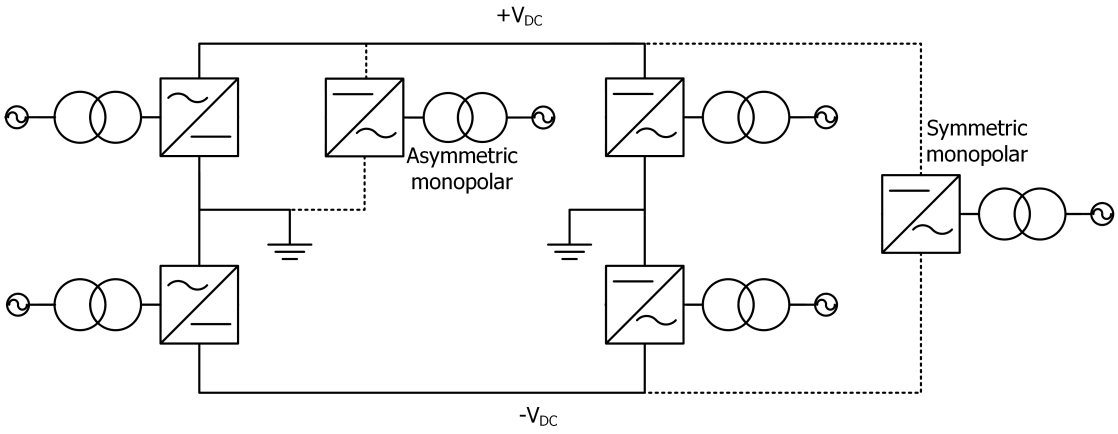


**Figure 7.9:** Interconnection of different HVDC configurations

However, DC links cannot be connected directly as shown in Figure 7.9. DC/DC converter with transformer coupling is an essential component for the interconnection of DC networks operating in different configurations which also provides the medium or high voltage steps between two DC systems.

The interconnection of bipolar and monopole HVDC networks can be performed by two-winding transformers or a three-winding transformer.

### 7.2.1. Interconnection by Two-Winding Transformers

In this topology for the interconnection of bipolar and monopole systems, DC/DC converter includes two separate two-winding transformers and four MMC. A return path on the neutral point of the converters is used on the bipolar side in order to keep continuous operation of the healthy pole by creating a path for the current to flow during the outage of one pole. Recently, ground electrodes are used as a return path; however, the power transmission systems may be affected by the flow of DC current to the ground resulting in corrosion of saturation of transformers. A neutral conductor instead of a ground electrode can be a solution for such problems in order to ensure a path for the current flow [77, 78].

#### Control Structure

Control of DC/AC/DC converter using two two-winding transformers includes AC voltage controllers and power controllers. The converters on the monopole side set the AC voltage while the converters on bipolar side adjust power flow by supplying the required currents for the desired power level. The control structure is shown in Figure 7.10.

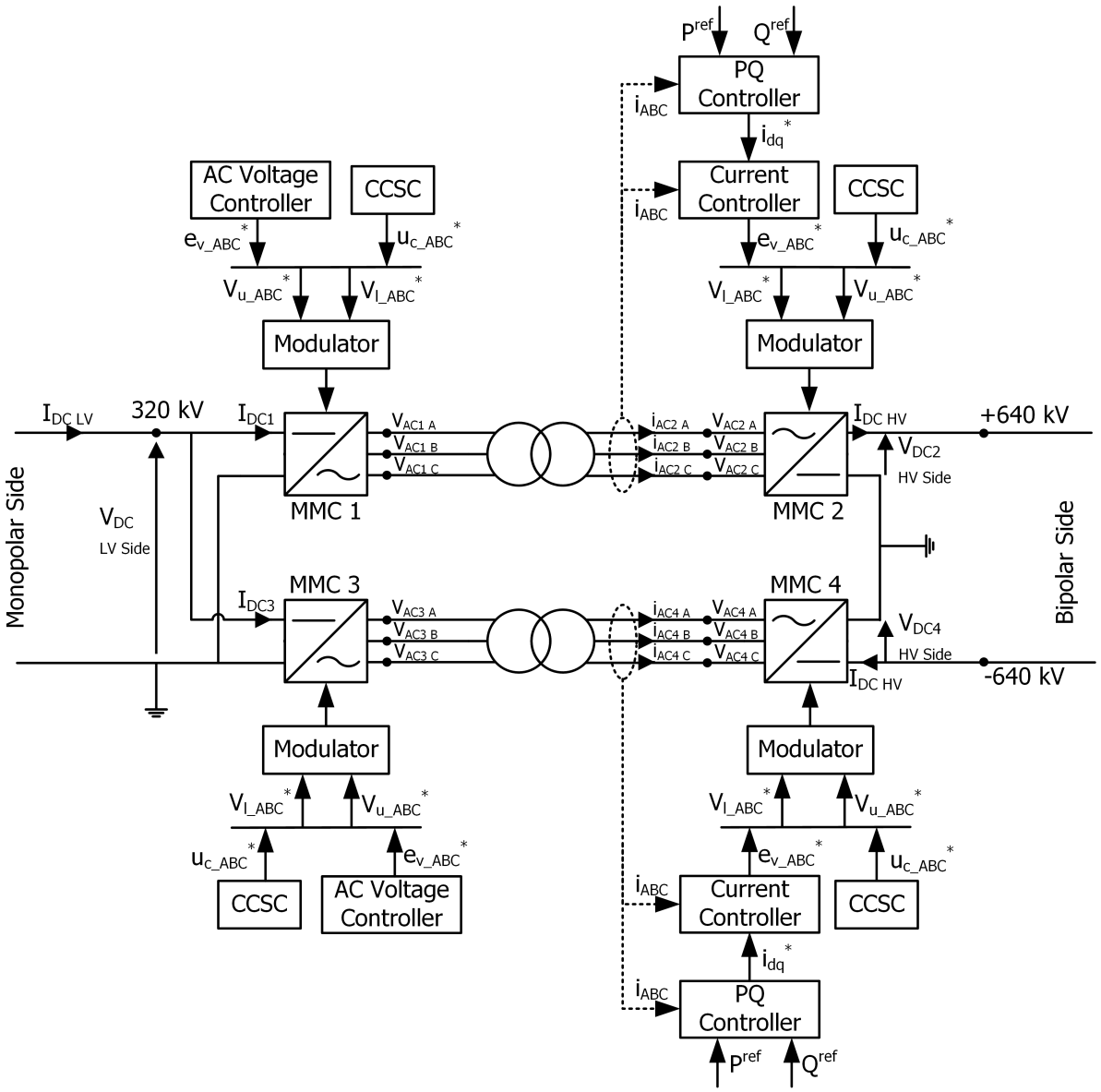


**Figure 7.10:** Interconnection by two-winding transformers

### Simulation Results

The interconnection of different HVDC schemes using two-winding transformers is simulated in Matlab/Simulink. The low voltage side is adjusted as asymmetric monopole configuration while the high voltage side is a bipolar HVDC system. As shown in Figure 7.10, the current on the monopole side is separated into two which halves the power rating of the converters. Simulation parameters for the transformers and converters are given in Table 7.3 and Table 7.4.

**Table 7.3:** Design parameters of the two-winding transformers used in the simulation of DC/AC/DC converter

| | |
|---|---|
| **Nominal power** | 600 MVA |
| **Maximum phase voltages, $V_1$, $V_2$ (max)** | 320 kV , 640 kV |
| **Turns ratio** | 1:2 |
| **Frequency** | 50 Hz |
| **Type** | Two-winding Y-Y |
| **Resistance** | 1 mΩ |
| **Reactance** | 0.18 pu |

**Table 7.4:** Design parameters of the converters used in the simulation of DC/AC/DC converter with two-winding transformers (MMC 1 and 3 are on the monopole side, MMC 2 and 4 are on the bipolar side)

| | **MMC 1, 3** | **MMC 2, 4** |
|---|---|---|
| **Power, P** | 500 MW | 500 MW |
| **Number of submodules in one phase leg** | 200 | 200 |
| **DC voltage, $V_{DC}$** | 320 kV | ±640 kV |
| **AC voltage (phase max), $V_{AC}$** | 320 kV | 640 kV |
| **Frequency on AC side, f** | 50 Hz | 50 Hz |
| **Submodule capacitance, C** | 5 mF | 2.5 mF |
| **Proportional gain of current controller for P, $k_P$** | | 4 |
| **Proportional gain of current controller for Q, $k_P$** | | 6 |
| **Integral time constant of current controller for P, $T_I$** | | 0.04 |
| **Integral time constant of current controller for Q, $T_I$** | | 0.004 |
| **Proportional gain of power controller for P and Q, $k_P$** | | 10 |
| **Integral time constant of power controller for P, $T_I$** | | 0.01 |
| **Integral time constant of power controller for Q, $T_I$** | | 0.001 |
| **Proportional gain of CCSC, $k_P$** | 0.02 | 0.02 |
| **Resonant gain of CCSC, $k_r$** | 0.8 | 0.8 |
| **Cut-off frequency of CCSC, $\omega_c$** | 80 rad/s | 80 rad/s |

The power flow is tested by changing the total active power reference from -1000 MW to 500 MW (-500 MW to 250 MW for each converter) at t=1.5 s while the reactive power is kept at 0. Figure 7.11 shows the power plots for one of the converters on both monopole and bipolar sides. As seen in the Figure, each converter carries half of the total power of the system.

Figure 7.12 shows DC voltages and currents on both monopole and bipolar sides. DC currents change their direction and magnitude in order to meet the active power demand as seen in the figure.

Three phase AC waveforms on each side of the transformer are shown in Figure 7.13. AC voltage is set by the converters on the monopole side, while the currents are adjusted by the converters on the bipolar side in order to meet the power demand of the system. Since there is an active power change at t=1.5 s, the magnitude of the AC current changes at this time instant while the voltage is kept constant.

Upper and lower arm cell voltages of the converters are shown in Figure 7.14 in order to check the proper operation of MMC. Submodule capacitor voltages have 1 pu average value during all operation states as seen in the figure.

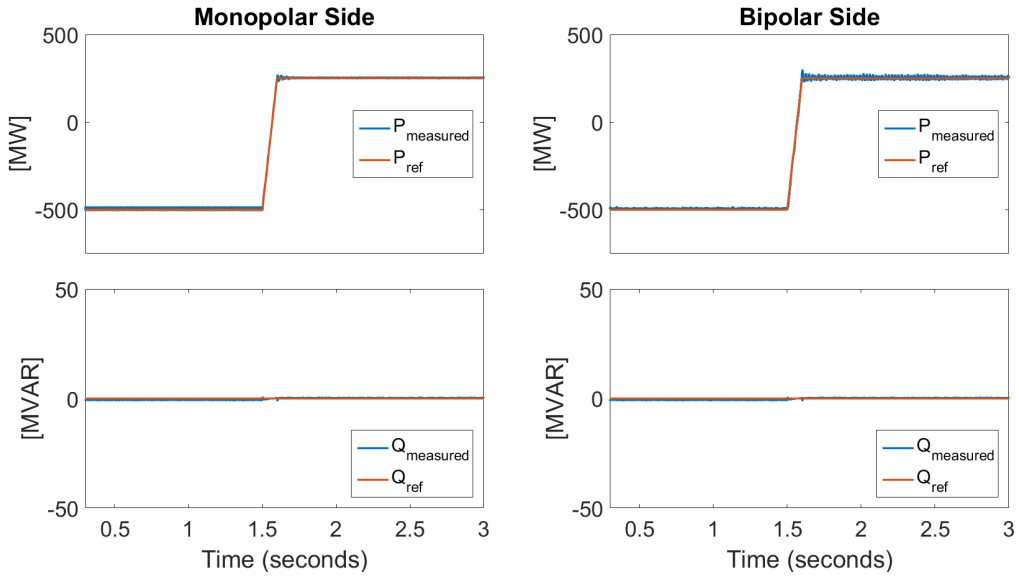


**Figure 7.11:** Power flow in one of the converters on monopole and bipolar sides

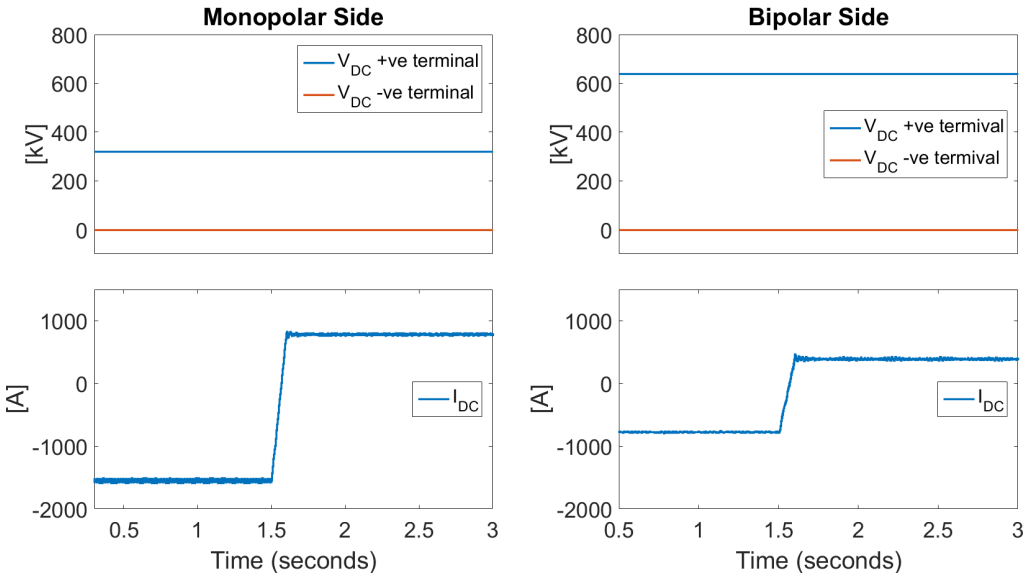


**Figure 7.12:** DC voltages and currents of one of the converters on monopole and bipolar sides

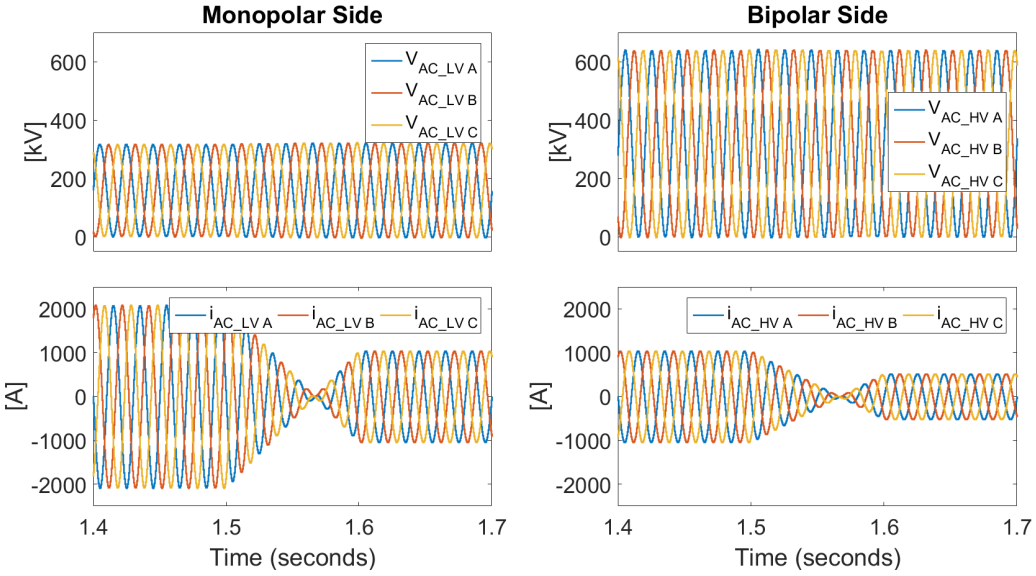


**Figure 7.13:** AC voltages and currents on both side of the one of the transformer

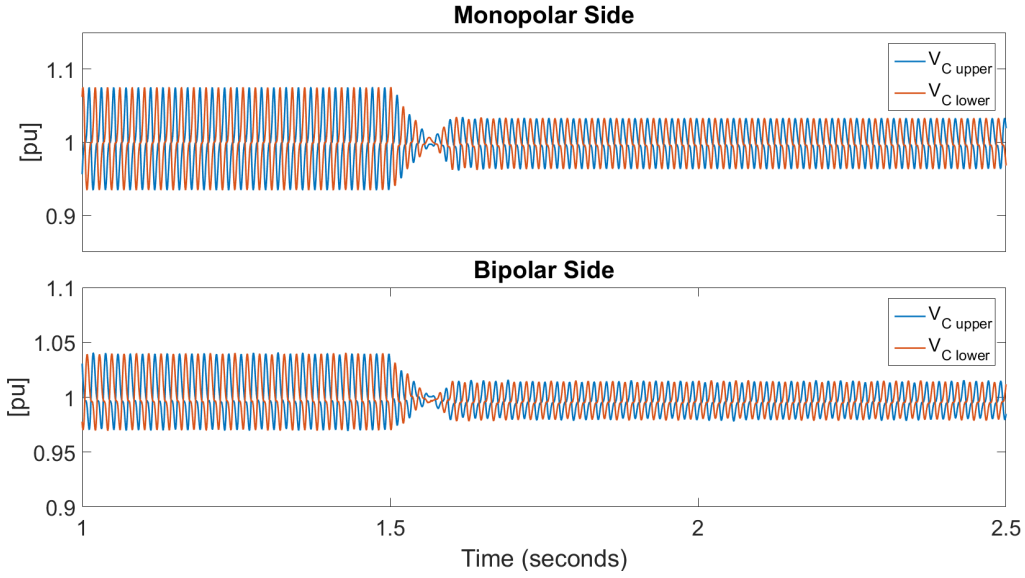


**Figure 7.14:** Upper and lower submodule capacitor voltages of MMC

### 7.2.2. Interconnection by a Three-Winding Transformer

The interconnection of bipolar and monopole systems can be performed by a three-winding transformer instead of two two-winding transformers. This system includes 3 MMC (2 on bipolar side, 1 on monopole side) and a three-winding transformer, which decreases the number of components and thus the footprint size and investment costs of the converter station compared to use of two two-winding transformers with 4 MMC.

#### Control Structure

Similar to converter with two-winding transformers, connection via a three-winding transformer includes

AC voltage controlled and power controlled MMC. The MMC on the monopole side controls the three phase AC voltage in the middle stage while two converters on the bipolar side controls power flow. Each converter has its circulating current suppressing controller. Control structure of the system with a three-winding transformer is shown in Figure 7.15.

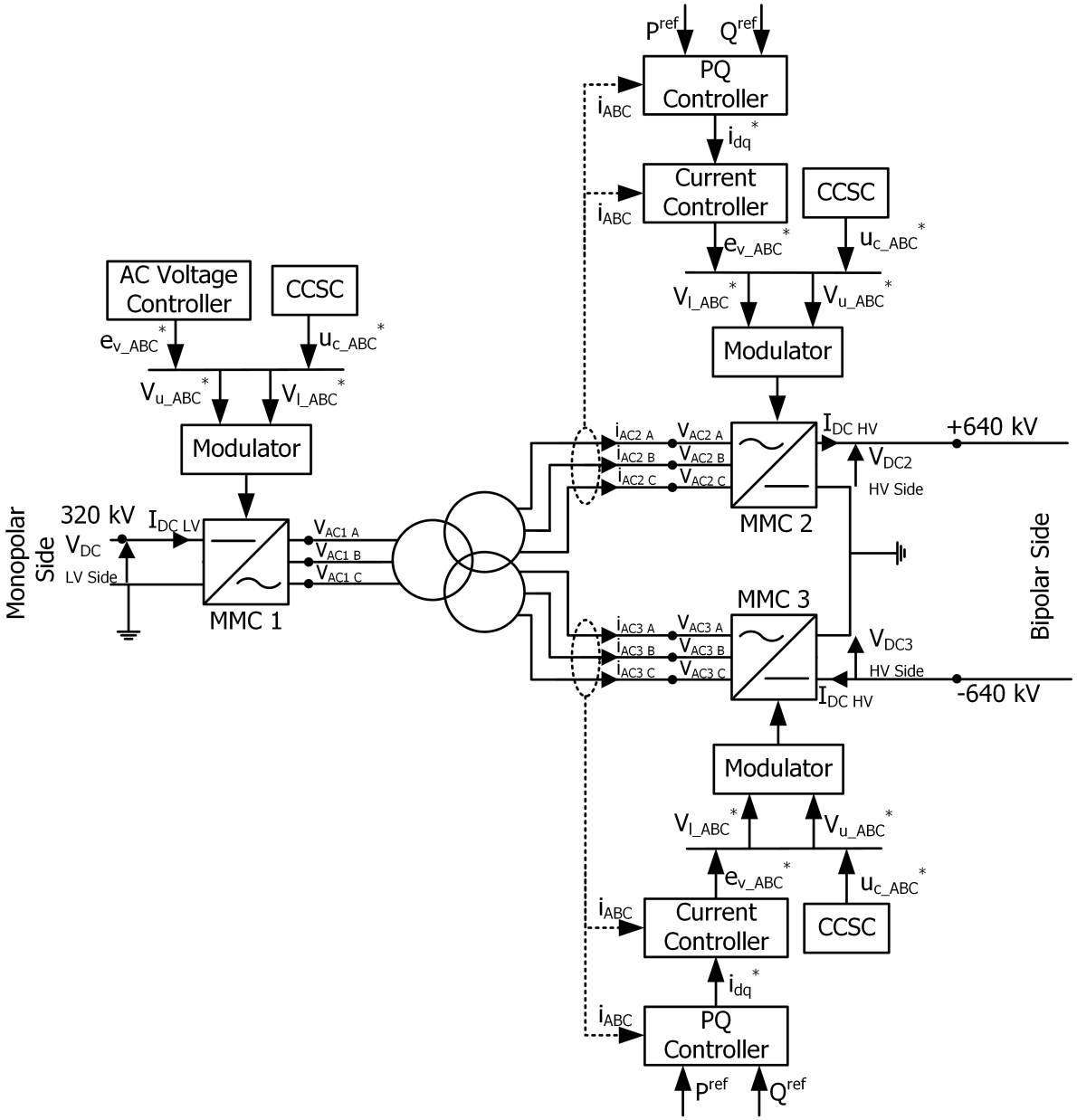


**Figure 7.15:** The control structure of the DC/AC/DC converter with a three-winding transformer

### Simulation Results with a Fault on Bipolar Side

The simulation of the DC/DC converter connecting bipolar and monopole HVDC networks is performed in order to test independent power flow on both poles of bipolar side and verify the ability of power flow even though one pole is out of service. During the true operation of the system, half of the power is supplied by two converters on the bipolar side while the converter on the monopole side should be able to carry the total power. One of the poles of bipolar side may be disconnected due to a fault in the converter or a maintenance on the link. In this situation, half of the power flow should still be

achieved by the healthy pole without changing any power settings. If the total power flow has to be kept constant, the power demand from the healthy pole can be doubled. Changes in the converter and transformer parameters are shown in Table 7.5 and Table 7.6 while the other parameters are kept the same with Table 7.4.

**Table 7.5:** Design parameters of the converters used in the simulation of DC/AC/DC converter with three-winding transformers

| | **MMC (monopole)** | **MMC (bipolar)** |
|---|---|---|
| **Power, P** | 1000 MW | 500 MW |
| **Submodule capacitance, C** | 10 mF | 2.5 mF |
| **Proportional gain of CCSC, $k_P$** | 0.02 | 0.02 |
| **Resonant gain of CCSC, $k_r$** | 0.8 | 5 |
| **Cut-off frequency of CCSC, $\omega_c$** | 80 rad/s | 5 rad/s |

**Table 7.6:** Design parameters of the three-winding transformers used in the simulation of DC/AC/DC converter

| | |
|---|---|
| **Nominal power** | 1200 MVA |
| **Maximum phase voltages, $V_1$, $V_2$ (max)** | 320 kV , 640 kV |
| **Turns ratio** | 1:2 |
| **Frequency** | 50 Hz |
| **Type** | Three-winding Y-Y |
| **Resistance** | 1 mΩ |
| **Reactance** | 0.18 pu |

In order to verify the above mentioned scenario, the total active and reactive power are kept constant at 1000 MW and 0, respectively, and one of the poles of bipolar side is disconnected at t=1 s as seen in Figure 7.16. No change on the power reference is applied till t=2 s while power reference of the healthy pole is doubled at t=2 s in order to meet the total power requirement of the system.

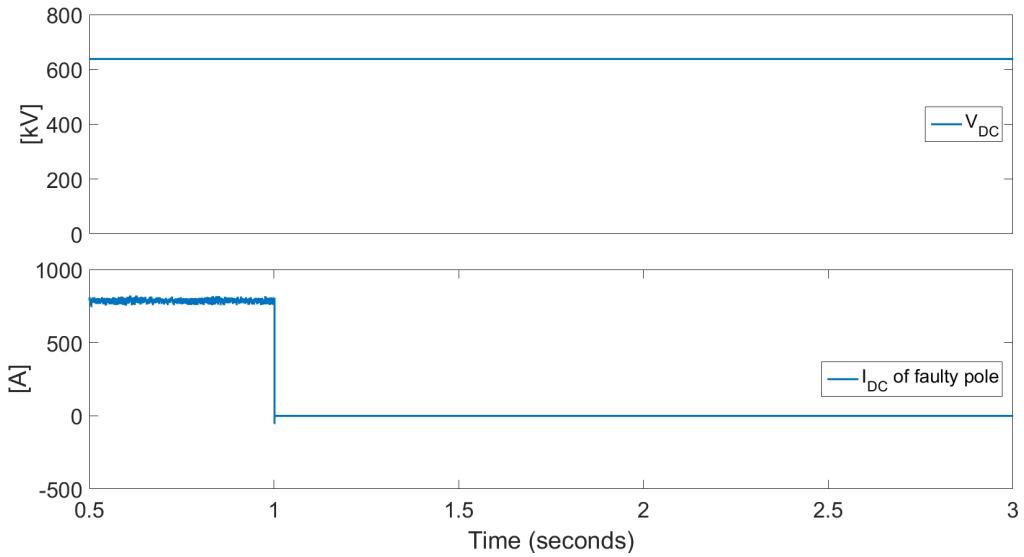


**Figure 7.16:** DC voltage and current on the faulty pole of bipolar side

Figure 7.17 shows that half of the active power (500 MW) can be transmitted to monopole side when there is a fault on one of the poles of bipolar side without changing any power reference. However, the total power transfer (1000 MW) can be achieved via healthy pole when all the power is demanded from the healthy pole at t=2 s.

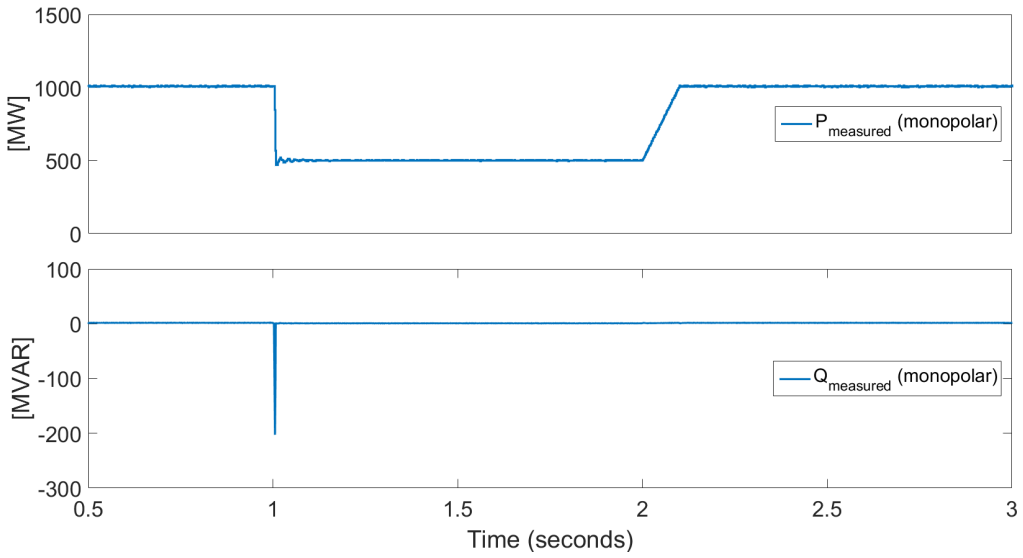


**Figure 7.17:** Active and reactive power flow on the monopole side

As seen in Figure 7.18, DC current decreases to half of its previous value during the time interval between t=1 s and t=2 s since there is no current flow from one of the bipolar side while the DC voltage is constant. The DC current doubles at t=2 s due to the increase in the power reference in order to meet the total power demand. Because of the same reason, the AC current of the monopole side converter decreases at t=1 s and it returns its previous value at t=2 s while the AC voltage is kept constant by the AC voltage controller as seen in Figure 7.19.

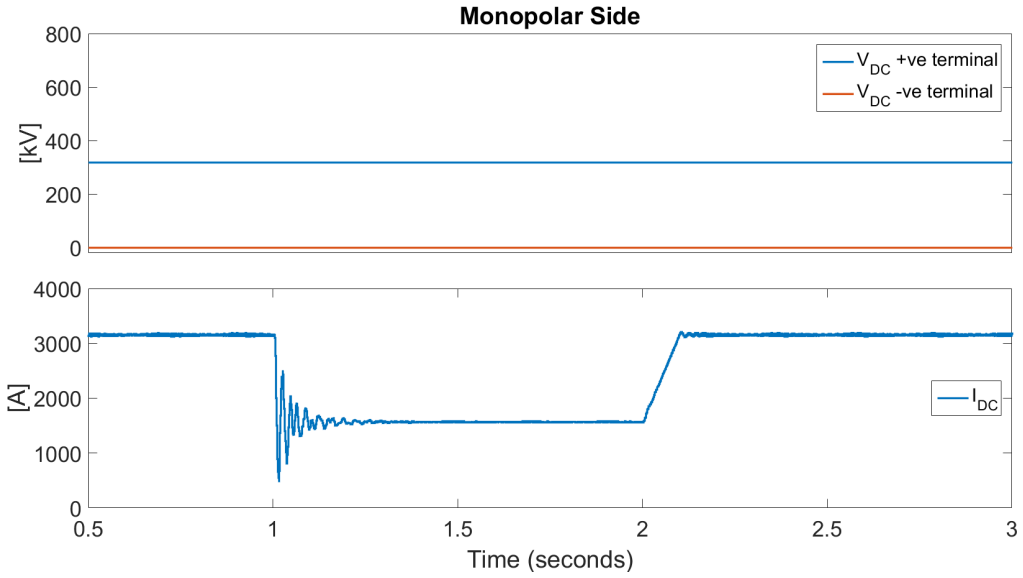


**Figure 7.18:** DC voltage and current on the monopole side

As seen in Figure 7.20, the power is transmitted by both converters on the bipolar side each carrying half of total power (500 MW) until t=1 s. The power reference is not changed until t=2 s on the healthy pole of the bipolar side, and it is doubled after this time instant in order to meet the total power demand of 1000 MW.

Figure 7.21 shows that DC voltage and current of the healthy pole are slightly affected by the dis-

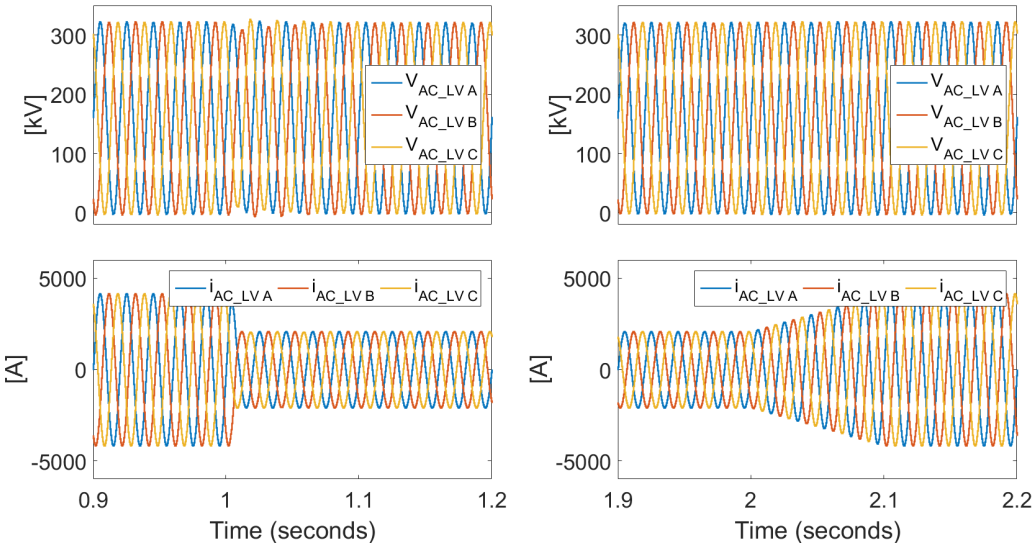


**Figure 7.19:** AC side voltage and current waveforms of the monopole side converter around time t=1 s and t=2 s

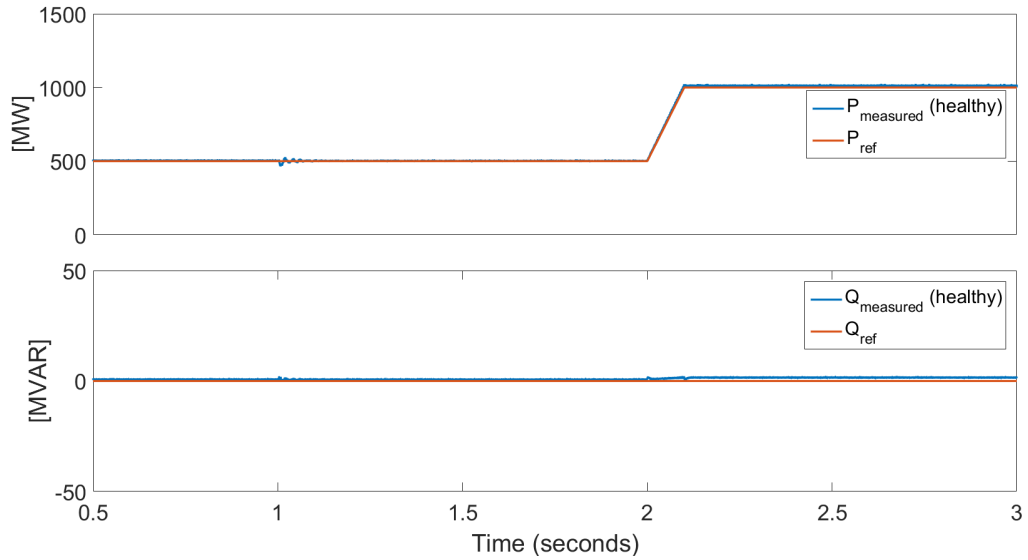


**Figure 7.20:** Active and reactive power flow on the healthy pole of bipolar side

connection of one pole of bipolar system. DC current increases at t=2 s in order to provide total power flow. Due to the same reason, the amplitude of the AC current increases at t=2 s while the AC voltage is constant during the whole operation of the converter as shown in Figure 7.22.

Figure 7.23 shows that upper and lower submodule voltages of MMC on both sides have an average value of 1 pu during the whole operation of the converters.

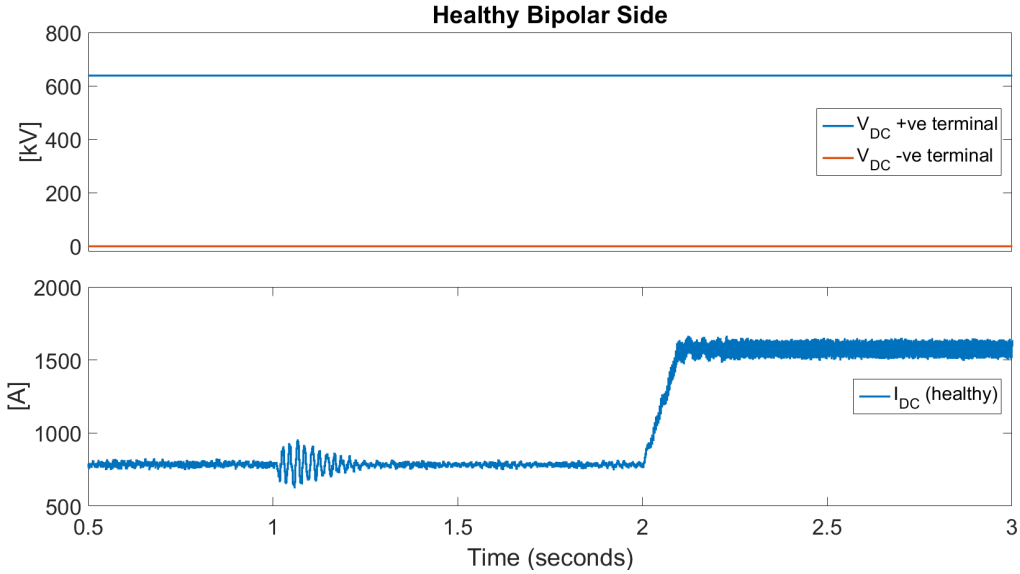


**Figure 7.21:** DC voltage and current of the healthy pole

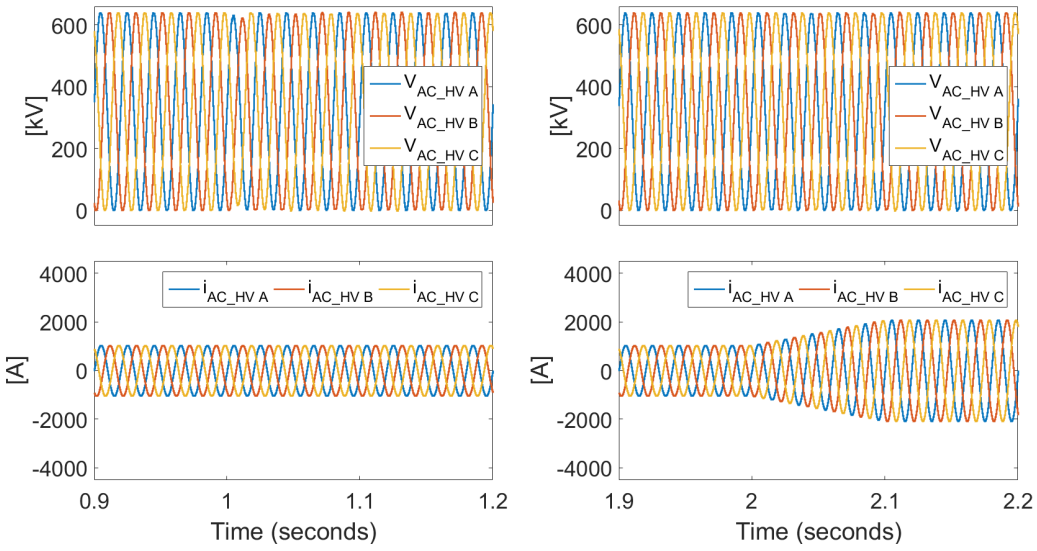


**Figure 7.22:** AC voltage and current waveforms of MMC on the healthy side

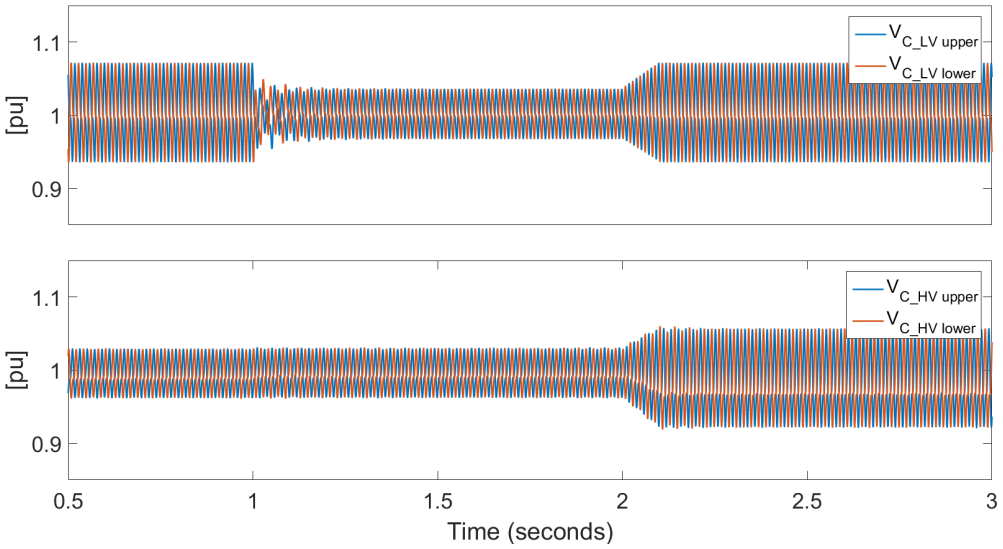


**Figure 7.23:** MMC upper and lower arm cell capacitor voltages of monopole and bipolar side converters

# 8

# AC Side Frequency vs. MMC Component Sizing

*This chapter focuses on the effect of AC side frequency change of front-to-front connected two MMC on the size of passive components used in the DC/DC converter. The simulation results are presented for the specified frequency, inductance and capacitance values for the converters described in previous chapters.*

## 8.1. Introduction

Although 50 Hz frequency is used for the simulation of MMC based DC/DC converters, AC side frequency of DC/AC/DC connected converters does not have to match with the AC grid frequency. In other words, it can be chosen freely. The frequency in between two MMC has a significant effect on passive components sizing. As described in Section 4.3, the submodule capacitance value is inversely proportional to frequency. Therefore, the capacitance value, thus the area occupied by the submodule capacitor, can be decreased by increasing the frequency value, which becomes even more important for the offshore applications where the size of the housing is limited. The increase of the frequency also decreases the core size of the transformer. The limiting factor for the frequency choice is the switching losses since the increase in the AC frequency requires switching of submodules at a higher rate which causes higher switching losses.

The effect of AC side frequency on sizing of passive components is analysed on DC/DC converter without transformer coupling connecting two similar HVDC systems, with transformer coupling connecting two similar configuration operating at different voltages and with 3-winding transformer coupling connecting two different HVDC configurations.

## 8.2. Increased Frequency without Transformer Coupling

AC side frequency is analysed on the MMC based DC/DC converter without transformer coupling connecting two symmetrical monopole HVDC systems operating at same voltages in order to observe its effect on component sizing. The simulation results for the 50 Hz middle stage AC frequency are shown in Section 6.2 while the frequency is increased to 300 Hz in this section which allows reduced submodule capacitance, arm and AC side inductance decreasing the space occupied by these components. Table 8.1 compares component values used in the system with 50 Hz middle AC frequency to the values used in 300 Hz system. In the component sizing the information and formula given in Section 4.3 are considered for the minimum sizes of the components.

Firstly, the operation of the converter is observed at 300 Hz without changing the component sizes; i.e. using the component values for 50 Hz operation. Power, DC and AC waveforms are shown in

**Table 8.1:** Component sizing for the middle AC stage frequency of 50 Hz and 300 Hz

| | Cell Capacitance, C | Arm inductance, $L_a$ | AC side inductance, $L_{out}$ |
|---|---|---|---|
| **f=50 Hz** | 2.5 mF | 44.1 mH (0.15 pu) | 52.9 mH (0.18 pu) |
| **f=300 Hz** | 0.5 mF | 8.8 mH | 10.6 mH |

Figure 8.1. As seen in the figure, there is a considerable amount of oscillation in the DC current, thus in the power. Moreover, the sinusoidal AC waveforms of 50 Hz situation are also lost at 300 Hz operation with high component values. The reason of this situation may be the mismatch between the slow response of the converter due to large component values and the fast operation of the AC side.

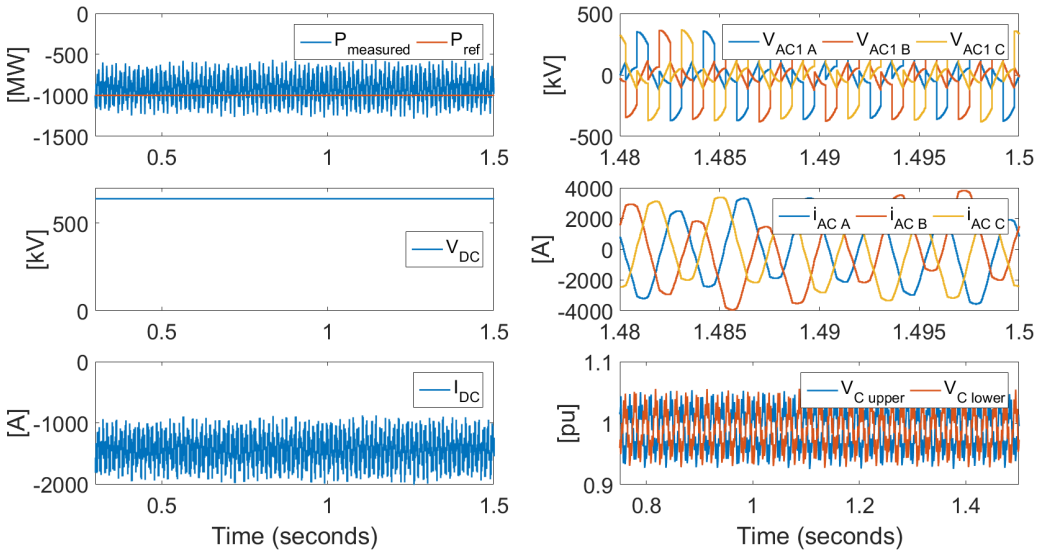


**Figure 8.1:** The response of the converter with high component values at 300 Hz

In order to test the correct operation of the converter with increased AC side frequency the component sizes are also adjusted according to Table 8.1. As the component sizes are inversely proportional to the frequency as explained in Section 4.3, capacitance and inductance values are decreased almost proportionally with the increase in AC side frequency and the comparable performance with the 50 Hz operation is obtained. A scenario is set such that the power reference is changed from -1000 MW to 500 MW as in the case of 50 Hz AC frequency at t=1.5 s. Figure 8.2 shows the converter power time interval between t=0.3 s and t=3 s. It can be seen that converter power tracks the reference value during the operation of the MMC based DC/DC converter with increased frequency.

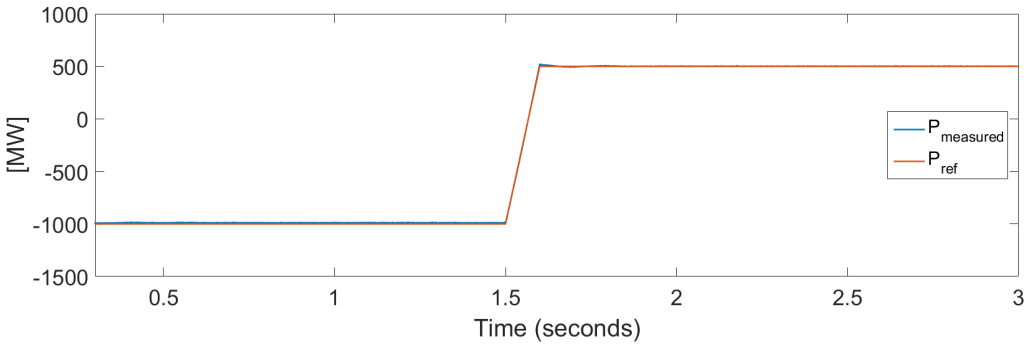


**Figure 8.2:** Reference and measured power of the converter

DC waveforms are presented in Figure 8.3. It shows that DC current changes its direction and magnitude in order to meet the power demand while the DC voltage is kept constant at 640 kV between converter terminals.

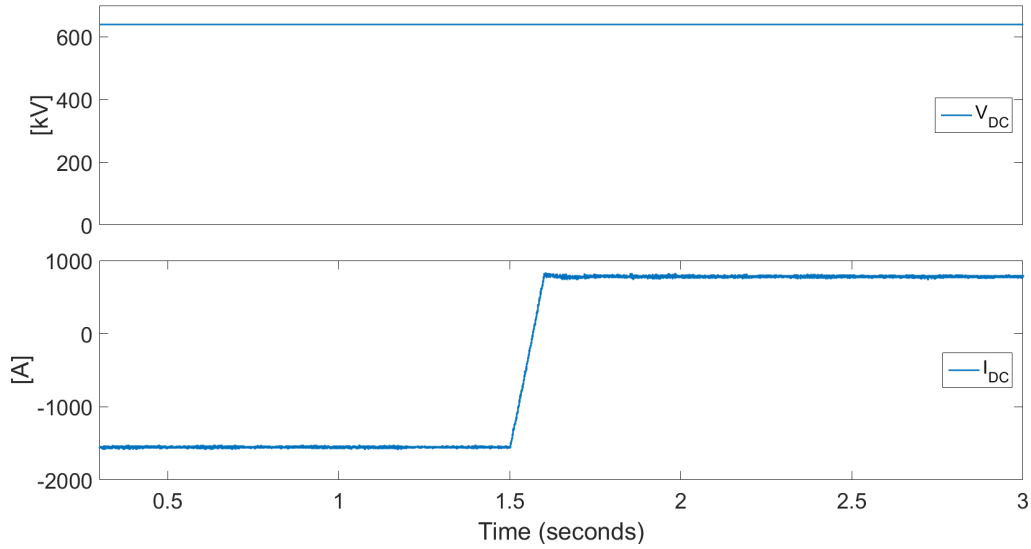


**Figure 8.3:** DC voltage and current at one terminal of the DC/DC converter

AC waveforms on the middle AC stage of MMC based DC/AC/DC converter are shown for two time intervals in Figure 8.4 in order to observe AC waveforms in 300 Hz frequency clearly. As seen in the figure, AC voltage is kept constant by the voltage controlled MMC while the AC current changes its amplitude depending on the power demand. Since the magnitude of the power transferred is decreased from 1000 MW to 500 MW at time t=1.5 s , the amplitude of the AC current is halved after t=1.5 s.

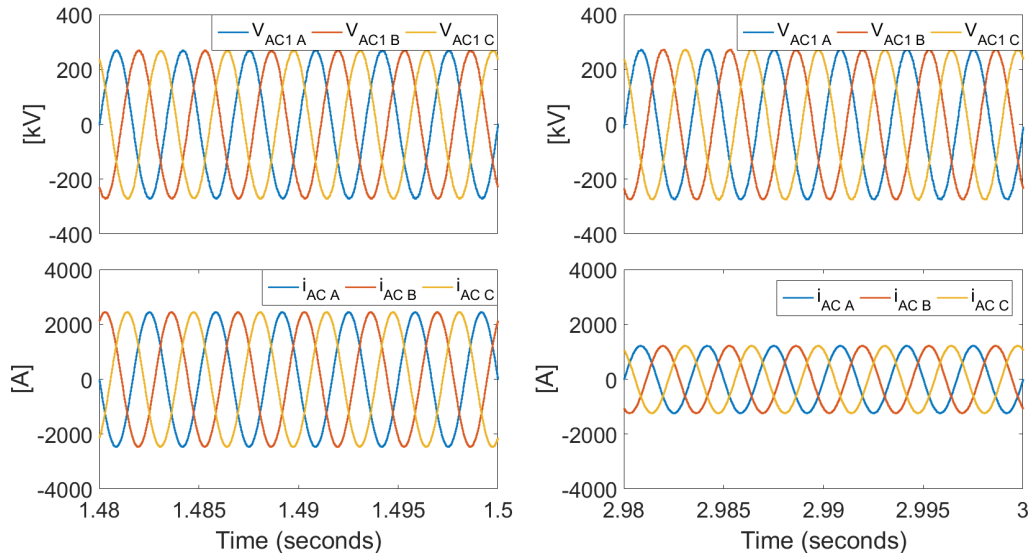


**Figure 8.4:** AC voltage and current waveforms on the middle AC stage

Converter submodule voltages for one of the upper and lower arm cells which belong to one of the MMC forming DC/AC/DC converter are shown in Figure 8.5. The plots are shown for two time intervals from t=1.48 s to t=1.5 s and from t=2.98 s to t=3 s in order to observe waveforms clearly. The figure

shows that the submodule voltages are at 1 pu average level during the operation of the converter at all power levels. As seen in the plot belonging to time interval between t=2.98 s and t=3 s, cell voltages have less ripple compared to first time interval since the current has a lower value resulting from less power demand.

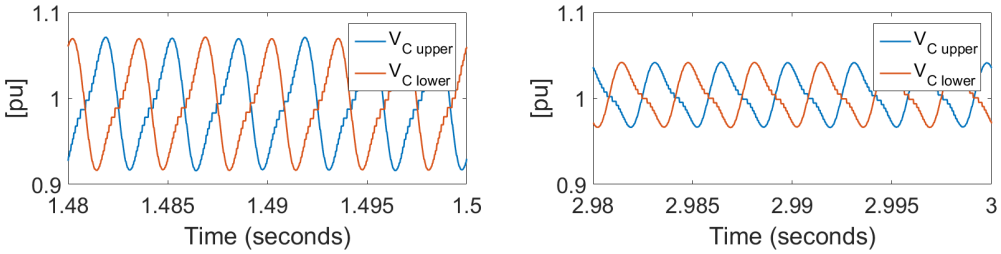


**Figure 8.5:** Upper and lower arm submodule voltages of one of the MMC

As a result, the simulation results show that the converter operates properly with the increased AC side frequency which allows significantly to decrease component values as shown in Table 8.1. Therefore, it is possible to save space in the converter station since lower inductance and submodule capacitances occupy less area.

## 8.3. Increased Frequency with 2-winding Transformer

In order to observe the effect of frequency on the system performance, the simulation is firstly performed with increased frequency with old component sizes; i.e. component sizes of 50 Hz case. The waveforms of the converter on low voltage side are shown in Figure 8.6. When compared to converter without transformer coupling, DC current, AC voltage and AC currents are much better thanks to the galvanic insulation although there are still undesired ripples on AC voltage. While cell capacitors are properly charged and discharged, the average value of the upper and lower capacitor voltages is slightly higher than 1 pu, which may require readjustment of controller gains.

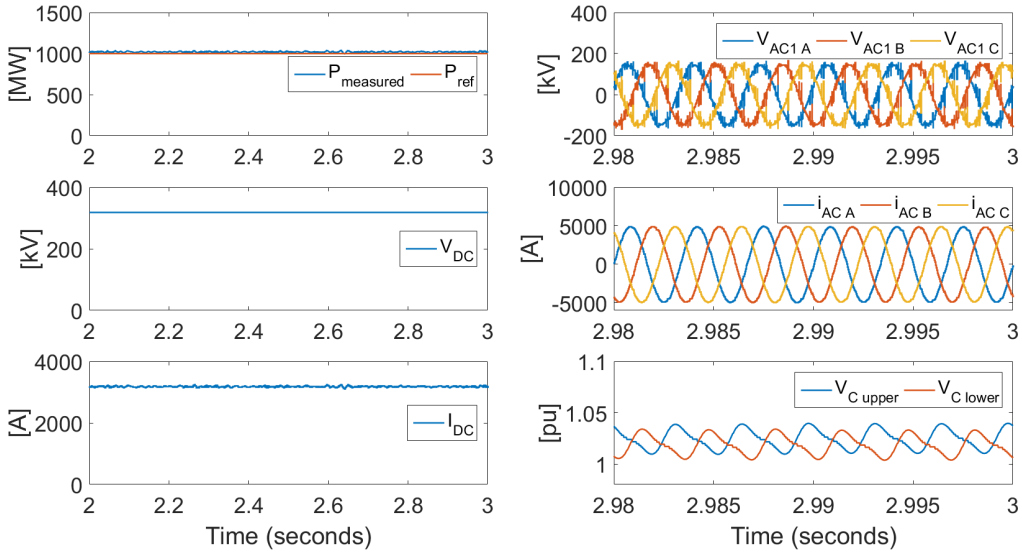


**Figure 8.6:** The response of the converter with transformer coupling at 300 Hz operation with high component values

Transformer coupled DC/AC/DC converter connecting similar HVDC configurations operating at different voltage levels is verified for the increased AC side frequency with lower component sizes. The

increase in the frequency allows to decrease submodule capacitance, arm and transformer inductance values, thus the size of the converter station. Table 8.2 compares the component values for increased frequency with the ones used in the system with 50 Hz. As seen on the table, component sizes for 300 Hz operation are calculated considering the fact that they are inversely proportional to the AC side frequency.

**Table 8.2:** Component sizing for the transformer coupled converter for 50 Hz and 300 Hz

| | **Low Voltage** | | | **High Voltage** | | |
|---|---|---|---|---|---|---|
| | **MMC1** | | **Transformer** | | **MMC2** | |
| | **C** | **$L_a$** | **$L_{tr}$(LV)** | **$L_{tr}$(HV)** | **C** | **$L_a$** |
| **f=50 Hz** | 10 mF | 11 mH | 13.2 mH | 52.9 mH | 2.5 mF | 44.1 mH |
| **f=300 Hz** | 1.6 mF | 1.8 mH | 2.2 mH | 8.8 mH | 0.4 mF | 7.4 mH |

The power reference is changed from -500 MW to 1000 MW at t=1.5 s in order to test the performance of the converter operating with the higher frequency on the AC side with the decreased component values given in Table 8.2. The power flow between two terminals of the converter is shown in Figure 8.7. It shows that the converter tracks the reference power during the all operation points.

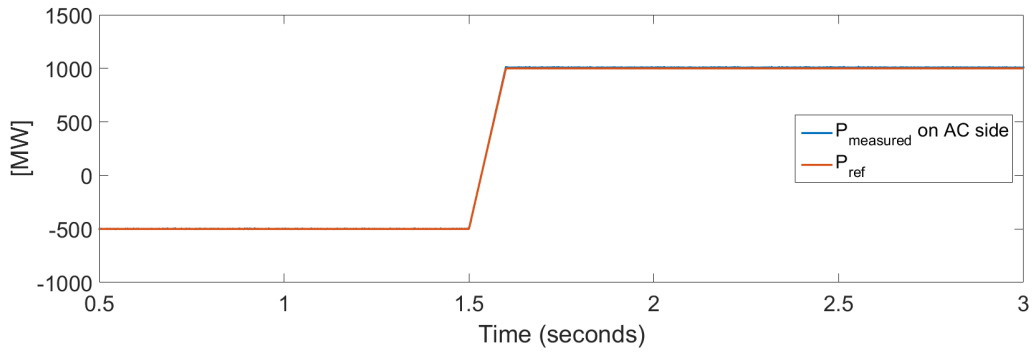


**Figure 8.7:** Reference and the measured power of the converter with transformer coupling

DC voltage and current plots for low voltage and high voltage sides are shown in Figure 8.8 and Figure 8.9, respectively. As seen in the figures, DC voltages are kept constant at 320 kV and 640 kV while the current changes its magnitude and direction in order to provide the power demand. Since the power is almost equal on DC terminals, the current has higher values on low voltage side while it is lower on high voltage side.

AC waveforms for low voltage and high voltage side of the converter are plotted in Figure 8.10 and Figure 8.11, respectively, for two time intervals where the power is -500 MW and 1000 MW in order to observe waveforms in 300 Hz plainly. During both time intervals from t=1.48 s to t=1.5 s and from t=2.98 s to t=3 s, AC voltage is kept constant by the voltage controlled MMC while the current has arranged by the other MMC in order to meet the power reference. The increase in the amplitude of the current can be seen in both figures for the second interval at which the amplitude of the power is increased from 500 MW to 1000 MW.

Figure 8.12 shows the MMC submodule voltage waveforms in per unit scale for both low voltage and high voltage converters for the two time intervals. It can be seen that the average of submodule voltages are at 1 pu level during the all operation of converter and the ripple increases with the increase in current.

The simulation results for the DC/DC converter connecting DC networks at different voltage levels show that it is possible to decrease capacitance and inductance values by increasing the AC side frequency as shown in Table 8.2. In addition to decreasing submodule capacitor and arm inductor sizes,

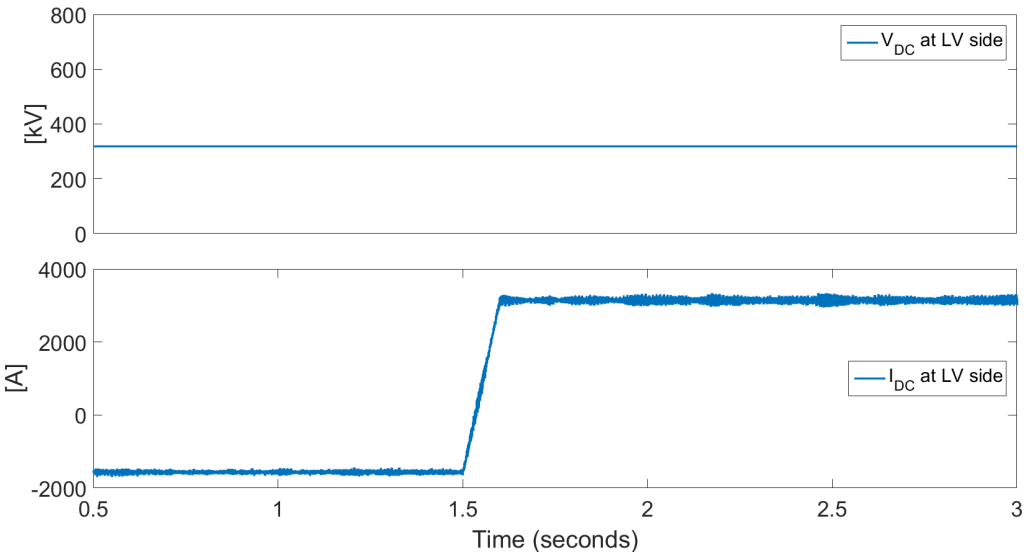


**Figure 8.8:** DC voltage and current on low voltage side

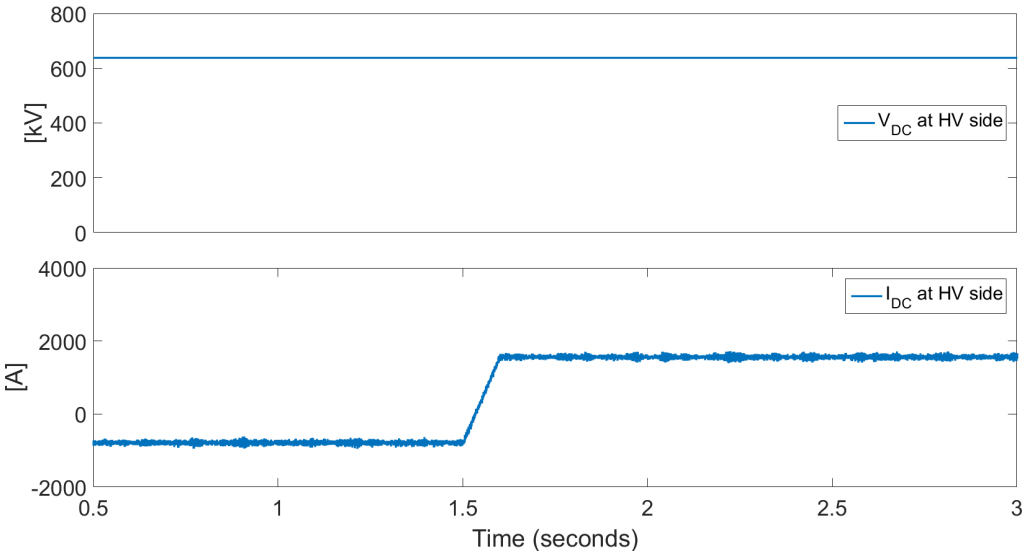


**Figure 8.9:** DC voltage and current on high voltage side

increasing the AC side frequency also benefits to decrease transformer size. Although core cross-sectional area (A) is inversely proportional to the frequency (f) according to transformer emf equation (emf=4.44fNAB), the relation is not straightforward due to the other factors of transformer design such as cooling equipments or insulation of windings. However, it is still expected to decreases the transformer size significantly [43].

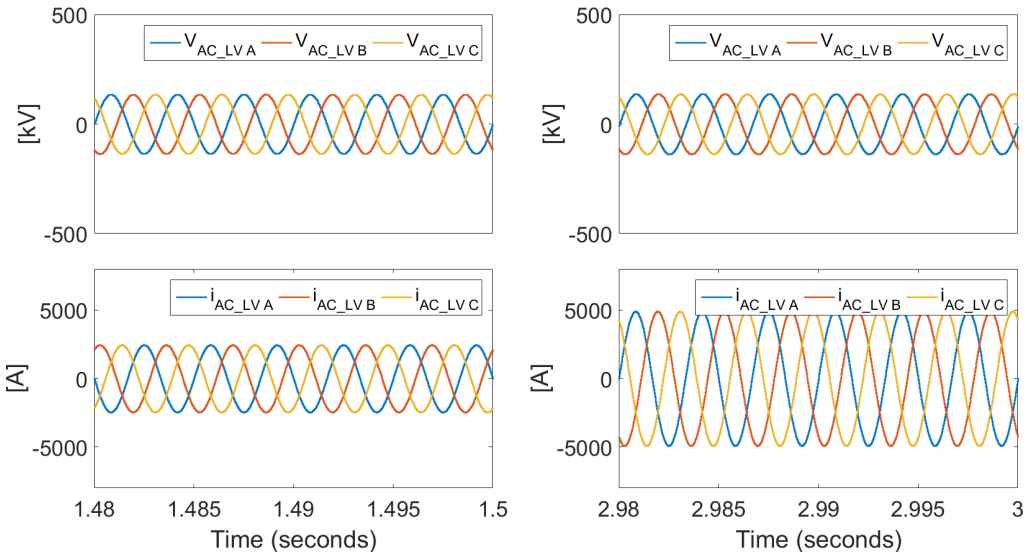


**Figure 8.10:** AC waveforms on low voltage side

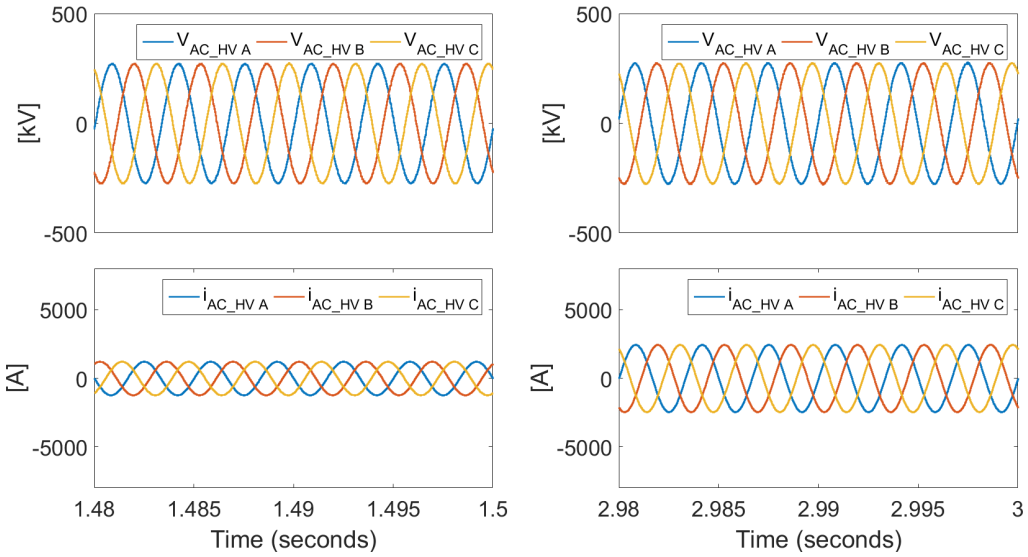


**Figure 8.11:** AC waveforms on high voltage side

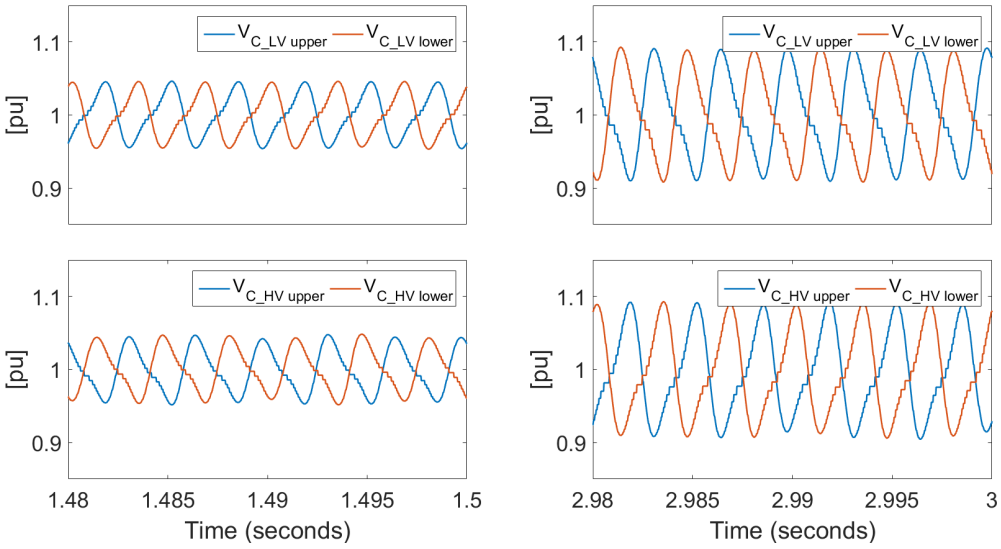


**Figure 8.12:** Upper and lower arm submodule voltages for both high voltage and low voltage converters

## 8.4. Increased Frequency with 3-winding Transformer

DC/DC converter connecting monopole and bipolar systems operating at different voltage levels is tested for higher AC frequency in order to check its performance and functionality. As expected, cell capacitance, arm and transformer inductance values can be decreased thanks to increase in frequency. Table 8.3 shows the component values for both 50 Hz system used in Section 7.2.2 and 300 Hz system.

**Table 8.3:** Component sizing for 3-winding transformer coupled converter

| | **Low Voltage** | | | | **High Voltage** | |
|---|---|---|---|---|---|---|
| | **MMC1** | | **Transformer** | | **MMC2 & MMC3** | |
| | **C** | **$L_a$** | **$L_{tr}$(LV)** | **$L_{tr}$(HV)** | **C** | **$L_a$** |
| **f=50 Hz** | 10 mF | 15.3 mH (0.15 pu) | 18.3 mH (0.18 pu) | 73.3 mH | 2.5 mF | 61.1 mH |
| **f=300 Hz** | 1.6 mF | 2.5 mH | 3.1 mH | 12.2 mH | 0.4 mF | 10.2 mH |

The total power flow on the converter is provided by the two MMC on bipolar side. Therefore, the power reference for each bipolar side MMC is the half of the total power. The power reference for each MMC is changed from -500 MW to 250 MW at t=1.5 s in order to test the bidirectional power flow under higher frequency. The power flow on monopole side MMC and one of the bipolar side MMC are shown in Figure 8.13. As seen in the figure, power controlled MMC tracks the reference power and the total power transferred on the monopole side is -1000 MW until t=1.5 s and 500 MW after power switch.

DC voltage and current waveforms for the converter connecting asymmetric monopole and bipolar HVDC systems are shown in Figure 8.14. it can be seen that positive terminal voltages are constant at 320 kV and 640 kV for low voltage monopole and high voltage bipolar sides, respectively, while negative terminals are grounded. DC current changes its direction and magnitude according to the power setting.

Figure 8.15 shows AC waveforms under the frequency of 300 Hz for both monopole and bipolar side MMC. Voltage and current signals for both converters are plotted in two time intervals, namely from t=1.48 s to 1.5 s and t=2.98 s to t=3 s, in order to observe AC signals clearly. As seen in the figure, the frequency of the waveforms are 300 Hz and they have 120° phase difference. The amplitude of the currents are adjusted depending on the power flow between each side.

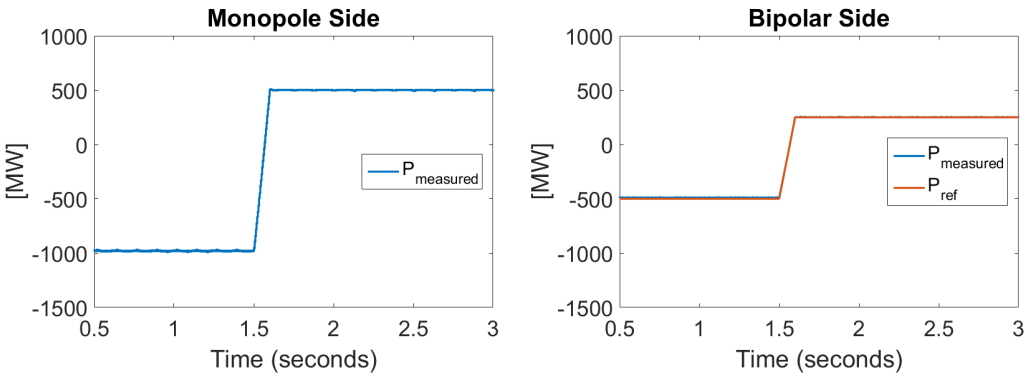


**Figure 8.13:** The power flow on monopole and bipolar sides of the DC/DC converter

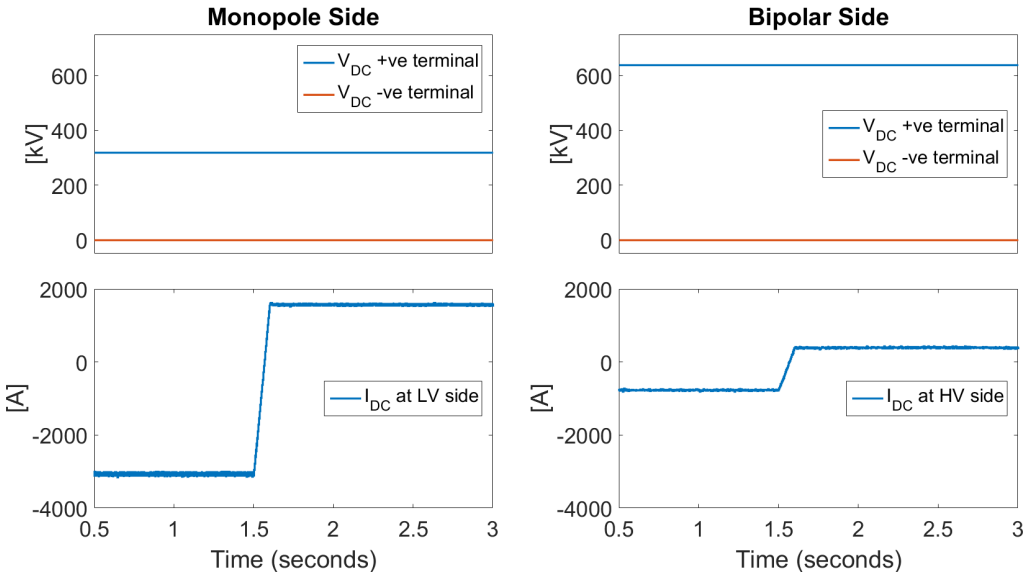


**Figure 8.14:** DC voltage and current plots for both monopole and bipolar sides

Upper and lower submodule voltages of the converters on both sides are shown in Figure 8.16. It shows that the average value of the cell voltages is 1 pu and the ripple changes depending on the current magnitude.

The simulation results for the 3-winding transformer coupled DC/DC converter show that the proper operation of MMC can be maintained under higher frequencies than the grid frequency which saves space in the converter station by decreasing the size of submodule capacitors, arm inductors and coupling transformer.

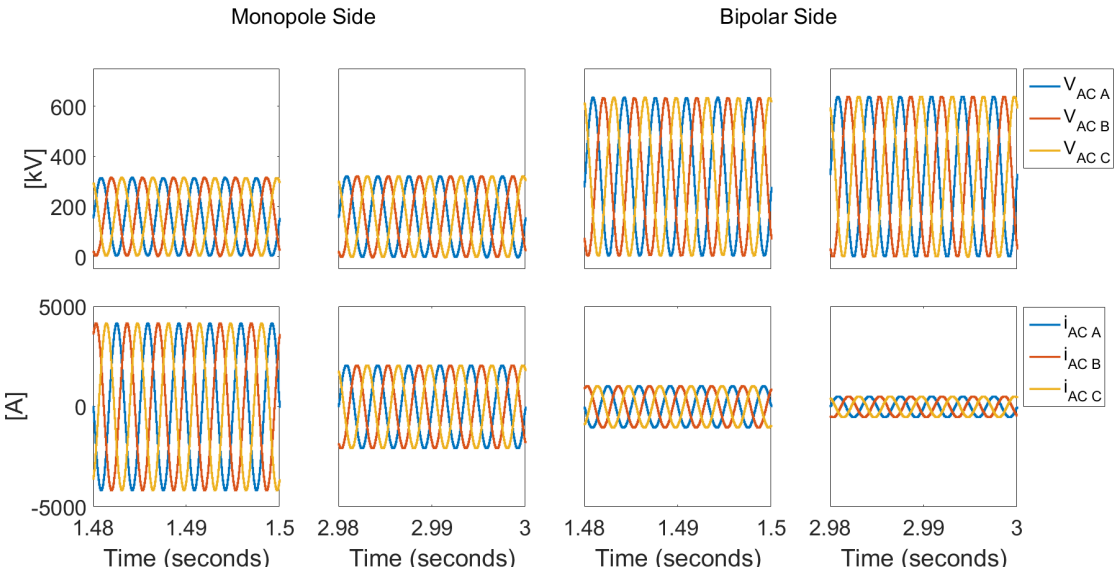


**Figure 8.15:** AC waveforms of monopole and bipolar converters plotted for two time intervals

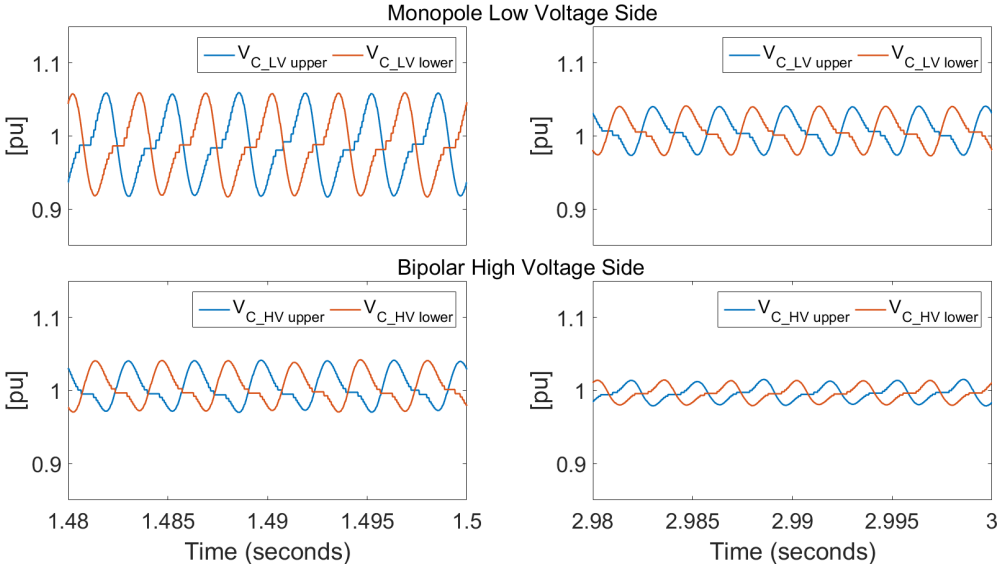


**Figure 8.16:** Submodule voltages of monopole and bipolar converters plotted for two time intervals

# 9

# Multi-terminal HVDC Grid

*A multi-terminal HVDC grid designed by CIGRE B4 working group is introduced in this chapter. Furthermore, DC/DC converters designed in previous chapters are verified in the MTDC system in order to test their performance.*

## 9.1. Introduction

A VSC based MTDC grid has been developed by the B4 working group of CIGRE including connections of both AC/DC and DC/DC. The schematic of the system is shown in Figure 9.1. The system consists of:

- Onshore AC systems, namely A (A0 and A1) and B (B0, B1, B2 and B3) shown in red in Figure 9.1.
- Offshore AC systems, namely C (C1 and C2), D1, E1 and F1 shown in yellow. C, D and F represent the offshore wind farms while E is the offshore oil/gas platform.
- DC nodes, namely Bb-B4 and Bm-B5 buses with only DC connections.
- VSC based HVDC systems, namely DCS1, DCS2 and DCS3.

DCS1 is a 2 terminal symmetric monopole system and it connects the offshore wind power generation bus, C1, to the onshore AC grid, A1. DCS2 is a 4 terminal symmetric monopole system which connects the offshore power plant at F1 and oil/gas platform at E1 to onshore grids B2 and B3. DCS3 is a 5 terminal bipolar meshed system with ±400 kV connecting offshore wind farms at C2 and D1 to the onshore AC grid. DCS3 also includes a DC/DC converter, Cd-B1, in order to control the power flow. Moreover, there is one more DC/DC converter, Cd-E1, which interconnects DCS2 and DCS3.

## 9.2. Test of DC/DC Converters in MTDC System

MMC based DC/DC converters designed in previous chapters are implemented in the MTDC grid in order to test their performance. The functionality of the MMC for interconnecting DC systems is verified by using them as Cd-B1 in DCS3 bipolar HVDC system and Cd-E1 interconnecting DCS2 and DCS3.

### 9.2.1. Converter Cd-B1 in DCS3 Bipolar System

Cd-B1 DC/DC converter with 50 Hz middle AC stage is tested in DCS3 meshed bipolar HVDC system shown in Figure 9.2 which is a subsystem of the total MTDC grid. As seen in the figure, the system provides interconnection of AC offshore and onshore grids via 4 AC/DC converters. Table 9.1 shows

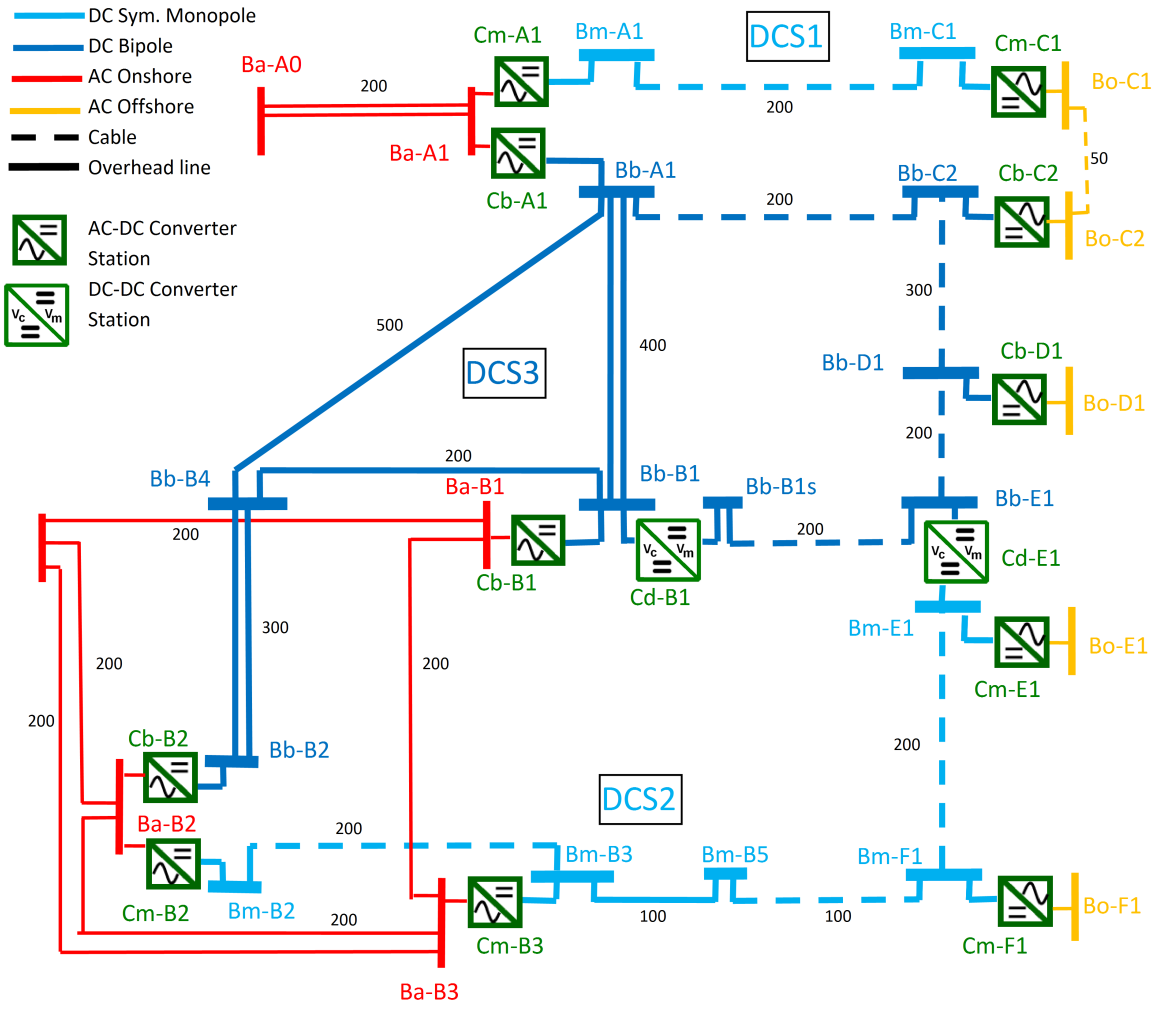


**Figure 9.1:** Multi-terminal DC grid designed by CIGRE B4 working group [79]

the converter settings and their operation modes.

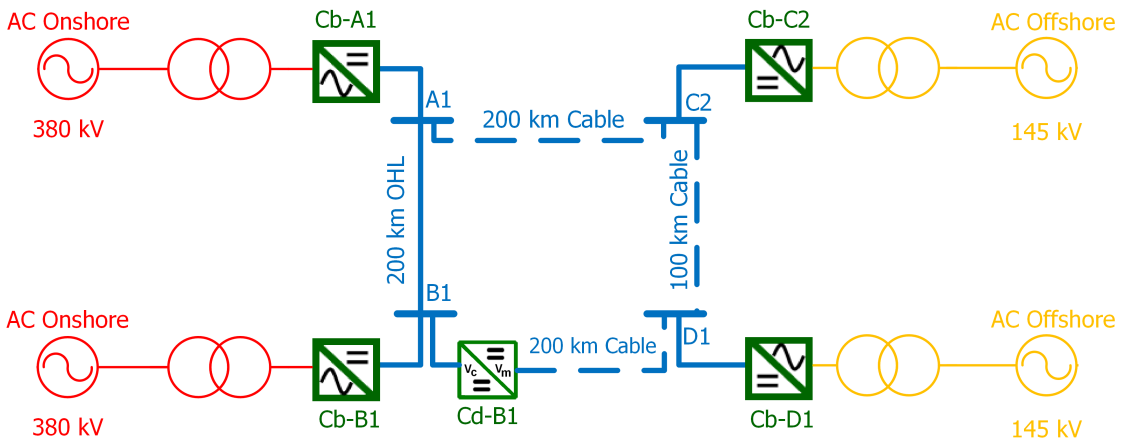


**Figure 9.2:** DCS3 meshed bipolar HVDC system

The meshed bipolar system also includes both DC overhead line (OHL) and cables in order to pro-

**Table 9.1:** Design parameters of the converters in DCS3 subsystem

| AC/DC converter station | Power rating [MVA] | DC voltage [kV] | Operation mode |
|---|---|---|---|
| Cb-A1 | 2x1200 | ±400 | $V_{DC}$=1.01 pu |
| Cb-B1 | 2x1200 | ±400 | P=800 MW |
| Cb-C2 | 2x400 | ±400 | P=-600 MW |
| Cb-D1 | 2x800 | ±400 | P=-1000 MW |

vide the connection between converter stations. Lengths and types of the lines between converter stations are given in Table 9.2 while the resistance, inductance and capacitance parameters of each type of line is given in Table 9.3.

**Table 9.2:** DC line information in DCS3 subsystem

| Line | Length [km] | Type |
|---|---|---|
| A1-B1 | 200 | OHL |
| A1-C2 | 200 | Cable |
| B1-D1 | 200 | Cable |
| C2-D1 | 100 | Cable |

**Table 9.3:** DC line parameters in DCS3 subsystem [79]

| Line Type | R [Ω/km] | L [mH/km] | C [$\mu$F/km] |
|---|---|---|---|
| DC OHL ±400 kV | 0.0114 | 0.9356 | 0.0123 |
| DC cable ±400 kV | 0.0095 | 2.1120 | 0.1906 |

DC/DC converter, Cd-B1, in DCS3 bipolar system is connected in between two buses operating at the same voltage levels and same configurations. Therefore, MMC based DC/DC converter without galvanic separation is used in the simulation. The function of the DC/DC converter in such a system is to provide desired power flow on the transmission lines. ProOfGrids Simulink files [80] are utilized and the required connections, line, voltage and power settings are adjusted for the simulation of MTDC grid. Average VSC models in ProOfGrids Simulink files are used as AC/DC converters and transmission lines are modelled using pi equivalent models. The simulation is performed with the scenario in which:

- Cb-A1 sets the DC voltage at 1.01 pu
- Cb-B1 transfers 800 MW active power to AC onshore grid
- Cb-C2 transfers 600 MW active power generated by offshore wind farms
- Cb-D1 transfers 1000 MW active power generated by offshore wind farms
- Cd-B1 transfers 300 MW from D1 to B1 until t=2.5 s, the power flow is changed to 150 MW from B1 to D1 at t=2.5 s.

The simulation is performed in two phases in order to observe the functionality of the DC/DC converter. Firstly, MTDC grid is simulated without DC/DC converter and power flows on lines are measured. Secondly, DC/DC converter CD-B1 is connected to the system and the expected values are observed for the power flows on transmission lines.

The converter powers of AC/DC converters are shown in Figure 9.3 without DC/DC converter. As seen in the figure, converters Cb-B1, Cb-C2 and Cb-D1 have fixed power levels set by the scenario while the power on Cb-A1 is adjusted depending on the power of other converters so that the remaining power flows on Cb-A1 and the DC voltage is kept constant at 1.01 pu (404 kV).

Powers flowing on DC OHL and cables between converter stations are shown in Figure 9.4. Although the converters adjust the amount of power transferred between AC and DC side, the power flowing

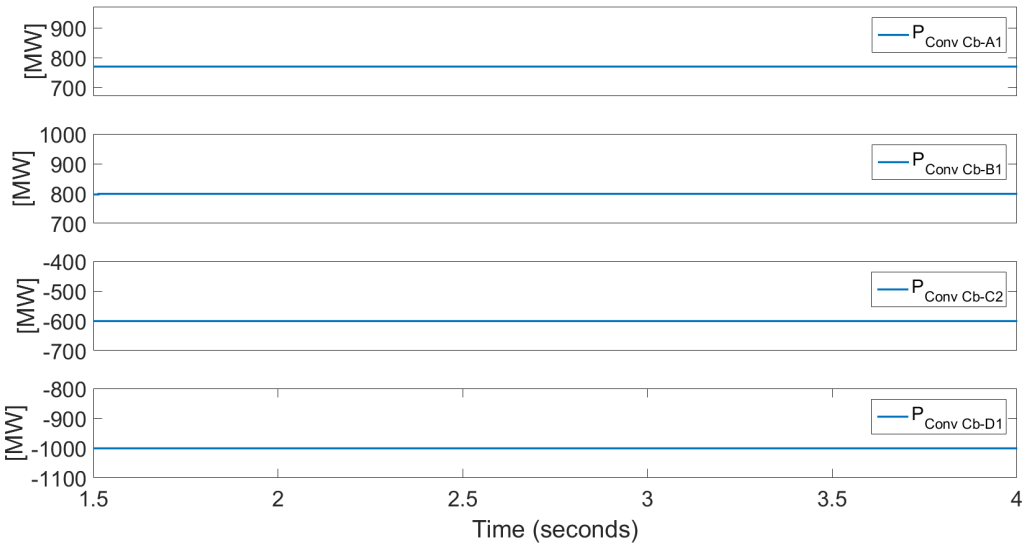


**Figure 9.3:** Power of AC/DC converters without DC/DC converter

on transmission lines is not controlled since each converter has connection with two DC lines. Hence the power flow on transmission lines is dependent on the impedances of each line without a DC/DC converter controlling power flow.

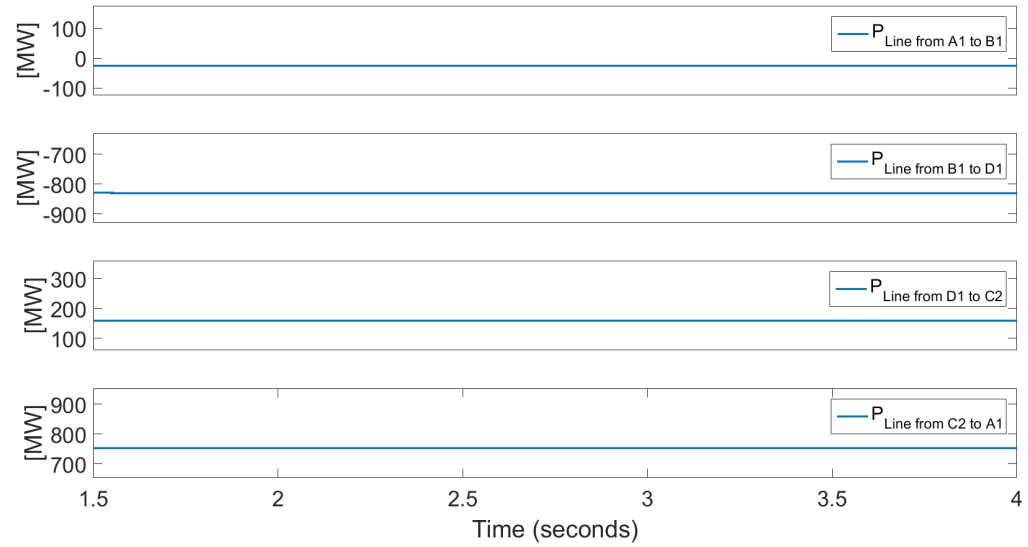


**Figure 9.4:** Power on transmission lines between AC/DC converters without DC/DC converter

DC voltage values for each bus in the bipolar MTDC system is shown in Figure 9.5. As seen in the figure, converter Cb-A1 sets the DC voltage to 404 kV corresponding 1.01 pu while the other voltages still in the operational frame for the DC systems with the upper limit at 1.05 pu and the lower limit at 0.95 pu as defined in [79].

In order to summarize power flow study in MTDC grid without DC/DC converter, all power flows between converter stations and the DC voltages are shown in Figure 9.6.

DC/DC converter, Cd-B1, designed as MMC based without transformer coupling is connected to

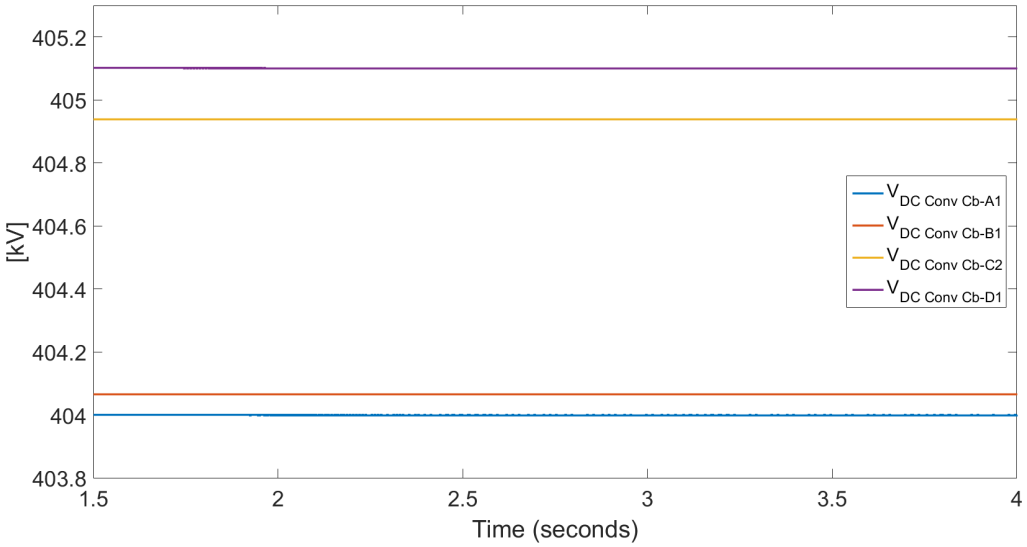


**Figure 9.5:** DC voltages at each AC/DC converters without DC/DC converter

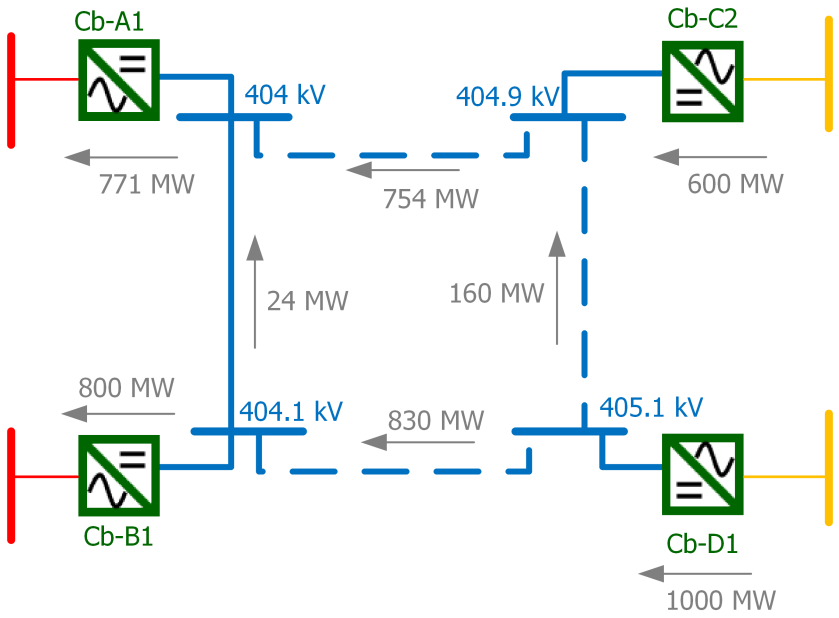


**Figure 9.6:** Power flow between converter stations and bus DC voltages

the system in order to control the power flow on transmission line between B1 and D1. In order to test the bidirectional power flow of DC/DC converter, the power reference is changed from -300 MW to 150 MW at t=2.5 s while the operation modes of AC/DC converters are kept the same as in Table 9.1. The converter powers are shown in Figure 9.7. It can be seen that converter powers have the adjusted values and they are not affected by the change in DC/DC converter power setting except a little oscillation for the converter Cb-A1 during the power change.

The powers flowing on transmission lines are shown in Figure 9.8. It can be observed that the change in the power flow adjusted by DC/DC converter, Cd-B1, can be seen in all powers flowing through DC lines. According to the setting, 300 MW of active power firstly flows from D1 to B1 till it changes direction and magnitude at t=2.5 s. After t=2.5 s, 150 MW of active power flows from B1 to D1 and the power flow on other lines changes its magnitude in order to keep the total AC/DC converter

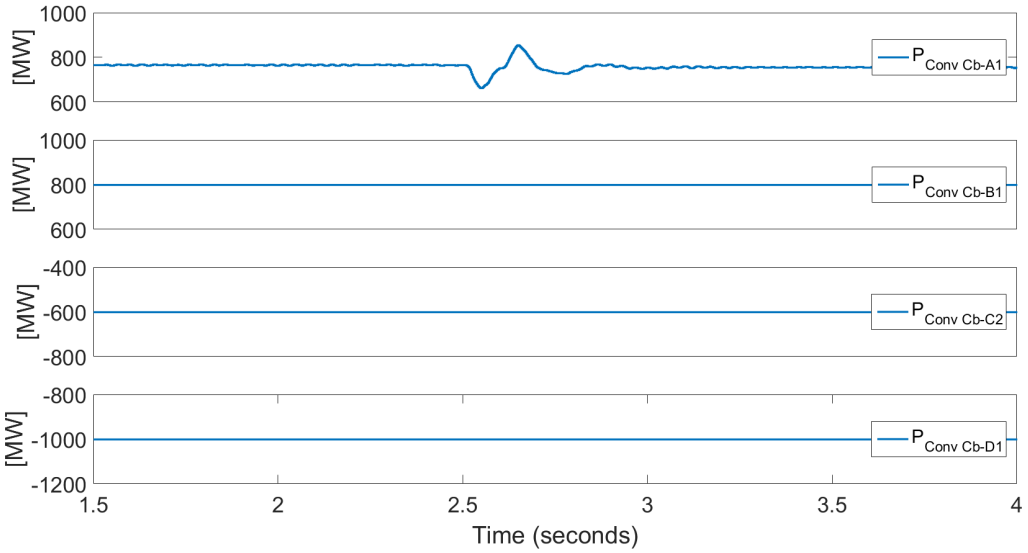


**Figure 9.7:** Power of AC/DC converters when DC/DC converter, Cd-B1, is connected

powers constant.

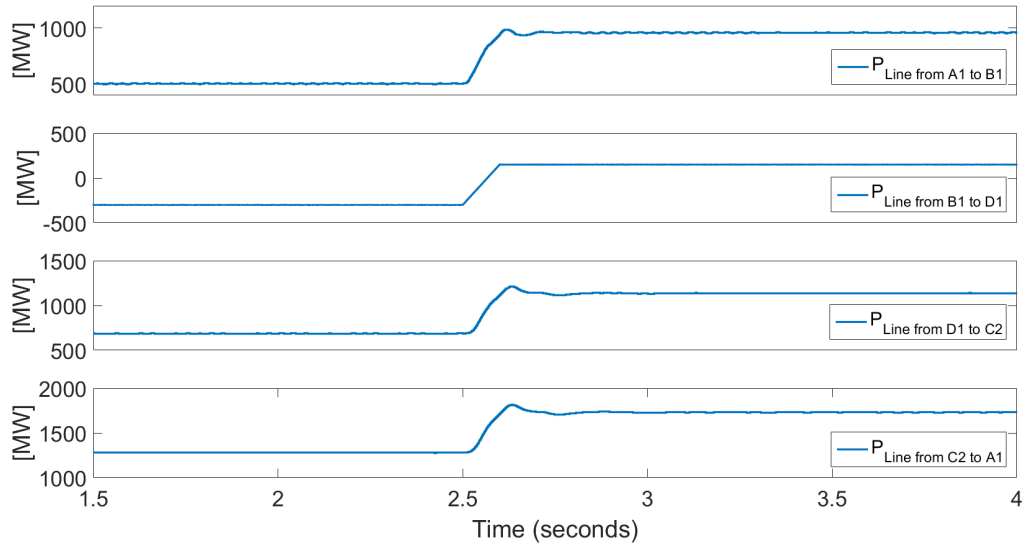


**Figure 9.8:** Power on transmission lines when DC/DC converter is connected

Figure 9.9 shows the DC voltages of the HVDC system. Although there is an oscillation during the power reversal of DC/DC converter, Cd-B1, all DC voltages are in operational limits.

The voltage and current waveforms on the AC side of MMC based DC/AC/DC converter used as Cd-B1 in the system are shown in Figure 9.10. It can be seen that the amplitude of the current decreases after t=2.5 s since the amount of power transferred is decreased from 300 MW to 150 MW while the AC voltage is not affected by the power reversal of the DC/AC/DC converter.

The power flow analysis is summarized in Figure 9.11a and Figure 9.11b showing all power flows and DC voltage values.

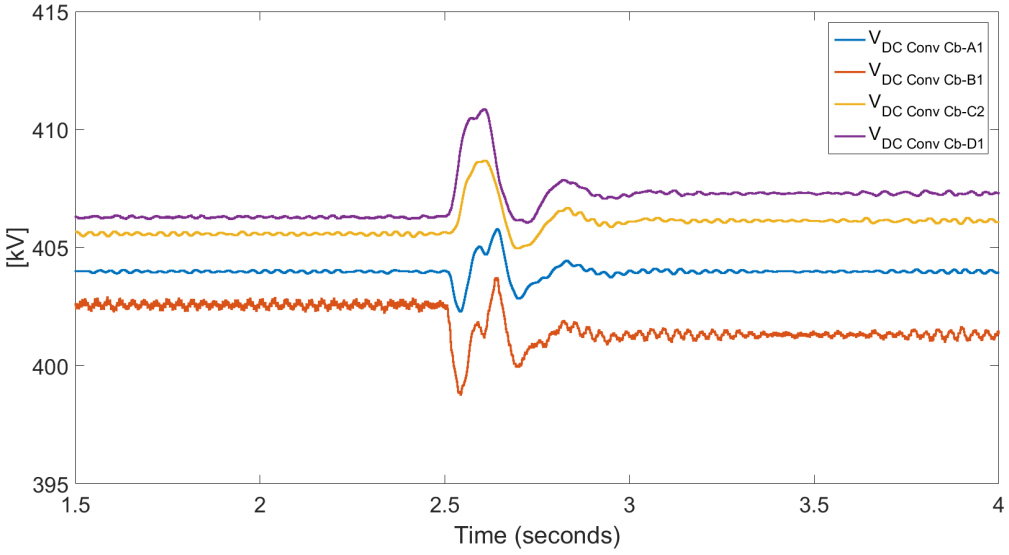


**Figure 9.9:** DC voltages at each AC/DC converters when Cd-B1 is connected

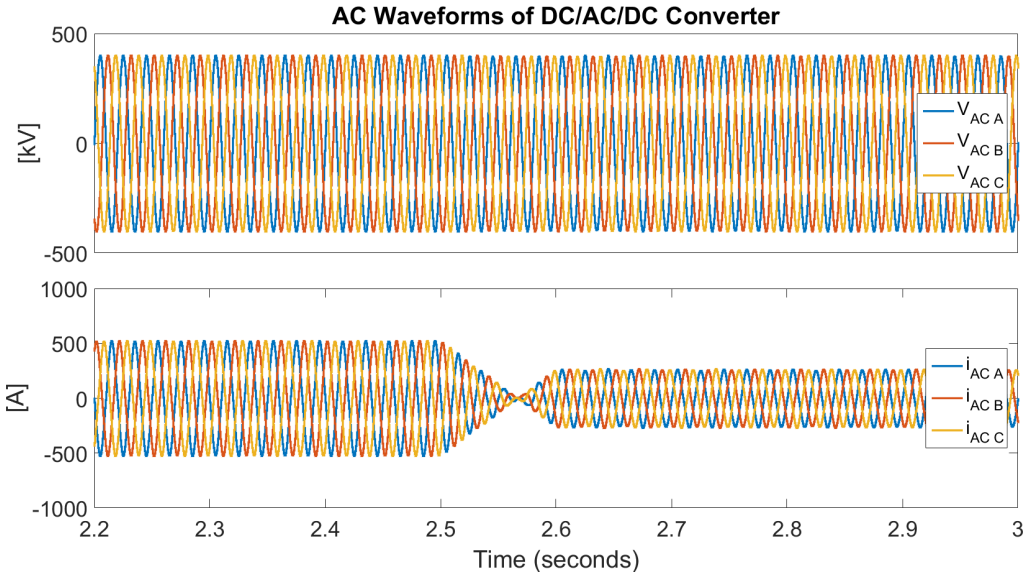


**Figure 9.10:** AC waveforms of MMC based DC/AC/DC converter, Cd-B1

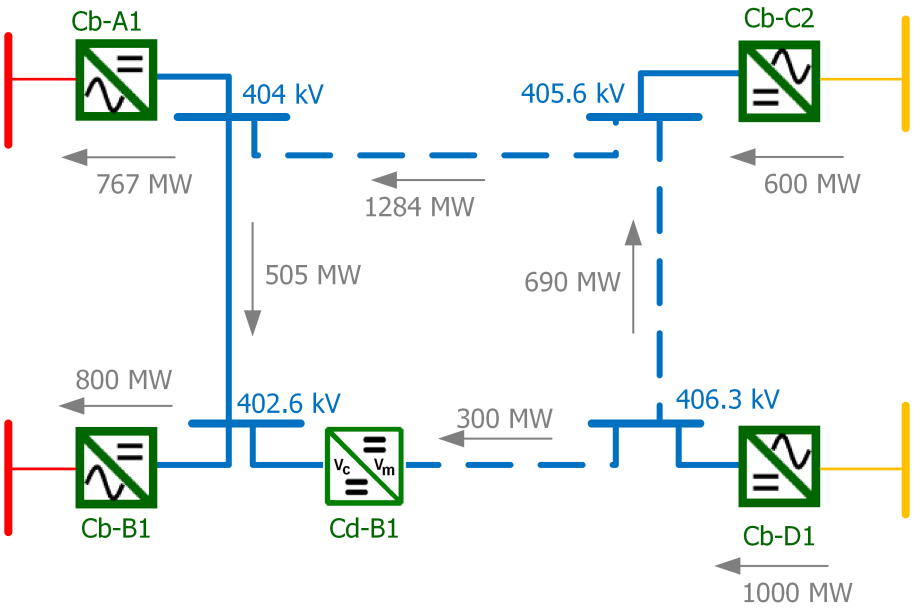


**(a)** Power flow between converter stations and DC voltages when $P_{Cd\text{-}B1}$=-300 MW

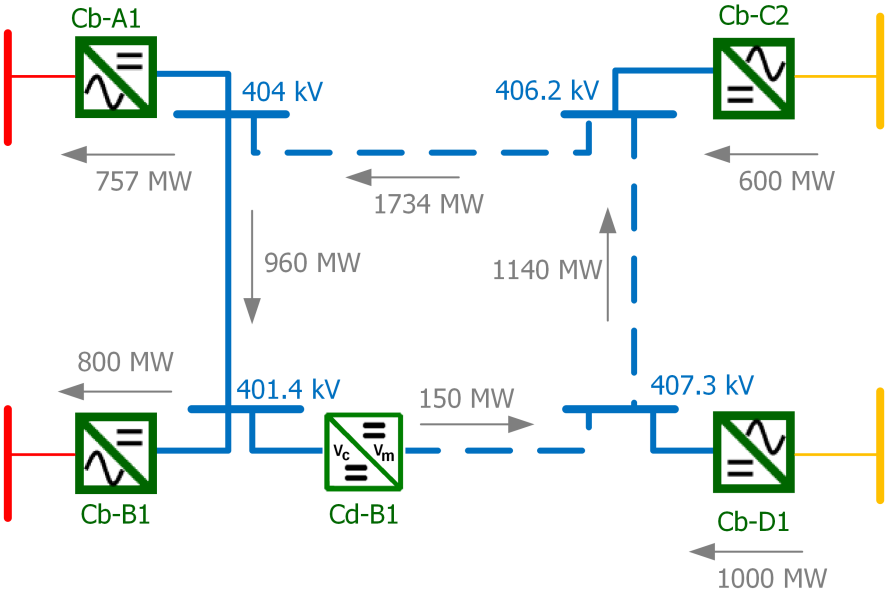


**(b)** Power flow between converter stations and DC voltages when $P_{Cd\text{-}B1}$=150 MW

**Figure 9.11:** Power flow analysis with DC/DC converter

### 9.2.2. Converter Cd-B1 with High Frequency on AC Stage

Converter Cd-B1 having a 50 Hz middle AC stage has been tested in a multi-terminal HVDC grid in Section 9.2.1. As explained in Chapter 8, the component sizing of the MMC based DC/DC converter can be decreased by increasing the AC side frequency. In this section, simulation of the system with DC/DC converter, Cd-B1, is presented with a middle AC stage frequency of 300 Hz and decreased submodule capacitance, arm inductance and AC line inductances in order to propose a more realistic solution while keeping the onshore and offshore AC systems at 50 Hz.

The results of the analysis are shown in Figures 9.12, 9.13 and 9.14 where the power flow on Cd-B1 is changed from -300 MW to 150 MW at t=2.5 s. As expected, the power flow is not affected by the

frequency change and the converter and transmission line powers are almost the same with the case of 50 Hz middle AC stage frequency as seen in Figure 9.12. Figure 9.13 shows that DC voltages at the converter stations have the same values with the previous case. AC waveforms on the middle AC stage of the DC/AC/DC converter, Cd-B1, are in 300 Hz as shown in Figure 9.14. During the power reversal the AC voltage is kept constant while AC current changes its magnitude in order to provide the power demand. Figure 9.14 also includes upper and lower arm submodule voltages, which are at 1 pu average level during the whole operation of the system.

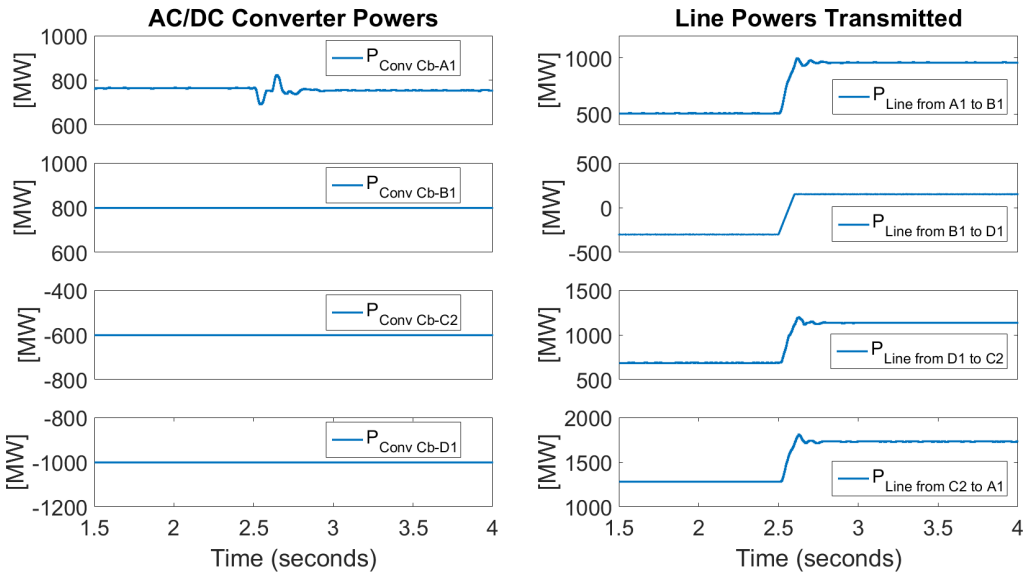


**Figure 9.12:** Converter and line powers

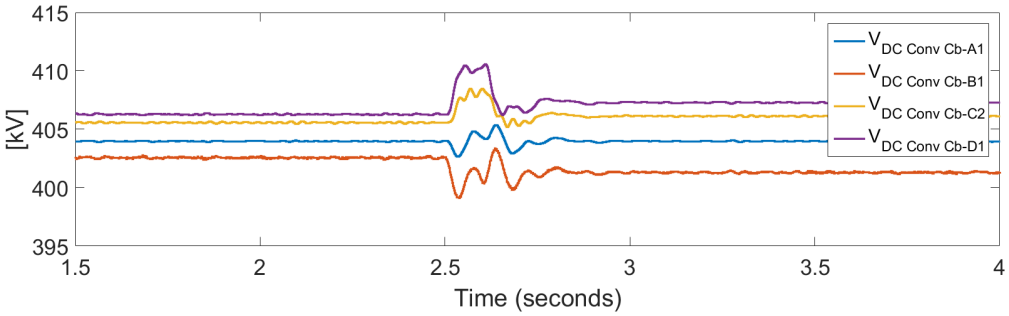


**Figure 9.13:** DC voltages at each AC/DC converter

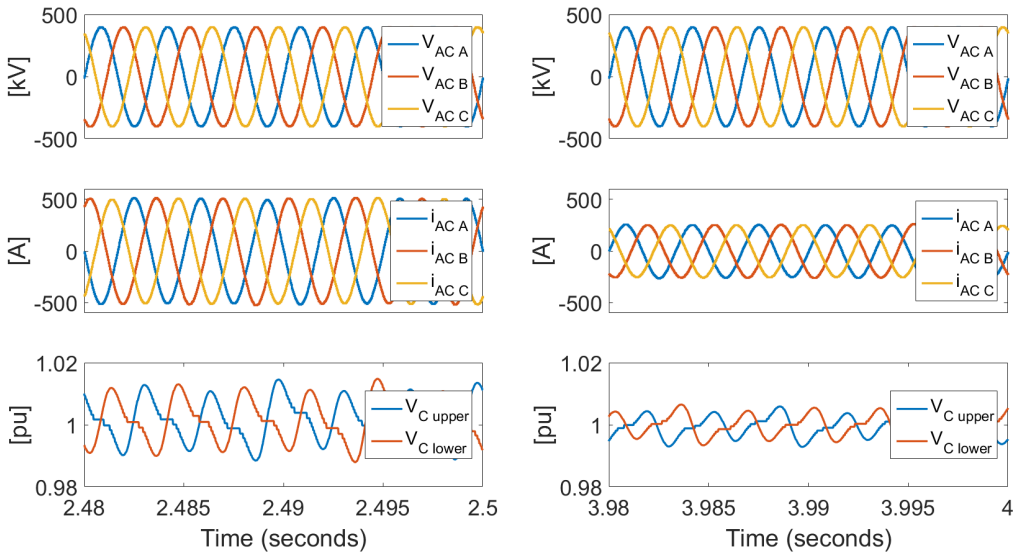


**Figure 9.14:** AC voltage, current and submodule voltages

### 9.2.3. Converter Cd-E1 Interconnecting Monopole and Bipolar Systems

The converter Cd-E1 is also verified by the DC/DC converter designed for interconnection of different HVDC configurations. For this purpose, previously constructed bipolar system is extended by adding the DCS2 monopole system to the MTDC grid. Monopole (light blue) and bipolar (blue) systems are shown in Figure 9.15. Additional offshore systems include an oil/gas platform at E1 which consumes power and power generation by wind farm at F1. On the onshore side, B1 and B3 are connected on AC side.

AC/DC converter settings and operation modes are shown in Table 9.4.

**Table 9.4:** Design parameters of the converters in MTDC grid

| AC/DC converter station | DC voltage [kV] | Operation mode |
|---|---|---|
| Cb-A1 | ±400 | $V_{DC}$=1.01 pu |
| Cb-B1 | ±400 | P=300 MW |
| Cb-C2 | ±400 | P=-500 MW |
| Cb-D1 | ±400 | P=-900 MW |
| Cm-E1 | ±100 | P=100 MW |
| Cm-F1 | ±100 | $V_{DC}$=0.99 pu |
| Cm-B3 | ±100 | P=400 MW |

As in DCS3 bipolar HVDC system, DCS2 provides the connection between converter stations via DC cables or overhead lines. Table 9.5 and Table 9.6 show length and type of lines between converter stations and resistance, inductance and capacitance values for the monopole system.

The simulation is performed using both converters Cd-B1 and Cd-E1 with a frequency of 300 Hz on AC stage. DC/DC converter without galvanic separation explained in Chapter 6 is used for Cd-B1 while galvanic separation via three-winding transformer introduced in Section 7.2.2 is used for Cd-E1. DC voltages of bipolar and monopole systems are set by converters at A1 and F1, respectively. As stated in [79], DC voltage in bipolar system is set to 1.01 pu (404 kV) while it is set to 0.99 pu (198 kV) in monopole system. In order to test the bidirectional power flow, the direction and magnitude of the power flow on the line B1-E1 are changed by DC/DC converter Cd-B1 from 300 MW (E1 to B1) to 150 MW (B1 to E1) at t=3 s while Cd-E1 changes the power flow from 400 MW (monopole to bipolar) to

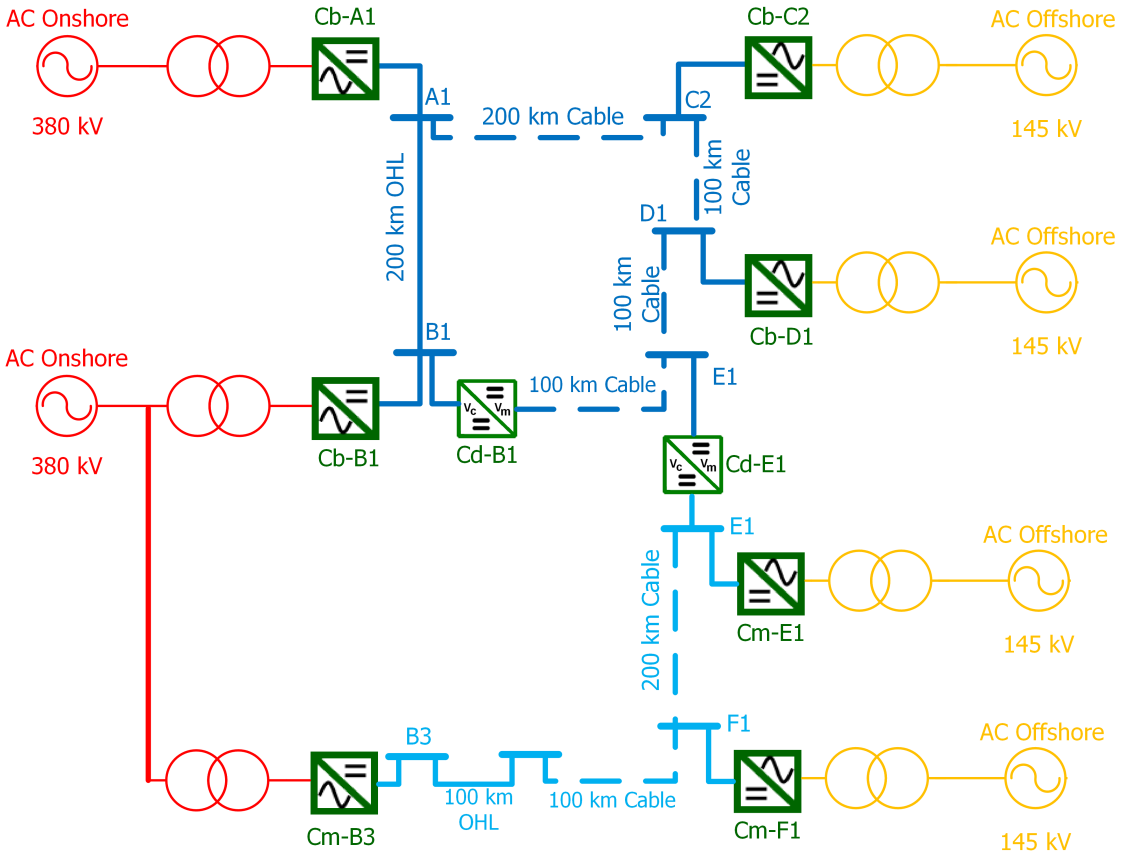


**Figure 9.15:** Monopole (light blue) and bipolar (blue) systems in MTDC grid

**Table 9.5:** DC line information in MTDC grid

| Line | Length [km] | Type |
|---|---|---|
| A1-B1 | 200 | OHL |
| A1-C2 | 200 | Cable |
| B1-E1 | 100 | Cable |
| C2-D1 | 100 | Cable |
| D1-E1 | 100 | Cable |
| E1-F1 | 200 | Cable |
| B3-F1 | 100 + 100 | OHL + Cable |

**Table 9.6:** DC line parameters in DCS2 monopole subsystem [79]

| Line Type | R [$\Omega$/km] | L [mH/km] | C [$\mu$F/km] |
|---|---|---|---|
| DC OHL monopole | 0.0133 | 0.8273 | 0.0139 |
| DC cable monopole | 0.0095 | 2.1110 | 0.2104 |

200 MW (bipolar to monopole) at t=6 s.

AC/DC converter powers in both bipolar and monopole systems are shown in Figure 9.16. As seen in the figure, power controlled converters have the adjusted power settings summarized in Table 9.4 while the converters controlling DC voltages, Cb-A1 and Cm-F1, affected by the power flow on the transmission lines.

Figure 9.17 shows the line powers between converter stations. Power flow from B1 to E1 is changed from -300 MW to 150 MW at t=3 s by DC/DC converter Cd-B1 while the power flow from monopole to

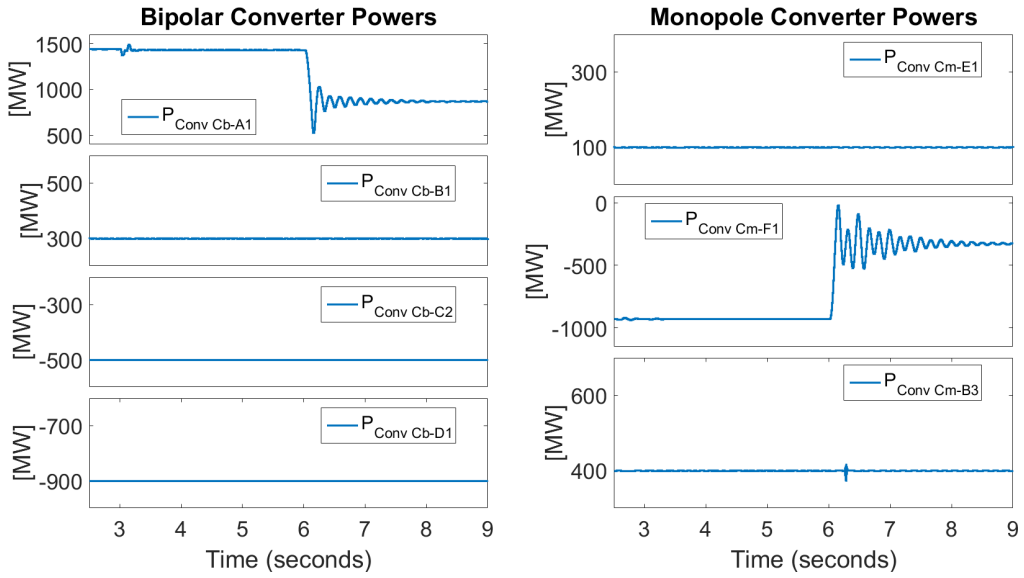


**Figure 9.16:** AC/DC converter powers in bipolar and monopole systems

bipolar system is changed from 400 MW to -200 MW at t=6 s. As seen in the Figure 9.17, the power transmitted on the other lines changes, accordingly and the oscillation of the power observed just after the power switch disappears in about 2 s.

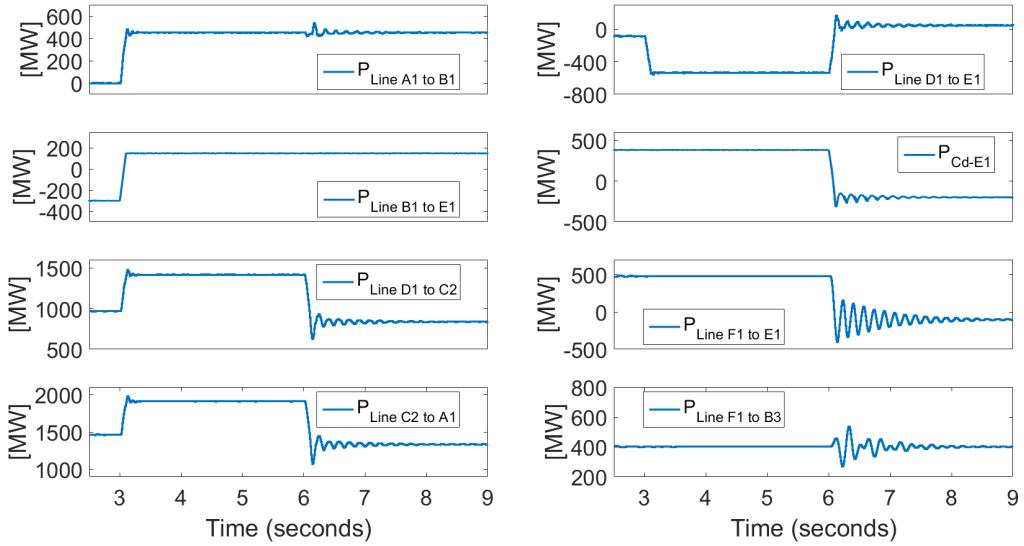


**Figure 9.17:** Transmitted line powers between converter stations

DC voltages of bipolar and monopole systems are shown in Figure 9.18. As seen in the figure, considerable amount of oscillation, especially on converter Cm-E1 which has a direct connection with DC/DC converter Cd-E1, is observed during the power changes on transmission lines. Since DC voltages are outside the limits of the multi-terminal grid codes during the transition, operation of the system has to be improved. In order to decrease oscillation, tuning of the controllers is re-examined and power and current controllers are slowed down. Figure 9.19 shows the result of the change in controller gains, thus the speed of the controller response, on DC voltages. Plots for the converter and line powers with the slowed down controllers can be found in Appendix E.

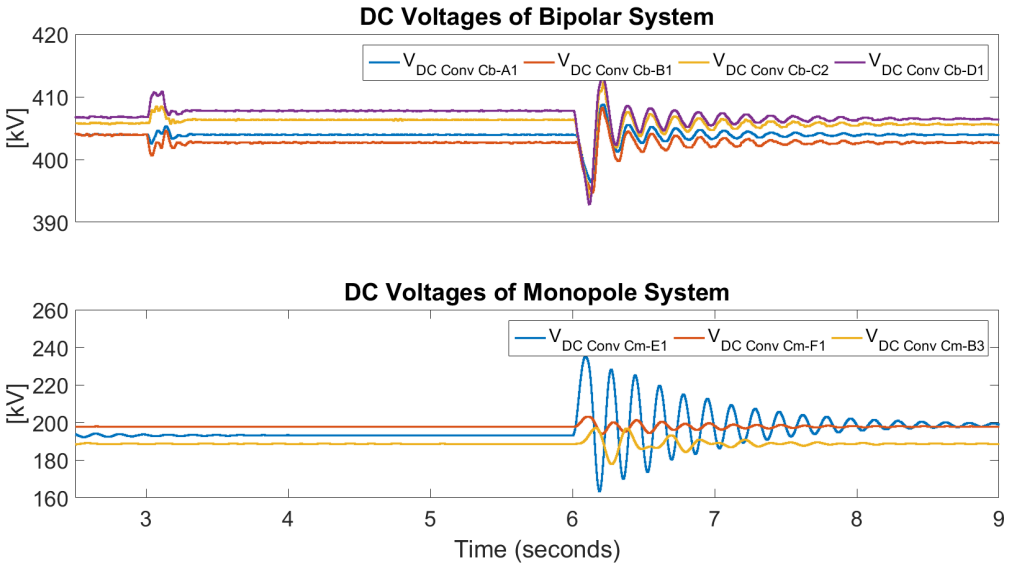


**Figure 9.18:** DC voltages at converter stations in bipolar and monopole systems

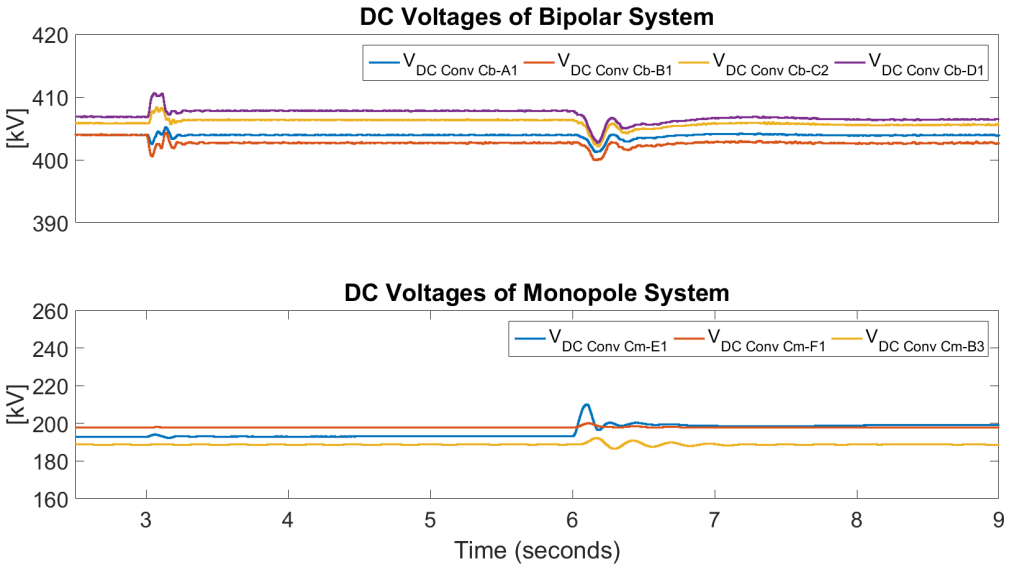


**Figure 9.19:** DC voltages at converter stations in bipolar and monopole systems with improved tuning of controllers

AC waveforms of DC/AC/DC converters, Cd-B1 and Cd-E1, operating at 300 Hz are shown in Figure 9.20 and Figure 9.21, respectively. As seen in the figures, AC voltages are constant during the all operation states of the converters while the AC currents change their magnitude according to power settings. Submodule voltages at around 1 pu level are also shown in these plots. Moreover, both figures show that the change in one converter does not affect the operation of other one.

The power flow analysis is summarized in Figure 9.22, Figure 9.23 and Figure 9.24 showing the all operation states of the converters. The power flow on transmission lines and the DC voltages at converter terminals are shown in these figures.

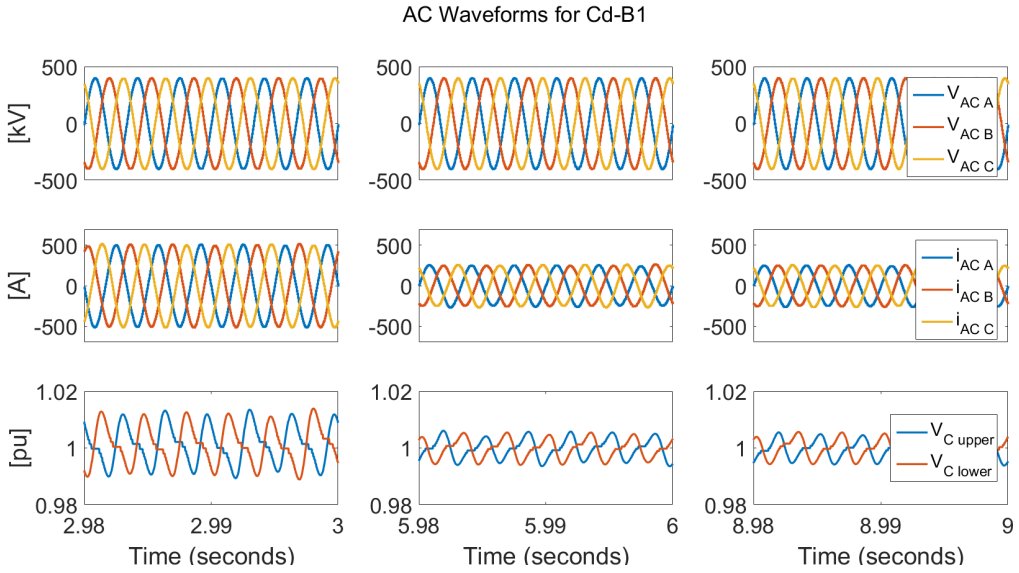


**Figure 9.20:** AC waveforms of Cd-B1 in bipolar system

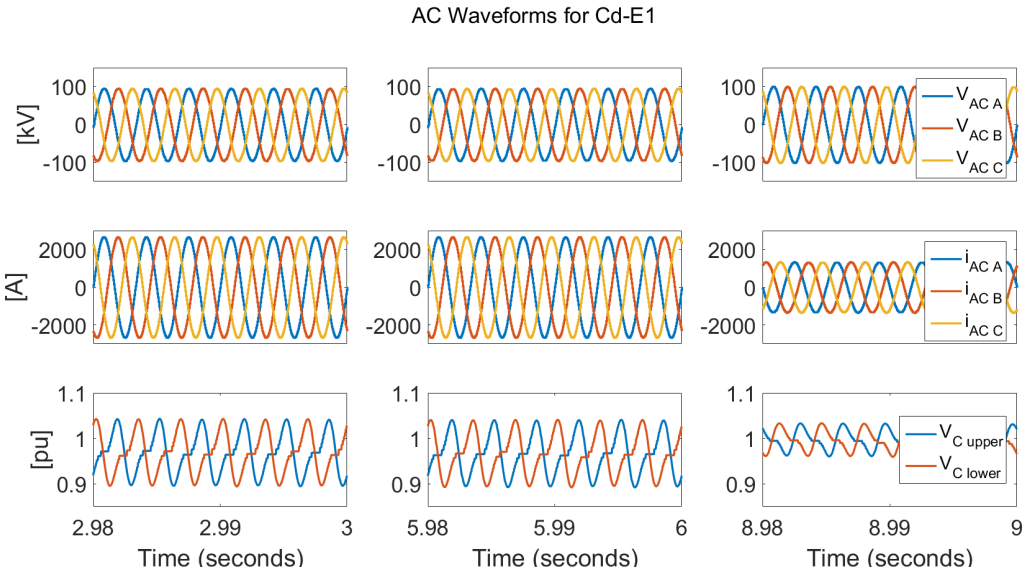


**Figure 9.21:** AC waveforms of Cd-E1 connecting bipolar and monopole systems with 300 Hz frequency

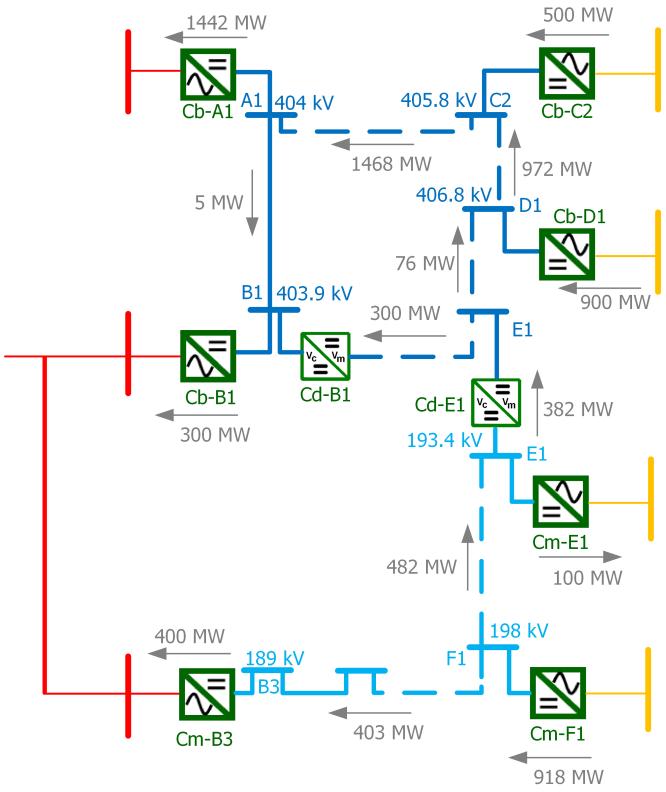


**Figure 9.22:** Power flow between converter stations and DC voltages when $P_{Cd\text{-}B1}$=-300 MW and $P_{Cd\text{-}E1}$=400 MW

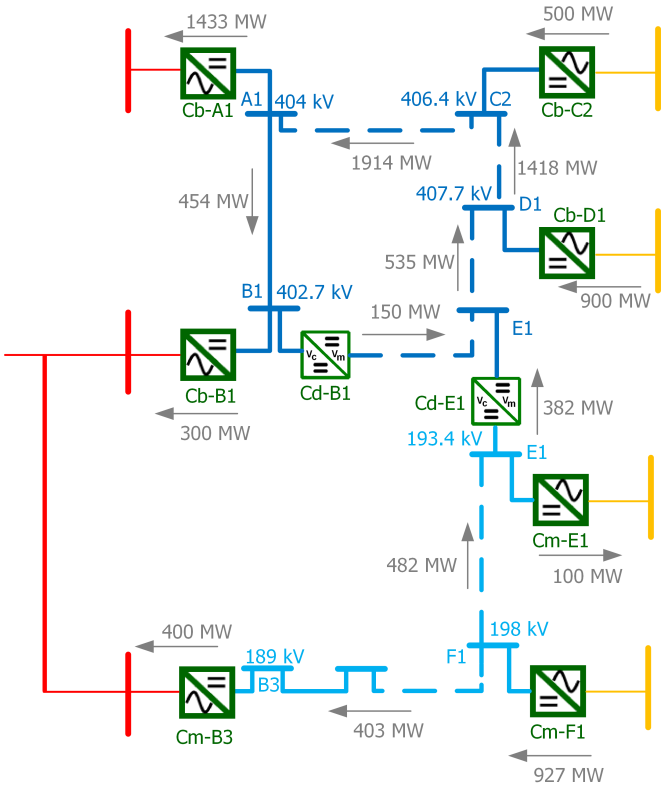


**Figure 9.23:** Power flow between converter stations and DC voltages when $P_{Cd\text{-}B1}$=150 MW and $P_{Cd\text{-}E1}$=400 MW

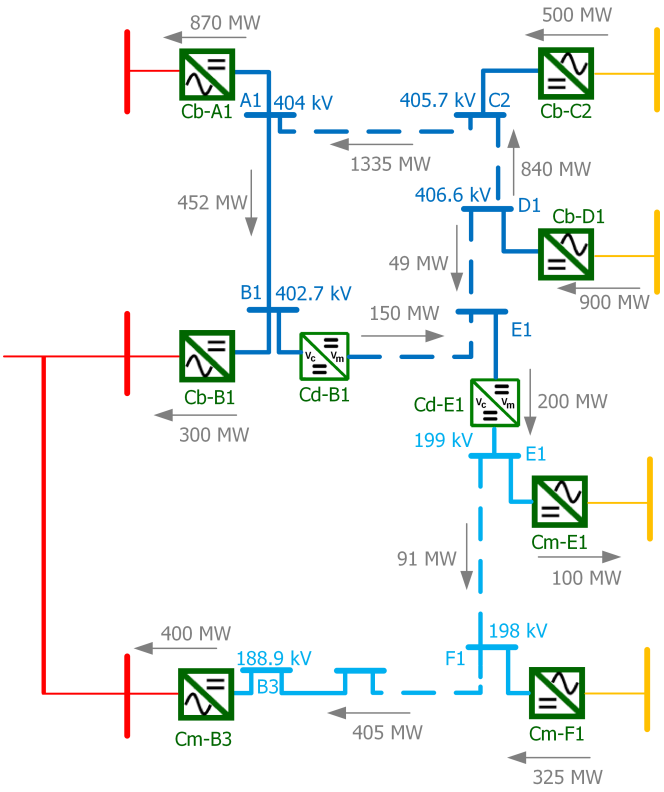


**Figure 9.24:** Power flow between converter stations and DC voltages when $P_{Cd\text{-}B1}$=150 MW and $P_{Cd\text{-}E1}$=-200 MW

### 9.2.4. Alternative Method for Connecting Monopole and Bipolar Systems

The connection of monopole DCS1 and bipolar DCS3 systems can be implemented by connecting two different systems on AC side instead of a direct connection on DC side via a DC/DC converter. Already existing AC/DC converters on the same onshore bus, A1, are used with this method which decreases the space and cost for the DC/DC converter. This connection includes two DC systems and an AC system at 50 Hz which also draws power in contrast to previously designed DC/AC/DC converters. Line powers become dependent on mainly AC/DC converter powers and DC/DC converter, Cd-B1, power flow. The layout of the system is shown in Figure 9.25. As seen in the figure, converters Cb-A1 and Cm-A1 are on the same bus while offshore wind power generation on C1 and C2 is connected via offshore cable. Figure 9.25 also shows the length of the lines connecting converter stations. The parameters for the additional offshore cable is given in Table 9.7.

**Table 9.7:** AC offshore cable parameters connecting Cm-C1 and Cb-C2 [79]

| Line Type | R [Ω/km] | L [mH/km] | C [$\mu$F/km] |
|---|---|---|---|
| AC 145 kV offshore cable | 0.0843 | 0.2526 | 0.1837 |

Converter settings and their operation modes are shown in Table 9.8.

The simulation is performed on Matlab/Simulink with Cd-B1 operating at 300 Hz on AC side and the interconnection of monopole and bipolar systems is accomplished by converters Cm-A1 and Cb-A1 located on the same bus. Converter and line powers are shown in Figure 9.26 and it shows that converter powers are almost constant during the whole operation of the system while the power reversal on Cd-B1 affects the transmitted powers on the lines.

Figure 9.27 shows DC voltages for both bipolar and monopole systems. As in the previous cases, Cd-A1 adjusts DC voltage of bipolar system at 1.01 pu corresponding 404 kV while Cm-A1 sets the DC

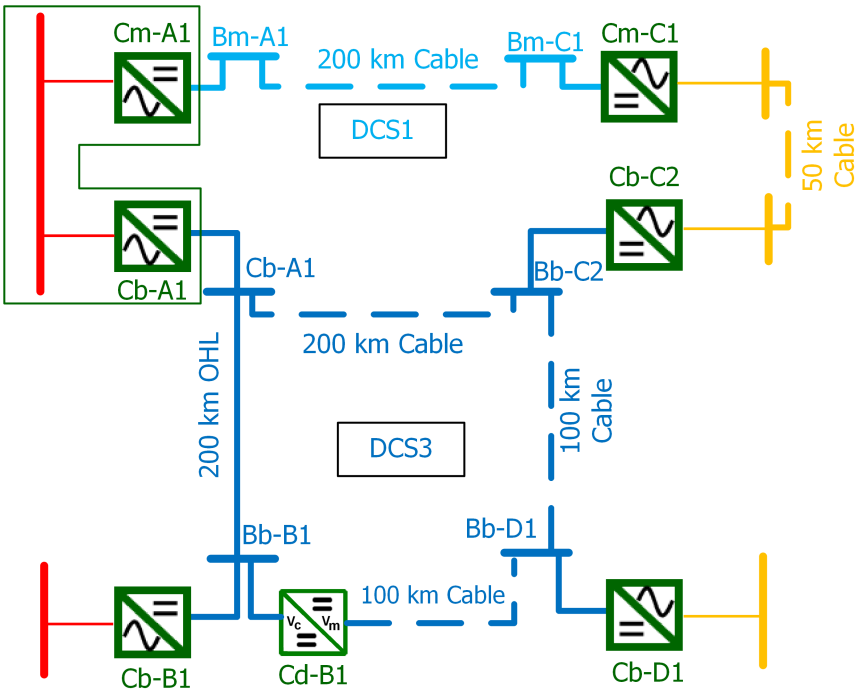


**Figure 9.25:** Layout of the monopole (light blue) and bipolar (blue) systems connection

**Table 9.8:** Design parameters of the converters in DCS3 and DCS1

| AC/DC converter station | DC voltage [kV] | Operation mode |
|---|---|---|
| Cb-A1 | ±400 | $V_{DC}$=1.01 pu |
| Cb-B1 | ±400 | P=800 MW |
| Cb-C2 | ±400 | P=-500 MW |
| Cb-D1 | ±400 | P=-900 MW |
| Cm-C1 | ±100 | P=-500 MW |
| Cm-A1 | ±100 | $V_{DC}$=1 pu |

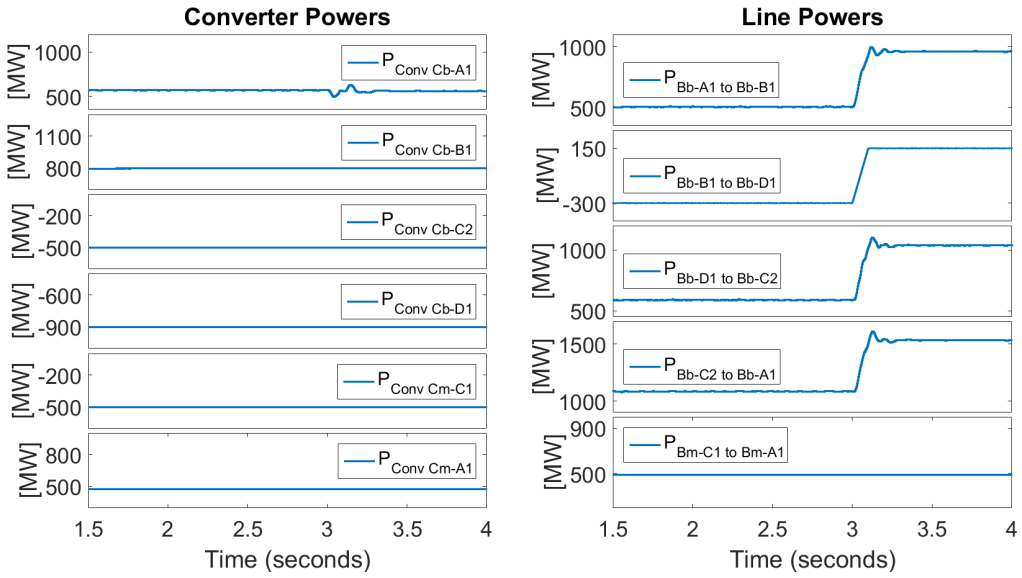


**Figure 9.26:** Converter and line powers of monopole and bipolar systems connected on bus A1

voltage of monopole system to 1 pu corresponding 200 kV.

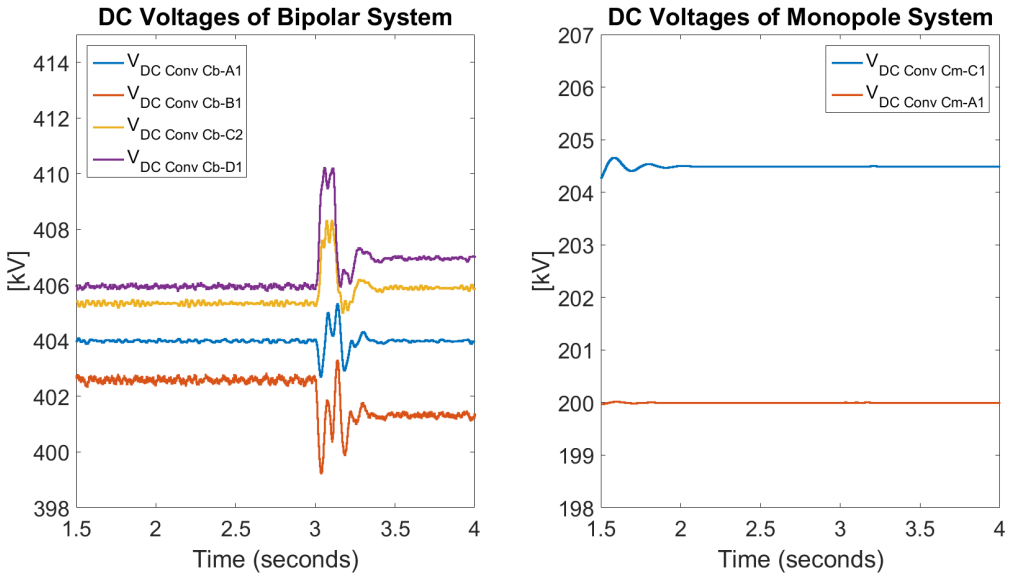


**Figure 9.27:** DC voltages of bipolar and monopole systems

AC voltage, current and submodule voltages of MMC based DC/DC converter Cd-B1 are shown in Figure 9.28. As seen in the figure, AC current and voltage has a sinusoidal waveforms, submodules are charged and discharged properly while the submodule voltage average is kept at 1 pu level.

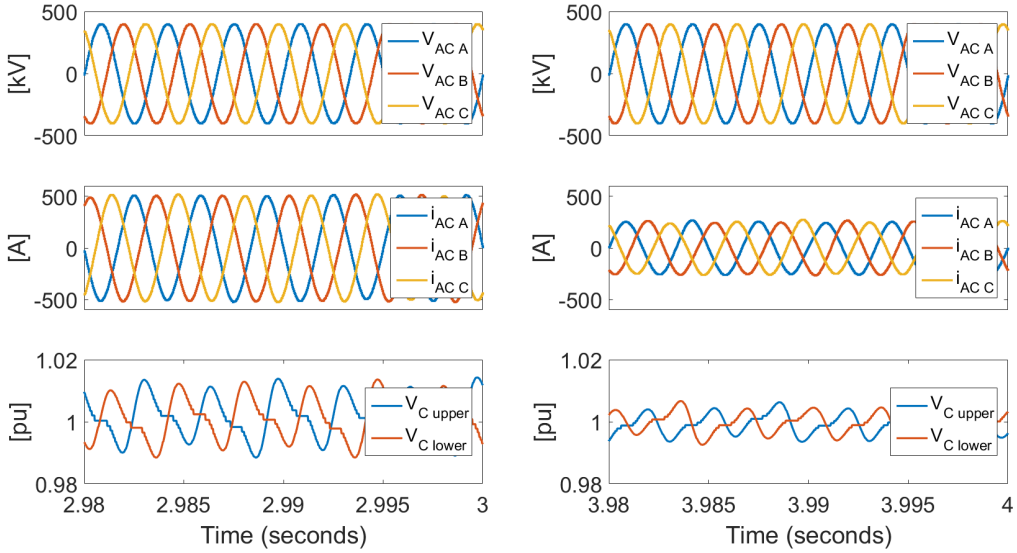


**Figure 9.28:** AC waveforms of Cd-B1 when DCS1 and DCS3 are connected

The summary of the power flow study with the connection of DCS1 and DCS3 is shown in Figure 9.29 for both direction of the powers on Cd-B1 together with the DC bus voltages.

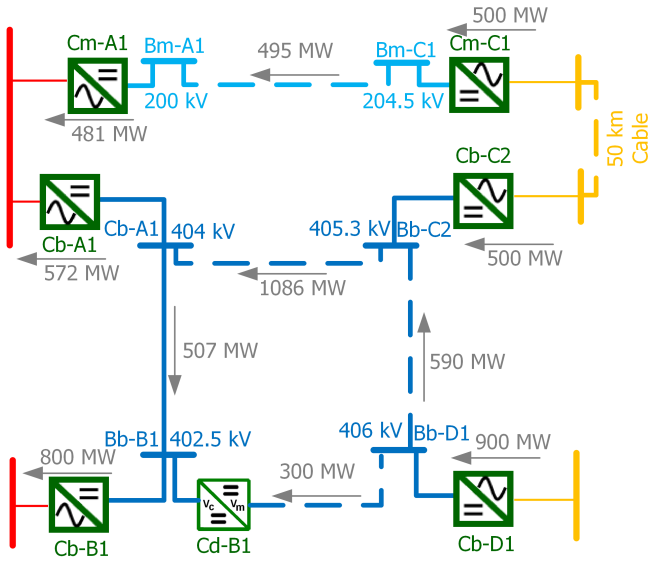


**(a)** Power flow between converter stations and DC voltages when $P_{Cd\text{-}B1}$=-300 MW

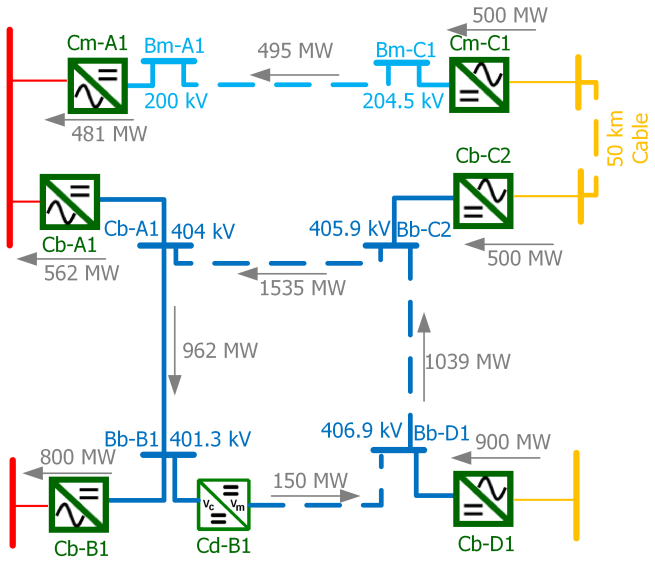


**(b)** Power flow between converter stations and DC voltages when $P_{Cd\text{-}B1}$=150 MW

**Figure 9.29:** Power flow analysis with alternative connection of monopole and bipolar systems

# 10

# Conclusion and Future Work

*This chapter summarizes the main results of the thesis and presents suggestions for future work.*

For the power transfer over long distances, VSC-based HVDC systems are favoured as they offer a flexible power control. The MMC is a prominent solution for high voltage and high power applications due to its high modularity, scalability and low switching losses. The increasing number of HVDC transmission lines and renewable energy generation requires the interconnection of DC networks in order to form a MTDC grid. In a MTDC system, interconnection of DC systems operating at different voltages and different configurations is inevitable. Therefore, DC/DC converters enter the scene.

Depending on the application and the characteristics of the DC networks to be connected, different DC/DC converters have been introduced in which front-to-front connection of two DC/AC converters forming a middle AC stage is common for all converter types for the high voltage and high power applications. MMC based DC/AC/DC converters have been analysed in this thesis after the basic analysis of MMC has been introduced.

A mathematical model of MMC has been simulated with phase shifted PWM technique for low number submodules. The mathematical model has been also verified by a switching model with 8 submodules per phase consisting of IGBT and capacitor connections in each cell and similar results have been obtained. Due to the increased simulation time for high number of submodules resulting from the increased number of signals to be compared for the modulation and generation of gate signals, nearest level modulation technique has been used for the further analysis with controlled voltage sources-based model. On this detailed MMC model with high number of submodules suitable for the high voltage applications, active and reactive power controls have been implemented before front-to-front connection of two MMC.

For the power flow control between two DC networks operating at similar voltages with similar configurations, front-to-front connected MMC based DC/AC/DC converter without transformer coupling has been proposed. Using vector control for power controllers and PR controllers for the circulating current suppression controller, the correct operation of the DC/DC converter has been observed for a power flow control study.

Connection of DC networks operating at different voltage levels or systems with different configurations has been achieved by using a transformer coupled DC/DC converter. The transformer has been used as a galvanic insulation on AC side which also adjusts the voltage level between converters on high voltage and low voltage sides. Monopole and bipolar HVDC networks have been connected via two two-winding transformers or a three-winding transformer and good performance of bidirectional power flow has been observed for all converters connecting different voltages and/or different configurations.

The effect of frequency change on component sizes of the MMC has been analysed on all types of DC/DC converters. In order to decrease submodule capacitor, arm inductor and transformer sizes,

increase in AC side frequency has been proposed which minimizes the main disadvantage of MMC resulting from the high number of submodule capacitors. The comparable performances of the converters have been observed with decreased component sizes and increased AC side frequency.

Designed DC/DC converters have been verified in terms of performance and functionality in a MTDC grid based on a system designed by Cigre B4 working group. The multi-terminal simulation models designed for ProOfGrids project performed in SINTEF Energy Research have been utilized and the required connections, line, voltage and power settings have been adjusted depending on the Cigre grid for the simulation of MTDC system. In MTDC grid, the converter designed for the connection of DC networks operating at the same voltage with same configurations and the converter connecting symmetric monopole and bipolar systems operating at different voltage levels have been both tested. The results have showed a good operation of converters in the MTDC system. Monopole and bipolar HVDC networks where the connection between them is provided by two AC/DC converters placed on the same bus have been also emphasized since it can be useful for the future development of a fully hybrid AC/DC transmission systems.

Several aspects can be relevant for further study and investigating the other features of MMC based DC/DC converters. Some ideas may include followings:

- The simulations have been performed based on the half bridge cell configuration. The full bridge topology for MMC submodules can be a next step for modelling of a MMC based DC/DC converter.
- Fault analysis of the converter has not been considered for the designs but DC transmission line faults are unavoidable especially for long distance transmissions and they could influence the performance of the whole MTDC system. The clearance of DC line faults feature of full bridge converter topology needs to be investigated.
- The main advantage of using MMC is that its low losses due to ability to operate at low switching frequencies. In order to test and verify this feature, a loss analysis should be implemented in the converter models. The calculation of losses is also useful to determine the AC side frequency on the middle stage. The balance between the component sizes and switching losses with increased AC frequency can be provided efficiently by loss calculation.
- The comparison of the DC/DC converters based on two level converters and MMC should be made in terms of losses, cost and area required for the converter station. MMC is also supposed to behave like a storage device due to the high number of capacitors; therefore, performing a speed comparison of MMC with the two level converter may be relevant.
- A prototype for laboratory hardware realization should be constructed in order to test control systems of MMC and verify the DC/DC converter operation.

# Appendix A

## Transformation between abc and dq Reference Frames

It should be noted that coefficients of active and reactive power equations change depending on the coefficient of Clark (from *abc* to $\alpha\beta$) and inverse Clark (from $\alpha\beta$ to *abc*) transformations.

**Power Invariant Transformation:** If the coefficients for Clark and inverse Clark transformation are $\sqrt{\frac{2}{3}}$ as shown below, active and reactive powers do not have any coefficient i.e. $P = V_d i_d$ , $Q = V_d i_q$

$$Clark\ Transformation: \sqrt{\frac{2}{3}}\begin{bmatrix} 1 & -\frac{1}{2} & -\frac{1}{2} \\ 0 & \frac{\sqrt{3}}{2} & -\frac{\sqrt{3}}{2} \end{bmatrix}$$

$$Inverse\ Clark\ Transformation: \sqrt{\frac{2}{3}}\begin{bmatrix} 1 & 0 \\ -\frac{1}{2} & \frac{\sqrt{3}}{2} \\ -\frac{1}{2} & -\frac{\sqrt{3}}{2} \end{bmatrix}$$

**Power Variant Transformation:** If the coefficient for Clark transformation is $\frac{2}{3}$ as shown below, active and reactive powers have a coefficient of $\frac{3}{2}$ i.e. $P = \frac{3}{2} V_d i_d$ , $Q = \frac{3}{2} V_d i_q$

$$Clark\ Transformation: \frac{2}{3}\begin{bmatrix} 1 & -\frac{1}{2} & -\frac{1}{2} \\ 0 & \frac{\sqrt{3}}{2} & -\frac{\sqrt{3}}{2} \end{bmatrix}$$

$$Inverse\ Clark\ Transformation: \begin{bmatrix} 1 & 0 \\ -\frac{1}{2} & \frac{\sqrt{3}}{2} \\ -\frac{1}{2} & -\frac{\sqrt{3}}{2} \end{bmatrix}$$

For both power invariant and power variant Clarke transformations, Park (from $\alpha\beta$ to $dq$) and inverse Park (from $dq$ to $\alpha\beta$) transformations are the same as shown below:

$$Park\ Transformation: \begin{bmatrix} \cos\theta & \sin\theta \\ -\sin\theta & \cos\theta \end{bmatrix}$$

$$Inverse\ Park\ Transformation: \begin{bmatrix} \cos\theta & -\sin\theta \\ \sin\theta & \cos\theta \end{bmatrix}$$

# Appendix B

## Matlab Code for Phase-Shifted PWM Modulation Algorithm

### Upper Arm Carrier Wave Generation

```
function yu = fcn(t)
%#codegen
coder.extrinsic('sawtooth')
n=8; %number of submodules in a leg
yu=zeros(n/2,1);
for i=1:n/2 %upper arm
yu(i) = sawtooth(2*pi*2000*t+(i-1)*360/(n/2)*2*pi/360, 0.5); %2 kHz
end
```

### Upper Arm Gate Signal Generation

```
function [Sl, state_cross, VClindex]  = fcn(Slold, Vlrefnew, VCl, i2, Tlnew, Tlold, Vlrefold)
%#codegen
coder.extrinsic('format')
format long
state_cross=0;
Sl=Slold;
n=8; %number of SM in a leg

for i=1:n/2 %upper arm
if(Tlold(i)-Vlrefold)*(Tlnew(i)-Vlrefnew)<0
    state_cross=1;
    ref_number=i;
    break
end
end
 [VClsorted, VClindex]=sort(VCl);

if state_cross==1 && Vlrefnew<Tlnew(ref_number)
    if i2>0
        for m=1:n/2
            if(Sl(VClindex(m))==0)
            Sl(VClindex(m))=1;
            break
            end
        end
    else
        for m=1:n/2
            if(Sl(VClindex((n/2)-(m-1)))==0)
            Sl(VClindex((n/2)-(m-1)))=1;
            break
            end
        end
    end
elseif state_cross==1 && Vlrefnew>=Tlnew(ref_number)
    if i2>0
        for m=1:n/2
            if(Sl(VClindex((n/2)-(m-1)))==1)
            Sl(VClindex((n/2)-(m-1)))=0;
            break
```

```
            end
        end
    else
        for m=1:n/2
            if(Sl(VClindex(m))==1)
            Sl(VClindex(m))=0;
            break
            end
        end
    end
else
     Sl=Slold;
end
```

## Lower Arm Carrier Wave Generation

```
function yl = fcn(t)
%#codegen
coder.extrinsic('sawtooth')
n=8; %number of submodules in a leg
yl=zeros(n/2,1);
for i=1:n/2 %lower arm
yl(i) = sawtooth(2*pi*2000*t+(i-1)*360/(n/2)*2*pi/360+360/n*2*pi/360, 0.5);
end
```

## Lower Arm Gate Signal Generation

```
function [Sl, state_cross, VClindex]  = fcn(Slold, Vlrefnew, VCl, i2, Tlnew, Tlold, Vlrefold)
%#codegen
coder.extrinsic('format')
format long
state_cross=0;
Sl=Slold;
n=8; %number of SM in  leg

for i=1:n/2 %lower arm
if(Tlold(i)-Vlrefold)*(Tlnew(i)-Vlrefnew)<0
    state_cross=6;
    ref_number=i;
    break
end
end
 [VClsorted, VClindex]=sort(VCl);

if state_cross==6 && Vlrefnew>Tlnew(ref_number)
    if i2>0
        for m=1:n/2
            if(Sl(VClindex((n/2)-(m-1)))==0)
            Sl(VClindex((n/2)-(m-1)))=1;
            break
            end
        end
    else
        for m=1:n/2
            if(Sl(VClindex(m))==0)
            Sl(VClindex(m))=1;
            break
            end
        end
    end
elseif state_cross==6 && Vlrefnew<=Tlnew(ref_number)
    if i2>0
        for m=1:n/2
```

```
                if(Sl(VClindex(m))==1)
                Sl(VClindex(m))=0;
                break
                end
            end
        else
            for m=1:n/2
                if(Sl(VClindex((n/2)-(m-1)))==1)
                Sl(VClindex((n/2)-(m-1)))=0;
                break
                end
            end
        end
    else
        Sl=Slold;
    end
```

# Appendix C

## Bode Plot of PR Controller Used in CCSC

The figure below shows the bode plot of PR controller used as a circulating current suppressing controller with the following parameters:

**Table 1:** Design parameters for the circulating current suppression using PR controller

| | |
|---|---|
| **AC side frequency** | 50 Hz |
| **$K_P$** | 0.06 |
| **$K_r$** | 5 |
| $\omega_c$ | 5 rad/s |

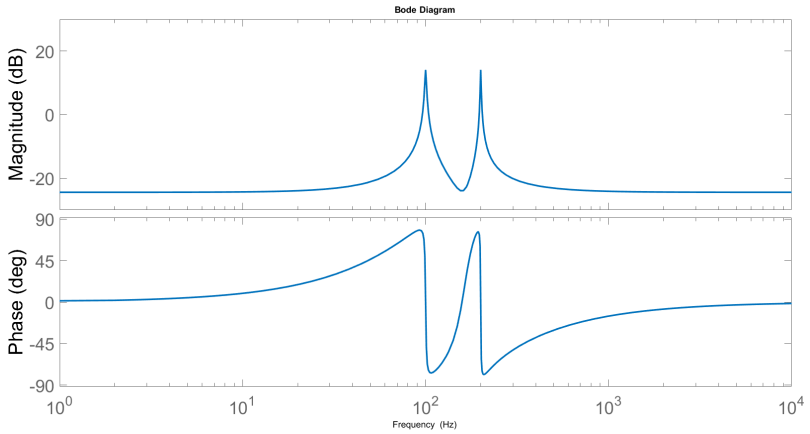


**Figure 1:** The bode plot of PR controller

# Appendix D

## Matlab Code for Multi-terminal DC Grid with 7 Converters

```
function varargout = ScenarioTemplate(varargin)
%#codegen
Ts = 0;
savemat = 1;
if  nargin>=2
    savemat = varargin{2};
elseif nargin>=1
    Ts = varargin{1};
end

nCvtr_ref = 16; % # number of references for each converter
nEl_mod_ctrl_ref = 10; % number of additional events
nSec_ctrl_ref = 16; % number of additional events

% definition of ref index
idx.enable_cvtr_intfc=1;
idx.enable_SVPWM_intfc=2;
idx.enable_PLL_intfc=3;
idx.enable_Vdc_ctrl_intfc=4;
idx.enable_PQ_ctrl_intfc=5;
idx.f_sw_ref=6;
idx.f_ref_PLL=7;
idx.Id_ref=8;
idx.Iq_ref=9;
idx.P_ref=10;
idx.Q_ref=11;
idx.Vdc_ref=12;
idx.cntcr_ctrl_intfc=13;
idx.enable_ICalibration_intfc=14;
idx.enable_VdcCalibration_intfc=15;
idx.enable_VCalibration_intfc=16;

% definition of Events index
idxE.SW1 = 1;
idxE.Fault1 = 2;

% definition of ref index
idxSC.Vdc_ref_max_A=1;
idxSC.Vdc_ref_min_A=2;
idxSC.droop_gain_A=3;
idxSC.Idc_ref_A=4;
idxSC.Vdc_ref_max_B=5;
idxSC.Vdc_ref_min_B=6;
idxSC.droop_gain_B=7;
idxSC.Idc_ref_B=8;
idxSC.Vdc_ref_max_C=9;
idxSC.Vdc_ref_min_C=10;
idxSC.droop_gain_C=11;
idxSC.Idc_ref_C=12;
idxSC.Vdc_ref_max_D=13;
idxSC.Vdc_ref_min_D=14;
idxSC.droop_gain_D=15;
idxSC.Idc_ref_D=16;

ts_ConvA = timeseries('ts_ConvA');
ts_ConvA = setinterpmethod(ts_ConvA, 'zoh');
```

```
ts_ConvB = timeseries('ts_ConvB');
ts_ConvB = setinterpmethod(ts_ConvB, 'zoh');
ts_ConvC = timeseries('ts_ConvC');
ts_ConvC = setinterpmethod(ts_ConvC, 'zoh');
ts_ConvD = timeseries('ts_ConvD');
ts_ConvD = setinterpmethod(ts_ConvD, 'zoh');
ts_ConvE1 = timeseries('ts_ConvE1');
ts_ConvE1 = setinterpmethod(ts_ConvB, 'zoh');
ts_ConvF = timeseries('ts_ConvF');
ts_ConvF = setinterpmethod(ts_ConvF, 'zoh');
ts_ConvG = timeseries('ts_ConvG');
ts_ConvG = setinterpmethod(ts_ConvG, 'zoh');
ts_Events = timeseries('ts_Events');
ts_Events = setinterpmethod(ts_Events, 'zoh');
ts_Secondary_control = timeseries('ts_Secondary_control');
ts_Secondary_control = setinterpmethod(ts_Secondary_control, 'zoh');

%% Initialization
f_sw_ref = 5000;

sA.data = zeros(1,nCvtr_ref); % Default initialization is zero.
sA.time = 0;
sA.data(idx.f_sw_ref) = f_sw_ref; % Initialize required variables.
sA.data(idx.f_ref_PLL) = 50;
ts_ConvA = addsample(ts_ConvA,sA);

sB.data = zeros(1,nCvtr_ref);
sB.time = 0;
sB.data(idx.f_sw_ref) = f_sw_ref;
sB.data(idx.f_ref_PLL) = 50;
ts_ConvB = addsample(ts_ConvB,sB);

sC.data = zeros(1,nCvtr_ref);
sC.time = 0;
sC.data(idx.f_sw_ref) = f_sw_ref;
sC.data(idx.f_ref_PLL) = 50;
ts_ConvC = addsample(ts_ConvC,sC);

sD.data = zeros(1,nCvtr_ref);
sD.time = 0;
sD.data(idx.f_sw_ref) = f_sw_ref;
sD.data(idx.f_ref_PLL) = 50;
ts_ConvD = addsample(ts_ConvD,sD);

sE1.data = zeros(1,nCvtr_ref);
sE1.time = 0;
sE1.data(idx.f_sw_ref) = f_sw_ref;
sE1.data(idx.f_ref_PLL) = 50;
ts_ConvE1 = addsample(ts_ConvE1,sE1);

sF.data = zeros(1,nCvtr_ref);
sF.time = 0;
sF.data(idx.f_sw_ref) = f_sw_ref;
sF.data(idx.f_ref_PLL) = 50;
ts_ConvF = addsample(ts_ConvF,sF);

sG.data = zeros(1,nCvtr_ref);
sG.time = 0;
sG.data(idx.f_sw_ref) = f_sw_ref;
sG.data(idx.f_ref_PLL) = 50;
ts_ConvG = addsample(ts_ConvG,sG);

sE.data = zeros(1,nEl_mod_ctrl_ref);
sE.time = 0;
ts_Events = addsample(ts_Events,sE);

sSC.data = zeros(1,nSec_ctrl_ref);
sSC.time = 0;
sSC.data(idxSC.Vdc_ref_max_A) = 1.1;
sSC.data(idxSC.Vdc_ref_min_A) = 1.1;
sSC.data(idxSC.droop_gain_A) = 0;
```

```
sSC.data(idxSC.Idc_ref_A) = 0;
sSC.data(idxSC.Vdc_ref_max_B) = 1.12;
sSC.data(idxSC.Vdc_ref_min_B) = 1.08;
sSC.data(idxSC.droop_gain_B) = 0;
sSC.data(idxSC.Idc_ref_B) = .8;
sSC.data(idxSC.Vdc_ref_max_C) = 1.14;
sSC.data(idxSC.Vdc_ref_min_C) = 1.06;
sSC.data(idxSC.droop_gain_C) = 0;
sSC.data(idxSC.Idc_ref_C) = .6;
sSC.data(idxSC.Vdc_ref_max_D) = 1.16;
sSC.data(idxSC.Vdc_ref_min_D) = 1.04;
sSC.data(idxSC.droop_gain_D) = 0;
sSC.data(idxSC.Idc_ref_D) = .7;

ts_Secondary_control = addsample(ts_Secondary_control,sSC);

% Events Definitions
% 1) set the new time:           sX.time = newtime
% 2) update the required data:   sX.data(index) = newvalue
% 3) add the sample:             ts_ConvX = addsample(ts_ConvX,sX);

%% Converter A1
% definition of event 1 A
sA.time = 0.01;
sA.data(idx.enable_SVPWM_intfc) = 1;
sA.data(idx.enable_PLL_intfc) = 1;
sA.data(idx.enable_Vdc_ctrl_intfc) = 1;
sA.data(idx.Vdc_ref) = 400e3*1.01;
sA.data(idx.cntcr_ctrl_intfc) = 1;
ts_ConvA = addsample(ts_ConvA,sA);

% definition of event 2 A
sA.time = 0.3;
sA.data(idx.enable_cvtr_intfc) = 1;
ts_ConvA = addsample(ts_ConvA,sA);


%% Converter B1
% definition of event 1 B
sB.time = 0.01;
sB.data(idx.enable_SVPWM_intfc) = 1;
sB.data(idx.enable_PLL_intfc) = 1;
sB.data(idx.enable_PQ_ctrl_intfc) = 1;
sB.data(idx.P_ref)=150e6;
sB.data(idx.Q_ref)=0;
sB.data(idx.cntcr_ctrl_intfc) = 1;
ts_ConvB = addsample(ts_ConvB,sB);

% definition of event 2 B
sB.time = 0.35;
sB.data(idx.enable_cvtr_intfc) = 1;
ts_ConvB = addsample(ts_ConvB,sB);


%% Converter C2
% definition of event 1 C
sC.time = 0.01;
sC.data(idx.enable_SVPWM_intfc) = 1;
sC.data(idx.enable_PLL_intfc) = 1;
sC.data(idx.enable_PQ_ctrl_intfc) = 1;
sC.data(idx.P_ref)=-250e6;
sC.data(idx.Q_ref)=0;
sC.data(idx.cntcr_ctrl_intfc) = 1;
ts_ConvC = addsample(ts_ConvC,sC);

% definition of event 2 C
sC.time = 0.25;
sC.data(idx.enable_cvtr_intfc) = 1;
ts_ConvC = addsample(ts_ConvC,sC);
```

```
%% Converter D1
% definition of event 1 D
sD.time = 0.01;
sD.data(idx.enable_SVPWM_intfc) = 1;
sD.data(idx.enable_PLL_intfc) = 1;
sD.data(idx.enable_PQ_ctrl_intfc) = 1;
sD.data(idx.P_ref)=-450e6;
sD.data(idx.Q_ref)=0;
sD.data(idx.cntcr_ctrl_intfc) = 1;
ts_ConvD = addsample(ts_ConvD,sD);

% definition of event 2 D
sD.time = 0.2;
sD.data(idx.enable_cvtr_intfc) = 1;
ts_ConvD = addsample(ts_ConvD,sD);

%% Converter E1
% definition of event 1 E1
sE1.time = 0.01;
sE1.data(idx.enable_SVPWM_intfc) = 1;
sE1.data(idx.enable_PLL_intfc) = 1;
sE1.data(idx.enable_PQ_ctrl_intfc) = 1;
sE1.data(idx.P_ref)=100e6;
sE1.data(idx.Q_ref)=0;
sE1.data(idx.cntcr_ctrl_intfc) = 1;
ts_ConvE1 = addsample(ts_ConvE1,sE1);

% definition of event 2 E1
sE1.time = 0.42;
sE1.data(idx.enable_cvtr_intfc) = 1;
ts_ConvE1 = addsample(ts_ConvE1,sE1);

%% Converter F1
% definition of event 1 F
sF.time = 0.01;
sF.data(idx.enable_SVPWM_intfc) = 1;
sF.data(idx.enable_PLL_intfc) = 1;
sF.data(idx.enable_Vdc_ctrl_intfc) = 1;
sF.data(idx.Vdc_ref) = 200e3*0.99;
sF.data(idx.cntcr_ctrl_intfc) = 1;
ts_ConvF = addsample(ts_ConvF,sF);

% definition of event 2 F
sF.time = 0.23;
sF.data(idx.enable_cvtr_intfc) = 1;
ts_ConvF = addsample(ts_ConvF,sF);

%% Converter B3
% definition of event 1 B3
sG.time = 0.01;
sG.data(idx.enable_SVPWM_intfc) = 1;
sG.data(idx.enable_PLL_intfc) = 1;
sG.data(idx.enable_PQ_ctrl_intfc) = 1;
sG.data(idx.P_ref)=400e6;
sG.data(idx.Q_ref)=0;
sG.data(idx.cntcr_ctrl_intfc) = 1;
ts_ConvG = addsample(ts_ConvG,sG);

% definition of event 2 B
sG.time = 0.5;
sG.data(idx.enable_cvtr_intfc) = 1;
ts_ConvG = addsample(ts_ConvG,sG);

%% Events
% definition of event 1 E
sE.time = 0.01;
sE.data(idxE.SW1) = 1; % close breaker 1
ts_Events = addsample(ts_Events,sE);

%% END
```

```
% resample timeseries using uniform time with timestep Ts, start Tstart and end Tend
if Ts>0
    time = 0:Ts:ts_ConvA.Time(end);
    ts_ConvA = resample(ts_ConvA,time,'zoh');
    time = 0:Ts:ts_ConvB.Time(end);
    ts_ConvB = resample(ts_ConvB,time,'zoh');
    time = 0:Ts:ts_ConvC.Time(end);
    ts_ConvC = resample(ts_ConvC,time,'zoh');
    time = 0:Ts:ts_ConvD.Time(end);
    ts_ConvD = resample(ts_ConvD,time,'zoh');
    time = 0:Ts:ts_ConvE1.Time(end);
    ts_ConvE1 = resample(ts_ConvE1,time,'zoh');
    time = 0:Ts:ts_ConvF.Time(end);
    ts_ConvF = resample(ts_ConvF,time,'zoh');
    time = 0:Ts:ts_ConvG.Time(end);
    ts_ConvG = resample(ts_ConvG,time,'zoh');
    time = 0:Ts:ts_Events.Time(end);
    ts_Events = resample(ts_Events,time,'zoh');
    time = 0:Ts:ts_Secondary_control.Time(end);
    ts_Secondary_control = resample(ts_Secondary_control,time,'zoh');
end

if savemat==1
    % save ts to mat files
    mtx_A = [ts_ConvA.Time, ts_ConvA.Data];
    mtx_B = [ts_ConvB.Time, ts_ConvB.Data];
    mtx_C = [ts_ConvC.Time, ts_ConvC.Data];
    mtx_D = [ts_ConvD.Time, ts_ConvD.Data];
    mtx_E1 = [ts_ConvE1.Time, ts_ConvE1.Data];
    mtx_F = [ts_ConvF.Time, ts_ConvF.Data];
    mtx_G = [ts_ConvG.Time, ts_ConvG.Data];
    mtx_E = [ts_Events.Time, ts_Events.Data];
    mtx_SC = [ts_Secondary_control.Time, ts_Secondary_control.Data];

    mtx_AA = mtx_A'; %#ok<NASGU>
    mtx_BB = mtx_B'; %#ok<NASGU>
    mtx_CC = mtx_C'; %#ok<NASGU>
    mtx_DD = mtx_D'; %#ok<NASGU>
    mtx_E1E1 = mtx_E1'; %#ok<NASGU>
    mtx_FF = mtx_F'; %#ok<NASGU>
    mtx_GG = mtx_G'; %#ok<NASGU>
    mtx_EE = mtx_E'; %#ok<NASGU>
    mtx_SCSC = mtx_SC'; %#ok<NASGU>

    save('Scenario_ConvA.mat','mtx_AA','-v4');
    save('Scenario_ConvB.mat','mtx_BB','-v4');
    save('Scenario_ConvC.mat','mtx_CC','-v4');
    save('Scenario_ConvD.mat','mtx_DD','-v4');
    save('Scenario_ConvE1.mat','mtx_E1E1','-v4');
    save('Scenario_ConvF.mat','mtx_FF','-v4');
    save('Scenario_ConvG.mat','mtx_GG','-v4');
    save('Scenario_Events.mat','mtx_EE','-v4');
    save('Scenario_Secondary_control.mat','mtx_SCSC','-v4');

    varargout = cell(1);
else
    varargout = {ts_ConvA ts_ConvB ts_ConvC ts_ConvD ts_ConvE1 ts_ConvF ts_ConvG ts_Events
                 ts_Secondary_control idx idxE idxSC}; %#ok<EMCA>
end
```

# Appendix E

## Power Plots for Improved Controllers in MTDC Grid

Converter and transmission line powers with the slower power and current controllers are shown in the figures below.

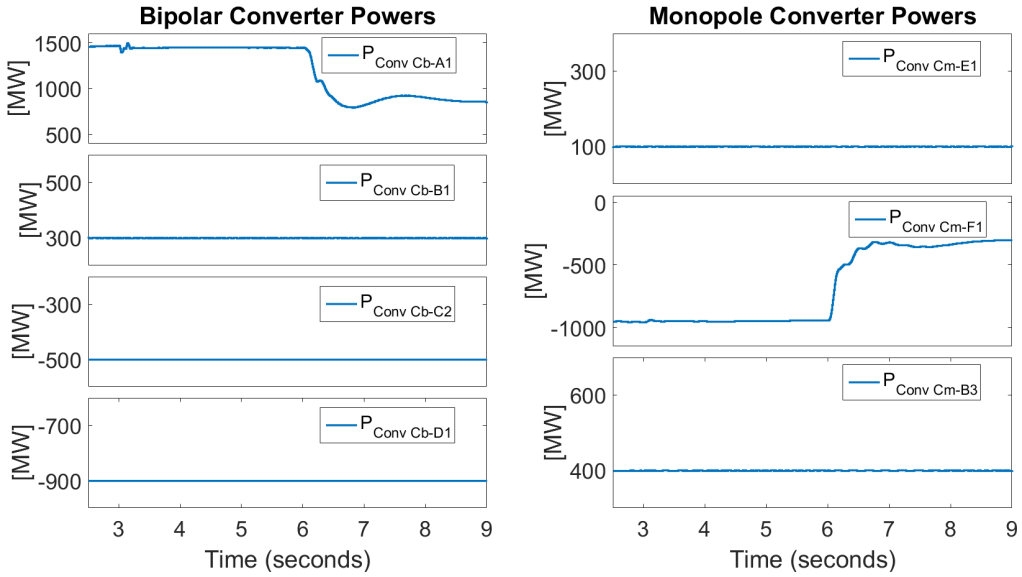


**Figure 2:** AC/DC converter powers with improved controllers

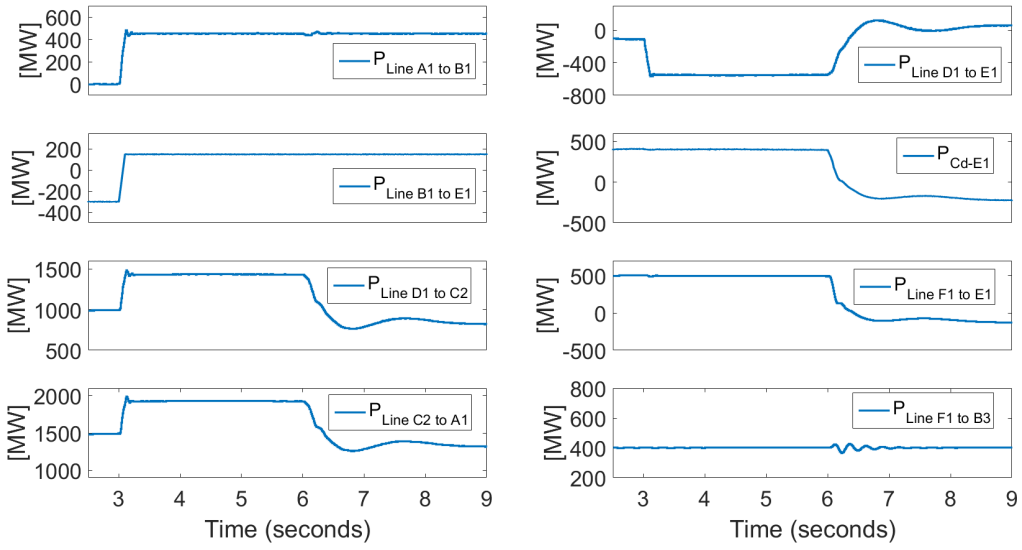


**Figure 3:** Transmission line powers between converter stations with improved controllers

# Bibliography


[1] L. Doman, *Eia projects 48consumption by 2040,* (2016).

[2] A. Whiteman, T. Rinke, J. Esparrago, and S. Elsayed, *Renewable capacity statistics 2016,* (2016).

[3] IEA-ETSAP and IRENA2016, *Wind power technology brief,* (2016).

[4] S. P. Engel, M. Stieneker, N. Soltau, S. Rabiee, H. Stagge, and R. W. D. Doncker, *Comparison of the modular multilevel dc converter and the dual-active bridge converter for power conversion in hvdc and mvdc grids,* IEEE Transactions on Power Electronics **30**, 124 (2015).

[5] T. Lüth, M. M. C. Merlin, and T. C. Green, *Modular multilevel dc/dc converter architectures for hvdc taps,* in *Power Electronics and Applications (EPE'14-ECCE Europe), 2014 16th European Conference on* (2014) pp. 1–10.

[6] F. Wang, Y. Pei, D. Boroyevich, R. Burgos, and K. Ngo, *Ac vs. dc distribution for off-shore power delivery,* in *Industrial Electronics, 2008. IECON 2008. 34th Annual Conference of IEEE* (2008) pp. 2113–2118.

[7] ABB, *Dolwin2 largest offshore wind hvdc grid connection in the world,* (2015).

[8] G. P. Adam, O. Anaya-Lara, and G. Burt, *Multi-terminal dc transmission system based on modular multilevel converter,* in *Universities Power Engineering Conference (UPEC), 2009 Proceedings of the 44th International* (2009) pp. 1–5.

[9] K. R. Padiyar, *Multiterminal and multi-infeed dc systems,* in *HVDC Power Transmission Systems*, p. 205–206.

[10] N. R. Chaudhuri, B. Chaudhuri, R. Majumder, and A. Yazdani, *Multi-terminal direct-current grids: modeling, analysis, and control*.

[11] C. Kamerbeek, *Dnv gl advises on world's first multi-terminal vsc hvdc transmission project integrating clean energy into china's regional power composition mix,* (2014).

[12] X. Li, Z. Yuan, J. Fu, Y. Wang, T. Liu, and Z. Zhu, *Nanao multi-terminal vsc-hvdc project for integrating large-scale wind generation,* in *2014 IEEE PES General Meeting | Conference Exposition* (2014) pp. 1–5.

[13] Y. Wang and R. Marquardt, *Future hvdc-grids employing modular multilevel converters and hybrid dc-breakers,* in *Power Electronics and Applications (EPE), 2013 15th European Conference on* (2013) pp. 1–8.

[14] D. Das, J. Pan, and S. Bala, *Hvdc light for large offshore wind farm integration,* in *2012 IEEE Power Electronics and Machines in Wind Applications* (2012) pp. 1–7.

[15] Siemens-AG-Energy-Sector, *The smart way hvdc plus – one step ahead,* (2011).

[16] Alstom-Grid, *Hvdc-vsc: transmission technology of the future,* (2011).

[17] K. Schmitt, *Siemens to deliver new hvdc technology for low-loss power supply via submarine cable to san francisco,* (2007).

[18] M. Guarnieri, *The alternating evolution of dc power transmission [historical],* IEEE Industrial Electronics Magazine **7**, 60 (2013).

[19] J. Arrillaga, *High voltage direct current transmission*, 29 (Iet, 1998).

[20] B. V. Lundin, *Hvdc transmission capacity growing,* (2013).

[21] E. Tedeschi, *Power electronics in future power systems lecture notes,* Lecture 2, Norwegian University of Science and Technology, Trondheim (2015).

[22] ABB, *Why hvdc, technical advantages,* .

[23] AskjaEnergy, *The iceland-europe interconnector,* (2012).

[24] J. Skog, H. v Asten, T. Worzyk, and T. Andersrød, *Norned—world's longest power cable,* CIGRE Session, Paris, France (2010).

[25] R. A. Mukhedkar, *Introduction to hvdc, lcc and vsc comparison, alstom,* .

[26] C.-K. Kim, V. K. Sood, G.-S. Jang, S.-J. Lim, and S.-J. Lee, *HVDC transmission: power conversion applications in power systems* (John Wiley & Sons, 2009).

[27] K. Eriksson, *Hvdc light and development of voltage source converters,* ABB review (2002).

[28] N. Flourentzou, V. G. Agelidis, and G. D. Demetriades, *Vsc-based hvdc power transmission systems: An overview,* IEEE Transactions on Power Electronics **24**, 592 (2009).

[29] L. Ronström, M. Hoffstein, R. Pajo, and M. Lahtinen, *The estlink hvdc light transmission system,* in *Proc. CIGRE Regional Meeting on Security and Reliability of Electric Power Systems, Tallinn, Estonia* (2007).

[30] I. Mattsson, A. Ericsson, B. Railing, J. Miller, B. Williams, G. Moreau, and C. Clarke, *Murray link-the longest underground hvdc cable in the world,* in *Paper B4-103 presented at the Cigré conference, Paris, France, Aug* (2004).

[31] A. Lesnicar and R. Marquardt, *An innovative modular multilevel converter topology suitable for a wide power range,* in *Power Tech Conference Proceedings, 2003 IEEE Bologna*, Vol. 3 (2003) pp. 6 pp. Vol.3–.

[32] M. A. Reynolds, *Tres amigas super station - large scale application of vsc back-to-back technology,* in *Transmission and Distribution Conference and Exposition (T D), 2012 IEEE PES* (2012) pp. 1–5.

[33] ABB, *Hvdc light - it's time to connect,* ABB AB, Grid Systems - HVDC, Ludvika, Sweden (2013).

[34] Siemens, *Bipolar long-distance dc transmission,* HVDC Configuration - Long-distance power transmission.

[35] L. Mackay, T. Hailu, L. Ramirez-Elizondo, and P. Bauer, *Towards a dc distribution system - opportunities and challenges,* in *DC Microgrids (ICDCM), 2015 IEEE First International Conference on* (2015) pp. 215–220.

[36] Y. Yang, M. Jafar, P. Vaessen, A. Yanushekvich, Y. Fu, R. Marshall, T. Bosma, and M. Irvine, *Hybrid grid, towards a hybrid ac/dc transmission grid,* DNV GL Strategic Research and Innovation Position Paper 2-2015 , 29 (2015).

[37] W. Zhou, X. Wei, S. Zhang, G. Tang, Z. He, J. Zheng, Y. Dan, and C. Gao, *Development and test of a 200kv full-bridge based hybrid hvdc breaker,* in *Power Electronics and Applications (EPE'15 ECCE-Europe), 2015 17th European Conference on* (2015) pp. 1–7.

[38] C. Barker, C. Davidson, D. Trainer, and R. Whitehouse, *Requirements of dc-dc converters to facilitate large dc grids,* Cigre Session 2012 (2012).

[39] S. Kavungal Kolparambath, *DC/DC Converters in Multi-terminal HVDC System for Integrating Offshore Wind Farms*, Master's thesis, TU Delft, Delft University of Technology (2015).

[40] T. Lüth, M. M. C. Merlin, T. C. Green, C. D. Barker, F. Hassan, R. W. Critchley, R. W. Crookes, D. Trainer, and K. Dyke, *Choice of ac operating voltage in hv dc/ac/dc system,* in *2013 IEEE Power Energy Society General Meeting* (2013) pp. 1–5.

[41] T. Lüth, M. M. C. Merlin, T. C. Green, C. D. Barker, F. Hassan, R. W. Critchley, R. W. Crookes, and K. Dyke, *Performance of a dc/ac/dc vsc system to interconnect hvdc systems,* in *AC and DC Power Transmission (ACDC 2012), 10th IET International Conference on* (2012) pp. 1–6.

[42] G. P. Adam, K. H. Ahmed, and B. W. Williams, *Mixed cells modular multilevel converter,* in *2014 IEEE 23rd International Symposium on Industrial Electronics (ISIE)* (2014) pp. 1390–1395.

[43] T. Lüth, M. M. C. Merlin, T. C. Green, F. Hassan, and C. D. Barker, *High-frequency operation of a dc/ac/dc system for hvdc applications,* IEEE Transactions on Power Electronics **29**, 4107 (2014).

[44] S. Shi, Y. Yang, T. Zhu, F. Wang, and F. Zhuo, *High power dc/ac/dc converter based on different modulation strategies,* in *2016 IEEE 8th International Power Electronics and Motion Control Conference (IPEMC-ECCE Asia)* (2016) pp. 315–320.

[45] S. Kenzelmann, A. Rufer, D. Dujic, F. Canales, and Y. R. de Novaes, *A versatile dc/dc converter based on modular multilevel converter for energy collection and distribution,* in *Renewable Power Generation (RPG 2011), IET Conference on* (2011) pp. 1–6.

[46] A. Schön and M. M. Bakran, *High power hvdc-dc converters for the interconnection of hvdc lines with different line topologies,* in *2014 International Power Electronics Conference (IPEC-Hiroshima 2014 - ECCE ASIA)* (2014) pp. 3255–3262.

[47] S. K. Kolparambath, J. A. Suul, and E. Tedeschi, *Dc/dc converters for interconnecting independent hvdc systems into multiterminal dc grids,* in *2015 IEEE 13th Brazilian Power Electronics Conference and 1st Southern Power Electronics Conference (COBEP/SPEC)* (2015) pp. 1–6.

[48] P. S. Jones and C. C. Davidson, *Calculation of power losses for mmc-based vsc hvdc stations,* in *Power Electronics and Applications (EPE), 2013 15th European Conference on* (2013) pp. 1–10.

[49] G. Bergna-Diaz, *Modular Multilevel Converter Control for HVDC Operation, Optimal Shaping of the Circulating Current Signal for Internal Energy Regulation*, Ph.D. thesis, NTNU (2015).

[50] E. Solas, G. Abad, J. A. Barrena, A. Cárear, and S. Aurtenetxea, *Modelling, simulation and control of modular multilevel converter,* in *Power Electronics and Motion Control Conference (EPE/PEMC), 2010 14th International* (2010) pp. T2–90–T2–96.

[51] M. M. C. Merlin and T. C. Green, *Cell capacitor sizing in multilevel converters: cases of the modular multilevel converter and alternate arm converter,* IET Power Electronics **8**, 350 (2015).

[52] C. Barker, C. Davidson, D. Trainer, and R. Whitehouse, *Requirements of dc-dc converters to facilitate large dc grids,* Cigre Session 2012 (2012).

[53] E. Solas, G. Abad, J. A. Barrena, A. Carear, and S. Aurtenetxea, *Modulation of modular multilevel converter for hvdc application,* in *Power Electronics and Motion Control Conference (EPE/PEMC), 2010 14th International* (2010) pp. T2–84–T2–89.

[54] W. Yao, H. Hu, and Z. Lu, *Comparisons of space-vector modulation and carrier-based modulation of multilevel inverter,* IEEE Transactions on Power Electronics **23**, 45 (2008).

[55] Y. Deng, K. H. Teo, C. Duan, T. G. Habetler, and R. G. Harley, *A fast and generalized space vector modulation scheme for multilevel inverters,* IEEE Transactions on Power Electronics **29**, 5204 (2014).

[56] M. Hamdi, M. Hamouda, F. Fnaiech, and K. Al-Haddad, *Space vector pulse width modulation of multilevel inverters: A new method for selecting the appropriate small hexagon,* in *IECON 2012 - 38th Annual Conference on IEEE Industrial Electronics Society* (2012) pp. 774–779.

[57] H. Zhang, A. V. Jouanne, S. Dai, A. K. Wallace, and F. Wang, *Multilevel inverter modulation schemes to eliminate common-mode voltages,* IEEE Transactions on Industry Applications **36**, 1645 (2000).

[58] M. Huang, J. Zou, and X. Ma, *An improved phase-shifted carrier modulation for modular multilevel converter to suppress the influence of fluctuation of capacitor voltage,* IEEE Transactions on Power Electronics **PP**, 1 (2016).

[59] L. Lin, Y. Lin, Z. He, Y. Chen, J. Hu, and W. Li, *Improved nearest-level modulation for a modular multilevel converter with a lower submodule number,* IEEE Transactions on Power Electronics **31**, 5369 (2016).

[60] L. G. Franquelo, J. Rodriguez, J. I. Leon, S. Kouro, R. Portillo, and M. A. M. Prats, *The age of multilevel converters arrives,* IEEE Industrial Electronics Magazine **2**, 28 (2008).

[61] M. AnLezana, S. Kouro, J. Rodriguez, and B. Wu, *Level-shifted pwm for cascaded multilevel inverters with even power distribution,* in *2007 IEEE Power Electronics Specialists Conference* (2007) pp. 2373–2378.

[62] Y. Deng, Y. Wang, K. H. Teo, and R. G. Harley, *A simplified space vector modulation scheme for multilevel converters,* IEEE Transactions on Power Electronics **31**, 1873 (2016).

[63] M. Moranchel, E. J. Bueno, F. J. Rodriguez, and I. Sanz, *Implementation of nearest level modulation for modular multilevel converter,* in *2015 IEEE 6th International Symposium on Power Electronics for Distributed Generation Systems (PEDG)* (2015) pp. 1–5.

[64] Q. Tu, Z. Xu, and J. Zhang, *Circulating current suppressing controller in modular multilevel converter,* in *IECON 2010 - 36th Annual Conference on IEEE Industrial Electronics Society* (2010) pp. 3198–3202.

[65] D. G. Artjoms Timofejevs, *Control of MMC in HVDC Applications*, Master's thesis, Department of Energy Technology, Aalborg University, Denmark (2013).

[66] A. Antonopoulos, L. Angquist, and H. P. Nee, *On dynamics and voltage control of the modular multilevel converter,* in *Power Electronics and Applications, 2009. EPE '09. 13th European Conference on* (2009) pp. 1–10.

[67] Q. Tu, Z. Xu, and J. Zhang, *Circulating current suppressing controller in modular multilevel converter,* in *IECON 2010 - 36th Annual Conference on IEEE Industrial Electronics Society* (2010) pp. 3198–3202.

[68] Q. Tu, Z. Xu, and L. Xu, *Reduced switching-frequency modulation and circulating current suppression for modular multilevel converters,* IEEE Transactions on Power Delivery **26**, 2009 (2011).

[69] B. Bahrani, S. Debnath, and M. Saeedifard, *Circulating current suppression of the modular multilevel converter in a double-frequency rotating reference frame,* IEEE Transactions on Power Electronics **31**, 783 (2016).

[70] X. She, A. Huang, X. Ni, and R. Burgos, *Ac circulating currents suppression in modular multilevel converter,* in *IECON 2012 - 38th Annual Conference on IEEE Industrial Electronics Society* (2012) pp. 191–196.

[71] Y. Ma, L. Fan, and Z. Miao, *Integrated control and switching strategy for a grid-connected modular multilevel converter,* in *2015 IEEE Power Energy Society General Meeting* (2015) pp. 1–5.

[72] C. Du, *The control of VSC-HVDC and its use for large industrial power systems*, Master's thesis, Department of Electric Power Engineering Chalmers University of Technology, Goteborg, Sweden (2003).

[73] E. N. Abildgaard and M. Molinas, *Modelling and control of the modular multilevel converter (mmc),* Energy Procedia **20**, 227 (2012).

[74] C. Bajracharya, M. Molinas, J. A. Suul, T. M. Undeland, *et al.*, *Understanding of tuning techniques of converter controllers for vsc-hvdc,* in *Nordic Workshop on Power and Industrial Electronics (NORPIE/2008), June 9-11, 2008, Espoo, Finland* (Helsinki University of Technology, 2008).

[75] C. Bajracharya, *Control of VSC-HVDC for wind power*, Master's thesis, Department of Electric Power Engineering, Norwegian University of Science and Technology, Trondheim, Norway (2008).

[76] I. A. Gowaid, G. P. Adam, A. M. Massoud, S. Ahmed, D. Holliday, and B. W. Williams, *Quasi two-level operation of modular multilevel converter for use in a high-power dc transformer with dc fault isolation capability,* IEEE Transactions on Power Electronics **30**, 108 (2015).

[77] V. Jankov and M. Stobart, *Hvdc system performance with a neutral conductor,* in *High Voltage Engineering and Application (ICHVE), 2010 International Conference on* (2010) pp. 188–191.

[78] A. k. Marten, V. Vahrenholt, W. Fischer, K. Fuchs, F. Berger, and D. Westermann, *Substation layout for multi-terminal hvdc systems and neutral conductor arrangements for reduced field emissions,* in *AC and DC Power Transmission, 11th IET International Conference on* (2015) pp. 1–6.

[79] T. K. Vrana, Y. Yang, D. Jovcic, S. Dennetière, J. Jardini, and H. Saad, *The cigre b4 dc grid test system,* Electra **270**, 10 (2013).

[80] G. Bergna-Diaz, *User guide for proofgrids models in matlab/simulink,* SINTEF Energi AS, Trondheim, Norway **29** (2014).